Spring 2014

Seismic anisotropy and mantle flow beneath Africa and Arabia

Ahmed Abdalla Elsheikh

Department: Geosciences and Geological and Petroleum Engineering

SEISMIC ANISOTROPY AND MANTLE FLOW BENEATH AFRICA AND ARABIA

by

AHMED ABDALLA ELSHEIKH

A DISSERTATION

Presented to the Faculty of the Graduate School of the

MISSOURI UNIVERSITY OF SCIENCE AND TECHNOLOGY

In Partial Fulfillment of the Requirements for the Degree

DOCTOR OF PHILOSOPHY

in

GEOLOGY AND GEOPHYSICS

2014

Approved by:
Stephen Gao, Co-Advisor,
Kelly Liu Co-Advisor
Mohamed Abdelsalam Co-Advisor
Andreas Eckert
J David Rogers

PUBLICATION DISSERTATION OPTION

Pages 5-32, were submitted to The Journal of African Earth Sciences, pages 34-45 have been published in Geophysical Research Letters.

ABSTRACT

In spite of numerous studies, the mechanisms for the rifting, uplifting, and volcanism on the African plate remain enigmatic. The most popular hypotheses proposed for explaining these tectonic phenomena involve edge-driven small-scale mantle convection and the thermal or dynamic effects of one or more mantle plumes. In this study we use continental scale shear-wave splitting (SWS) measurements to provide additional constraints on the various models of rifting, uplifting, and volcanism of the Cameroon Volcanic Line (CVL) and the Arabian plate. The splitting of P-to-S converted phases at the core-mantle boundary on the receiver side (XKS including PKS, SKKS, and SKS) is one of the most effective approaches to constrain convective mantle flow patterns. A robust procedure involving automatic and manual batch processing to reliably assess and objectively rank shear-wave splitting parameters were used. The resulting 1532 pairs of splitting parameters show a NNE dominated fast direction. Spatial distribution of the splitting parameters in the CVL and Arabia is not consistent with the edge-driven small-scale mantle convection hypothesis, the mantle plume hypothesis, fossil fabrics formed by past tectonic events, or the fabric-forming process due to the absolute plate motion relative to the deep mantle.

The research suggests that the progressive thinning of the lithosphere through basal erosion by the flow leads to decompression melting is responsible for the formation of the CVL, and olivine lattice preferred orientation in the upper asthenosphere associated with the northward motion of the African plate since 150 Ma, most likely causes the observed anisotropy across the Red Sea.

ACKNOWLEDGMENTS

I would not have made it to this point and through my entire life without Allah the almighty blessings. God is the one, and only to deserves the absolute praise.

Only when I started thinking of what to write in my acknowledgement, I discovered it is much more difficult to convey the deep feelings and appreciation, and put it into words than writing an entire dissertation. My PhD advisor, Dr. Stephen Gao, my MS advisor, Dr. Mohamed Abdelsalam, and co-advisor, Dr. Kelly Liu, have shaped my life and future in many aspects. I learned from Dr. Gao what it means to be patient and a good listener and I am indebted to him for uplifting my skills in seismology, critical thinking, writing, speaking, and teaching. The level of knowledge, capability and experience he generously offered me, will guide my research and academic life.

Other than the academic and research polishing Dr. Abdelsalam has made on me, he demonstrated to me how to maintain a high level of professionalism, even in hardest circumstances. The constant inspiration, encouragement, and advice of Dr. Kelly Liu, has kept me progressing and advancing my research.

I would also like express my sincere thanks and appreciation to my committee members, Dr. Andreas Eckert and Dr. J. David Rogers, for being members of my committee and for their invaluable suggestions. Also, I thank Radcliffe for PhD financial support.

Special thanks to my family for their unwavering support and prayers throughout my life. My sincere and heartfelt gratitude go out to my mother, my father, my brothers and my sister. I wish to express special appreciation to my wife, Ghadeer Sirag for uncounted sacrifices she made so I can finish my study.

TABLE OF CONTENTS

LIST OF ILLUSTRATIONS

NOMENCLATURE

Symbol	Description
Φ	Fast polarization direction
δt	Splitting time

SECTION

1. INTRODUCTION

A longstanding problem with our understanding of the tectonics of the African plate is the deformation of the lithosphere and its dynamic interaction with the asthenosphere. Numerous studies have used different methods to study lithospheric deformation, but many fundamental questions regarding the formation of intra-continental volcanic lines such as the CVL and interaction between moving plates and the underlying asthenosphere are still poorly understood (Figure 1.1).

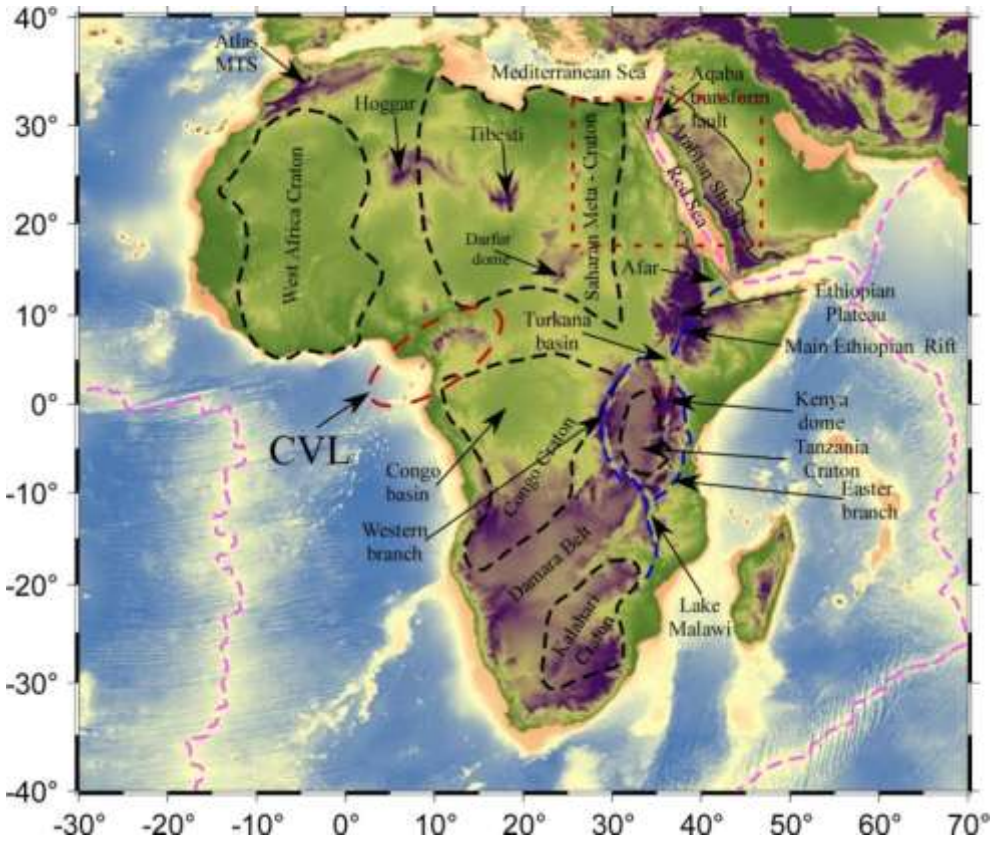

Figure 1.1. Major tectonic elements of the Afro-Arabian Rift System and East African Rift System.

This dissertation undertakes two seismic anisotropy studies using shear-wave splitting. The first project examines the upper mantle structure beneath the Cameroon Volcanic Line (Figure 1.1). This part of the study proposes a channel flow model that can explain the lack of age progression of the volcanoes in the CVL and the formation mechanism for both the continental and oceanic sections of the CVL.

The second part of the study investigates upper mantle anisotropy across the Red Sea (Figure 1.1). It is the first study that utilizes data recorded by the Egyptian National Seismic Network. The results suggests that seismic anisotropy is caused by simple shear in the boundary layer between the lithosphere and the asthenosphere associated with northward subduction of the African/Arabian plates over the past 150 Ma.

PAPER

I. MANTLE SEISMIC ANISOTROPY AND FORMATION OF THE CAMEROON VOLCANIC LINE BY LITHOSPHERIC BASAL EROSION

Abstract

The formation mechanism of intraplate volcanism such as that along the Cameroon Volcanic Line (CVL) is one of the controversial problems in global tectonics. Models proposed by previous studies include re-activation of ancient suture zones, lithospheric thinning by mantle plumes, and edge-driven mantle convection. To provide additional constraints on the models for the formation of the CVL, we measured shear-wave splitting parameters at 36 stations in the vicinity of the CVL using a robust procedure involving automatic batch processing and manual screening to reliably assess and objectively rank shear-wave splitting parameters (fast polarization directions and splitting times). The resulting 432 pairs of splitting parameters show a systematic spatial variation. Most of the measurements with ray-piercing points (at 200 km depth) beneath the CVL show a fast direction that is parallel to the volcanic line, while the fast directions along the coastline are parallel to the continental margin. The observations can best be interpreted using a model that involves a channel flow at the bottom of the lithosphere originated from the NE-ward movement of the asthenosphere relative to the African plate. We hypothesize that progressive thinning of the lithosphere through basal erosion by the flow leads to decompression melting and is responsible for the formation of the CVL. The model is consistent with the lack of age progression of the volcanoes in the

CVL, can explain the formation of both the continental and oceanic sections of the CVL, and is supported by previous geophysical observations and geodynamic modeling results.

1. Introduction

Most of the Earth's magmatism is associated with dehydration of minerals in subducting slabs and with decompression melting along mid-ocean ridges, and thus can be well-explained by the theory of plate tectonics [e.g., *Turcotte and Oxburgh, 1978; Courtillot et al., 2003*]. The formation mechanism for intraplate magmatism, on the other hand, remains enigmatic. Various models have been proposed to explain intraplate magmatism, including those involving mantle plumes [*Morgan, 1972; Courtillot et al., 2003*], tensional cracking in the lithosphere [*Turcotte and Oxburgh, 1978; Anderson, 2000*], and edge-driven convection (EDC) [*King and Anderson, 1998*].

The African plate is ideal for studying intraplate magmatism. It contains several intraplate volcanic segments or centers that are remote from the African plate boundaries (Figure 1). One of such segments is the NE-SW oriented Cameroon Volcanic Line (CVL), which consists of a continental and an oceanic section. The CVL intercepts with the Atlantic coastline at the joint point between the E-W and N-S segments of the coastline (Figure 2).

Many studies proposed that the CVL was the result of the NE-ward movement of the African plate over a mantle plume that is currently beneath St. Helena [e.g., *Morgan, 1983*] (Figure 1). This model predicts that the age of the volcanoes decreases toward the SW. Such an age progression, however, is not observed [e.g., *Fitton and Dunlop, 1985*].

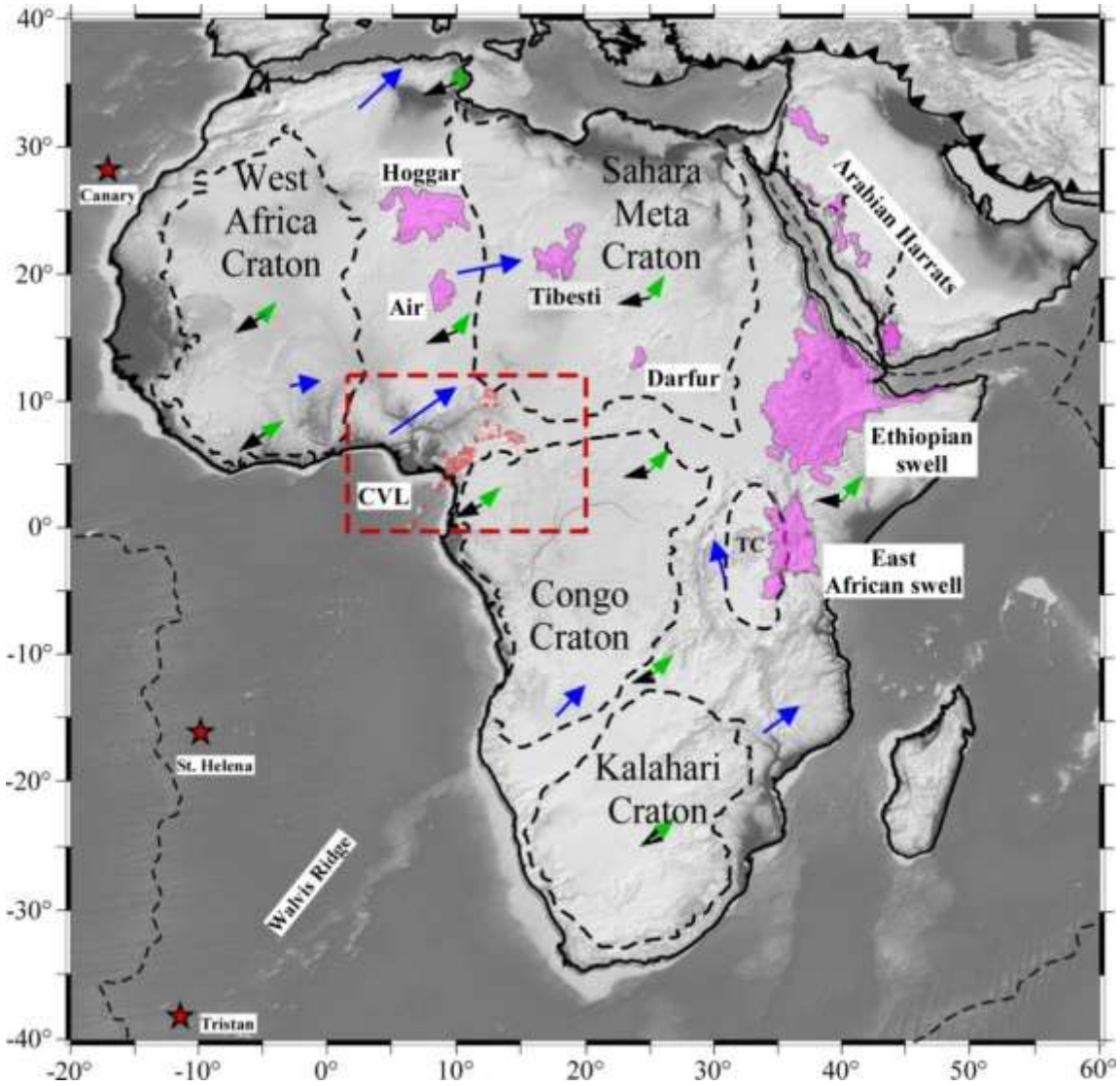

Figure 1. Topographic relief map of Africa showing major interplate volcanic centers and cratons [*Turcotte and Oxburgh, 1978; Abdelsalam et al., 2011*]. Cameroon Volcanic Line (CVL); Tanzania Craton (TC). The area inside the red dashed rectangle is shown in Figures 2 and 3. The green arrows represent absolute plate motion (APM) vectors calculated using the GMHRF model [*Doubrovine et al., 2012*] and the black arrows show APM vectors determined by the HS3-NUVEL1A model [*Gripp and Gordon, 2002*]. The blue arrows indicate the horizontal component of mantle flow predicted at 250 km depth [*Forte et al., 2010*]. Red stars represent the locations of the Atlantic mantle plumes [*Doubrovine et al., 2012*].

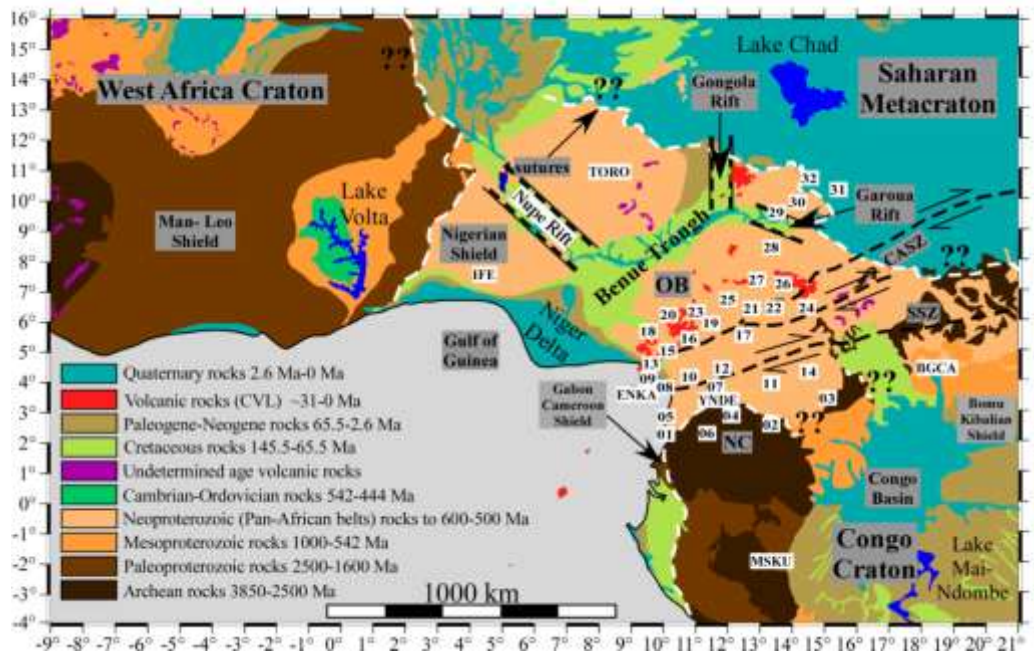

Figure 2. Major tectonic elements of western and central Africa showing the main geological subdivision units [*International Geological Map of Africa, 1990*]. The white squares and rectangular show the seismic stations used in the study.

Additionally, 3He/4He ratios measured along the CVL are lower than those observed at typical hotspots such as Loihi and Iceland [*Aka et al., 2004*], probably suggesting an upper-mantle origin of the magmatism. Other studies concluded that the CVL was due to decompression melting beneath re-activated shear zones on the African continent [e.g., *Fairhead, 1988*]. This model, while can explain the lack of age progression, cannot satisfactorily explain the existence of the oceanic section of the CVL. The third group of studies advocated edge-driven convection as the major cause of the CVL [*King and Ritsema, 2000; Koch et al., 2012; Milelli et al., 2012*]. This model suggests that the upwelling flow thins the lithosphere and creates a line of volcanoes parallel to the boundary between two areas with contrasting lithospheric thickness.

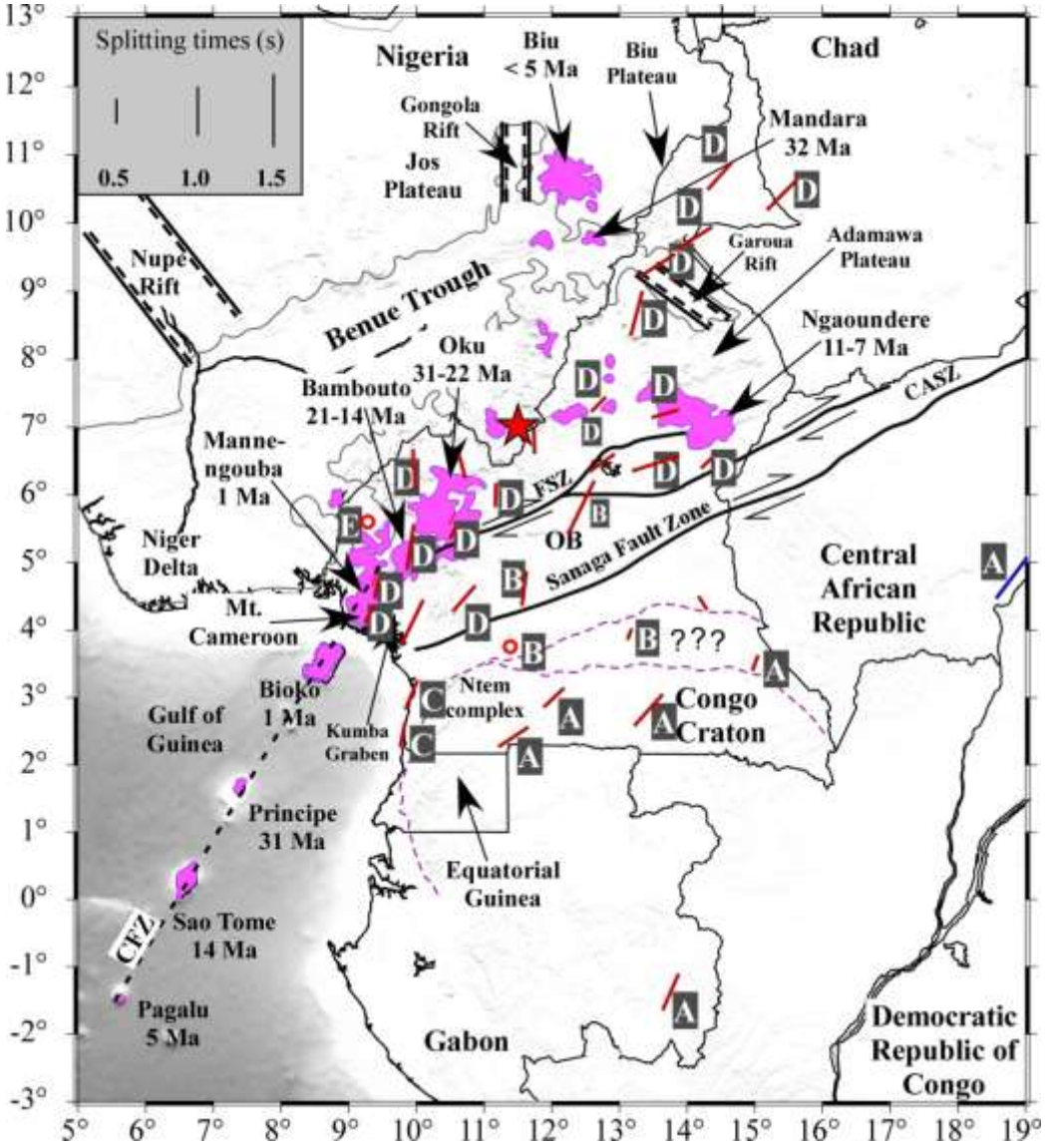

Figure 3. A map of the study area showing locations and ages of the Cameroon Volcanic Line (magenta features) [*Fitton and Dunlop, 1985; Fitton, 1987*] and previous shear-wave splitting measurements (red and blue bars). The orientation of the bars represents the fast direction (the length is proportional to the splitting time), and the red circles represent null measurements. The blue bar near the eastern edge of the figure represents the measurement from *Barruol and Ben Ismail* [2001], and the red bars and circles represent measurements from *Koch et al*. [2012]. FSZ, Foumban Shear Zone. CASZ, Central African Shear Zone. CFZ, Cameroon Fracture Zone [*Meyers et al., 1998; Reusch et al., 2010*]. OB, Oubanguides Belt. The dashed magenta line represents the northern edge of the Congo craton [*Schluter, 2006; Reusch et al., 2010*]. The red star shows the location of the Cameroon mantle plume [*Burke, 2001*]. The letters in the rectangles indicate the name of the sub-area that the stations belong to (see section 5.1).

In the study area, the northern edge of the Congo craton is a potential locale for the EDC to occur and thus could be responsible for the formation of the continental section of the CVL (Figure 2). However, this model cannot explain the orientation of the oceanic section of the CVL, because the anticipated strike of the zone of thinned oceanic lithosphere should be parallel to the coastline, while the actual CVL has a NE-SW strike. In addition, as described below, neither the plume nor the EDC model is supported by shear-wave splitting (SWS) measurements.

Splitting analysis of P-to-S converted phases at the core-mantle boundary on the receiver side, including the PKS, SKKS, and SKS (hereinafter collectively referred to as XKS) phases, is considered to be one of the most effective tools in measuring seismic anisotropy, which is mostly caused by deformational processes in the mantle [see *Silver, 1996*, *Savage, 1999*, and *Fouch and Rondenay, 2006* for reviews]. Numerous XKS splitting studies demonstrated that the spatial distribution of the two splitting parameters Φ, which is the polarization direction of the faster wave, and δt, the splitting time between the faster and slower waves, are crucial to understand mantle circulation patterns. The fast direction reflects the anisotropy orientation, while the splitting time quantifies the magnitude of mantle deformation [*Conrad and Behn, 2010; Kreemer, 2009*].

The coefficient of anisotropy is defined as $(V_{fast}-V_{slow})/V_{mean}$ where V_{fast} and V_{slow} are the fast and slow shear-wave velocities, respectively and V_{mean} is the mean velocity [Birch, 1960; Wolfe and Solomon, 1998]. The global average of the splitting time observed using teleseismic XKS waves is 1.0 s, which corresponds to a thickness of about 100 km for a 4% anisotropy [*Silver, 1996*]. Olivine lattice-preferred

orientations (LPO) likely forms as a result of dislocation creep deformation, leading to a macroscopic anisotropy in the upper mantle [e.g., *McKenzie, 1979; Ribe, 1989; Fouch and Rondenay, 2006; Conrad et al., 2007*]. Numerical modeling and experimental mineral physics studies indicate that under uniaxial compression, the olivine a-axis rotates to be orthogonal to the maximum compressional strain direction. Under pure shear, it becomes perpendicular to the shortening direction; and under progressive simple shear, it aligns parallel to the flow direction [*Ribe and Yu, 1991; Chastel et al., 1993; Zhang and Karato, 1995; Savage, 1999; Liu, 2009*]. Therefore, the fast direction may reveal the flow direction in the asthenosphere as observed in ocean basins, continental rifts, and passive margins [*Wolfe and Solomon, 1998; Gao et al., 1994, 1997, 2008, 2010; Refayee et al., 2013*].

In the lithosphere, Φ is primarily parallel to the trend of past tectonic events, as revealed at numerous locales [*McNamara et al., 1994; Liu et al., 1995; Silver, 1996; Barruol and Hoffmann, 1999; Fouch and Rondenay, 2006; Li and Chen, 2006; Liu, 2009*]. In addition, vertical magmatic dikes in the lithosphere can result in XKS splitting with a fast direction parallel to the main strike direction of the dikes [*Gao et al., 1997, 2010*]. This mechanism was suggested to explain rift-parallel fast directions detected in active continental rifts such as the Baikal rift zone [*Gao et al., 1997*], the East African rift system [*Gao et al., 1997, 2010; Kendall et al., 2005*], and failed rifts such as the southern Oklahoma aulacogen [Gao et al., 2008].

2. Geophysical background

The CVL is an ~1600 km elongated Y-shaped feature of Cenozoic volcanoes [e.g., *Fitton, 1987; Aka et al., 2004; Tokam et al., 2010; Reusch et al., 2010; Milelli et*

al.,2012] (Figure 3). It is located between the Congo craton to the south and the Oubanguides Belt to the north, which was created by the collision between four different terranes including the Sao Francisco and Congo cratons, the West African craton, and a Pan-African mobile domain during the formation of the Gondwana [e.g., *Castaing et al., 1994; Toteu et al., 2004; Begg et al., 2009; Tokam et al., 2010*]. The land section of the CVL includes several major volcanoes such as Mounts Cameroon, Manengouba, Bambouto, and Oku, and extends from the Gulf of Guinea all the way to the Chad frontier [e.g., *Aka et al., 2004*] (Figure 2). The oceanic section includes the islands of Annobon (formerly called Pagalu), Sao Tome, Principe, and Bioko (Figure 3). The Pan-African basement rocks almost cover the entire continental portion of the CVL with more than 60 anorogenic ring complexes exposed on the surface of the continental section of the CVL. The majority of these ring complexes are concentrated in the southwestern part of the continental section. The basement rocks exposed on the CVL are mainly alkaline (basalts, basanites, trachytes, and phonolites) with the exception of the nephelinitic lava that erupted near Mt. Etinde [*Fitton and Hughes, 1981; Fitton, 1987; Lee et al., 1994; Aka et al., 2004; Deruelle et al., 1991, 2007*].

Nearly all of the global and regional tomographic models agree that the CVL is underlain by upper mantle low-velocity anomalies, while the Congo and West Africa cratons are underlain by high-velocity anomalies [e.g., *King and Ritsema, 2011; Ritsema and Heijst, 2000; Priestley et al., 2008; Reusch et al., 2010*]. However, the lateral and depth extent of the upper mantle low-velocity anomalies beneath the CVL, which plays an important role for understanding the origin of the CVL, is still a subject of considerable debate [e.g., *Reusch et al., 2010*]. *King and Ritsema* [2000] used numerical

modeling constrained by seismic tomography results to understand the origin of African and South American intraplate volcanisms. They found relatively high seismic shear wave velocities in the mantle transition zone beneath the Congo and West African cratons and suggested that EDC from beneath the Congo craton is responsible for the formation of the CVL.

On a local scale, *Dorbath et al.* [1986] performed inversion of teleseismic P-wave travel-time residuals across the Adamawa Plateau and the central African shear zone (CASZ) in central Cameroon (Figure 3). They revealed a low-velocity anomaly beneath the Adamawa Plateau striking ENE at the depth of ~190 km. *Plomerova et al.* [1993] examined the lithospheric thickness and anisotropy within the upper mantle in the Adamawa Plateau using teleseismic P-and PKP-arrival times recorded by a network of 40 seismic stations deployed along the plateau. They concluded that a thinned lithosphere and a 2% low-velocity anomaly beneath the CASZ in Cameroon are caused by mantle upwelling. The most recent tomographic imaging using body-waves shows a tabular low-velocity anomaly beneath the CVL with a depth extension not less than 300 km [*Reusch et al., 2010*]. They argued that the low-velocity anomaly beneath the CVL is consistent with a model involving EDC along the northern boundary of the Congo craton.

Many studies have analyzed crustal structure beneath the study area using a variety of techniques including active and passive seismic source analysis [e.g., *Stuart et al., 1985; Dorbath et al., 1986; Tabod et al., 1992; Plomerova et al., 199139 3; Sandvol et al., 1998; Hansen et al., 2009; Obrebski et al., 2010; Tokam et al., 2010; Gallacher and Bastow, 2012] and gravity studies [e.g., Fairhead and Okereke, 1987; Djomani et al., 1995; Nnange et al., 2000; Toteu et al., 2004; Tadjou et al., 2009*]. *Tokam et al.*

[2010] used data from the Cameroon Broadband Seismic Experiment (CBSE) network, which consisted of 32 portable broad-band seismometers deployed between January 2005 and February 2007 across Cameroon, to investigate crustal structure beneath the CVL by utilizing P-wave receiver functions (RFs) and surface wave dispersion data. They found a thin crust of 26-31 km in thickness beneath the Garoua rift and the coastal plain (Figure 3), and a thicker crust of 43-48 km with a mafic lower crust beneath the Congo craton. The crustal thickness in the CVL and the Oubanguides Belt varies between 35 and 39 km (Figure 3). They suggested that the thin crust beneath the coastal plain is caused by the opening of the southern Atlantic Ocean, while the formation of the Benue Trough in the early Cretaceous thinned the crust in the Garoua rift. The thicker crust in the Congo craton was formed as a result of continent-continent collision in the development of the Gondwana. Recently, *Gallacher and Bastow* [2012] applied a RFs stacking technique [*Zhu and Kanamori, 2000*] using the CBSE data to study crustal structure beneath the CVL. Most of the crustal thickness measurements by *Gallacher and Bastow* [2012] are comparable with those obtained by *Tokam et al.* [2010].

3. Previous seismic anisotropy studies

During the past two decades, XKS splitting studies provided important constraints on various models for the formation, structure, and dynamics of various Cenozoic tectonic processes on the African plate including rifting, uplifting, volcanism, and lithosphere deformation [e.g., *Vinnik et al., 1989; Gao et al., 1997; Barruol and Hoffmann, 1999; Silver et al., 2001; Barruol and Ben Ismail, 2001; Gashawbeza et al., 2004; Walker et al., 2004; Kendall et al., 2005, 2006; Gao et al., 2010; Bagley and*

Nyblade, 2013]. In our study area, *Chevrot* [2000] conducted multichannel SKS splitting analysis to constrain seismic anisotropy beneath station BGCA (formerly called BNG). He suggested that the splitting parameters ($\Phi = 17 \pm 1.0°$ and $\delta t = 0.74 \pm 0.03$ s) observed at the station are due to the present-day movement of the African plate. For the same station, *Barruol and Hoffmann* [1999] found $\Phi = 29 \pm 4.0°$ and $\delta t = 0.84 \pm 0.11$ s. *Barruol and Ben Ismail* [2001] investigated upper mantle anisotropy beneath the African plate using data from the Incorporated Research Institutions for Seismology (IRIS) and GEOSCOPE stations including BGCA. They obtained a fast direction of $35 \pm 2.0°$ and a splitting time of 0.79 ± 0.06 s at BGCA.

Koch et al. [2012] reported station-averaged SKS and SKKS splitting parameters beneath Cameroon (Figure 3) using data from the CBSE and station MSKU. The study also used SWS results at station BGCA from *Barruol and Ben Ismail* [2001]. They identified four regions with different splitting parameters. The Congo craton and the Garoua rift have NE-SW fast directions and splitting times of about 1.0 s. Spatially varying fast directions and splitting times as small as 0.3 s are observed at the northern edge of the Congo craton and in the area between the CVL and the craton in central Cameroon (Figure 3). Along the CVL, the mean fast direction is about 30°, and the splitting times are 0.7 s. They suggested that the observed anisotropy beneath central and northeast Cameroon is associated with fossil anisotropy due to past collisional events, while most of the observed anisotropy beneath the CVL is related to EDC originated from variations in temperature between the Congo craton and the mobile belts that flank the northern boundary of the Congo craton [e.g., *King and Anderson, 1995; King and Anderson, 1998; King and Ritsema, 2000; Koch et al., 2012*] (Figure 3). According to

this model, the hotter materials beneath the Congo cratonic root propagate northward to the mobile belts, leading to mostly N-S fast directions in the CVL.

In this study, we take the advantage of the recently released broadband seismic data in a larger area surrounding the CVL than that in previous studies, including data from Cameroon, the Central African Republic, Gabon, and Nigeria, to provide additional constraints on the origin of the CVL. We conclude that SWS results favor a model that involves a lithospheric channel that developed as a result of gradual basal erosion by the underlying asthenosphere on the northern edge of the Congo craton. This mechanism in turn causes decompression melting and is responsible for the formation of both the continental and oceanic sections of the CVL.

4. Data and Methods

We use all the broadband XKS data recorded in the study area and archived until early 2013 at IRIS Data Management Center (DMC). The seismic events were selected based on the following criteria: For PKS, the epicentral distance range is 120-180°, and the cutoff magnitude is 5.8; for SKKS, the corresponding values are 95-180° and 5.6; and for SKS, they are 84-180° 200 and 5.6. In order to take the advantage of the sharper waveforms for all the PKS, SKKS, and SKS phases from deeper events, the cutoff magnitude is reduced by 0.1 units for events with a focal depth equal or greater than 100 km [*Liu and Gao, 2009, 2013*].

Figure 4 shows the distribution of the 204 events that produced at least one well-defined measurement. The majority of the events are located in the western Pacific and Nazca subduction zones. Thirty-six stations were found to produce at least one well-

defined XKS splitting measurement. One of the stations used in this study, BGCA in Central Africa, belongs to GEOSCOPE. This station has been operating since June 1994. Stations EKNA, IFE, and YNDE are part of the African Array, while station TORO is a Nigerian National Seismic Network station. In addition, we used data from station MSKU, which belongs to IRIS/USGS Global Seismographic Network in Masuku Gabon. This station belongs to IRIS/USGS Global Seismographic Network in Masuku Gabon, and has been operating since March 1999. The rest of the stations are from the CBSE [*Tokam et al., 2010*]. During our shear-wave-splitting analysis, we detected and corrected a misidentification of the vertical and E-W components at station IFE.

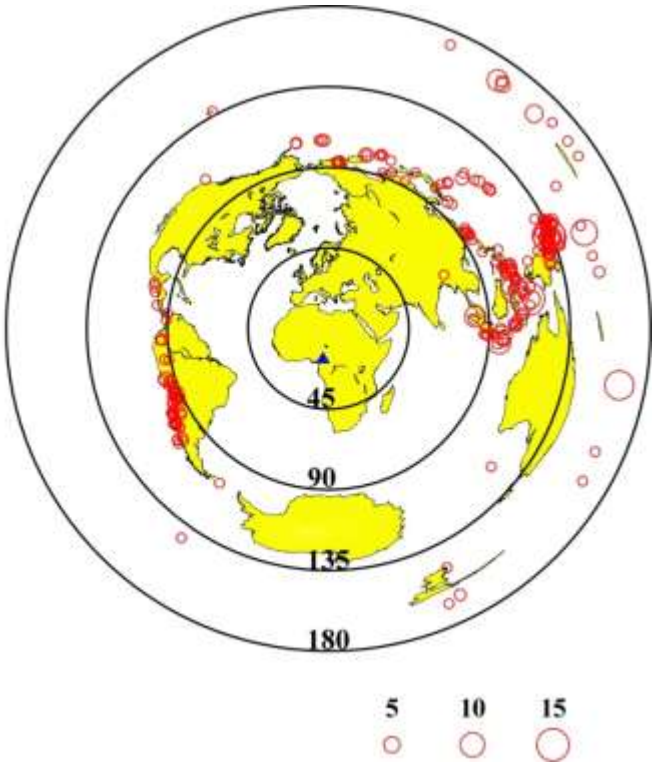

Figure 4. An azimuth equidistant projection map of the Earth showing the distribution of earthquakes used in the study (open dots). The radius of the dots is proportional to the number of resulting well-defined splitting measurements from the events. Circles and corresponding labels show the distance (in degree) to the center of the study area.

This study used a procedure for measuring and objectively ranking XKS splitting parameters based on the minimization of transverse energy method [*Silver and Chan, 1991; Liu et al., 2008; Gao and Liu, 2009; Liu, 2009; Gao et al., 2010; Liu and Gao, 2013*]. The seismograms were band-pass filtered in the 0.04-0.5 Hz range which is the most effective frequency band for enhancing the signal-to-noise ratio (S/N). The optimal XKS time window is visually verified and adjusted if necessary to exclude non-XKS arrivals [*Liu and Gao, 2013*]. The uncertainties in the measurements are calculated based on the inverse F-test [*Silver and Chan, 1991*].

Figure 5 shows examples of the original and corrected waveforms and their particle motion diagrams. The quality of the resulting measurements are ranked using the S/N on the original radial (Ror), original transverse (Rot), and corrected transverse (Rct) components [*Liu et al., 2008*]. We classified a measurement as a quality A measurement when Ror $\geq$ 10.0, Rot $\geq$ 2.0, and Rct/Rot $\leq$ 0.7, that is, outstanding energy on both the radial and transverse components is observed, and the resulting parameters were effective in reducing the energy on the transverse component [*Liu et al., 2008*]. For a quality B event, the corresponding values are 3.0 $\leq$ Ror < 10.0, Rot $\geq$ 2.0, and Rct/Rot $\leq$ 0.7. The ranking was manually screened and adjusted if necessary.

5. Results

A total of 432 pairs of quality A or B measurements were obtained after manual screening of the results (Figure 6). In addition, we observed null measurements at almost all of the stations. Null measurements are characterized by the lack of observable energy on the transverse component as a result of the backazimuth (BAZ) directions being either

parallel or perpendicular to the fast direction, or the media traveled by the XKS phase is isotropic [e.g., *Silver and Chan, 1991; Liu and Gao, 2013*]. Two or more null events with non-parallel or orthogonal back-azimuths indicate the paucity of anisotropy. Our results demonstrate that clear splitting is observed at all stations in the study area, and thus the null measurements are not used in the discussions below.

5.1. Spatial variations of SWS measurements

We divided the CVL and the adjacent regions into five sub-areas based on the characteristics of the SWS measurements and also on different tectonic provinces (Figures 2 and 3). Area A is on the Congo craton and includes stations CM02, 03, 04, 06, BGCA and MSKU and contains 208 pairs of SWS measurements.

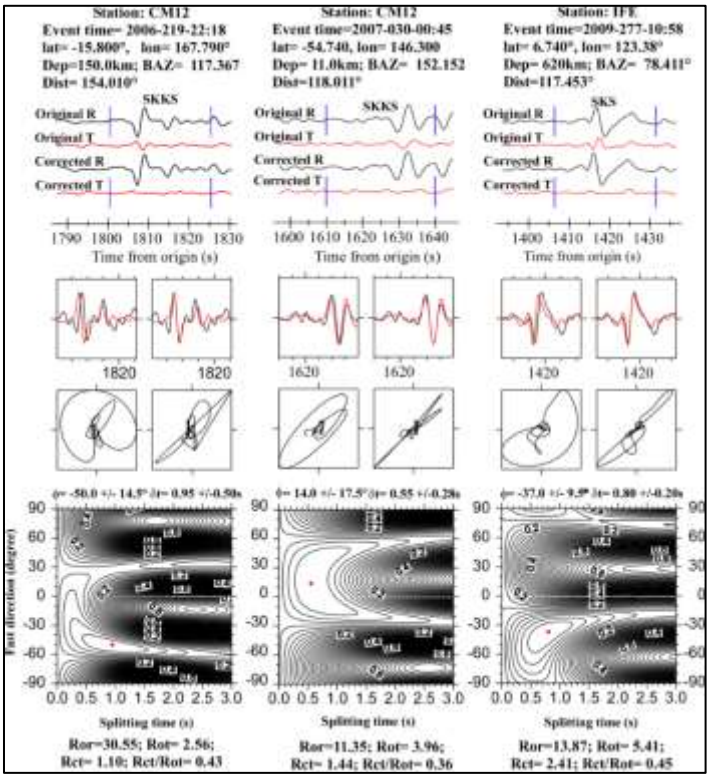

Figure 5. Example of original and corrected XKS radial and transverse components, their particle motion pattern, and the error functions.

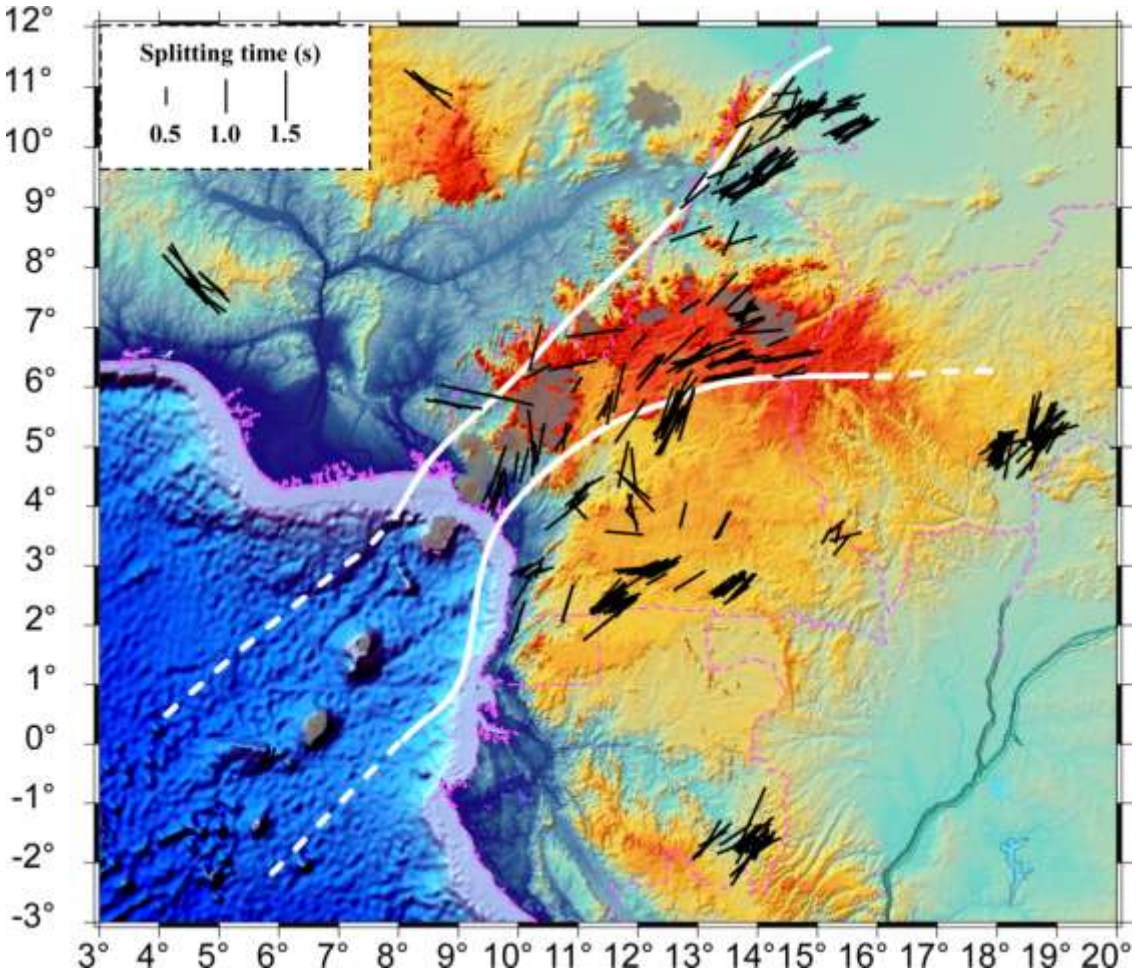

Figure 6. Resulting XKS splitting parameters plotted above ray-piercing points at the depth of 200 km (black bars). The color image in the background shows the topographic relief of the study area. The white lines represent the boundary of the low-velocity zone at the depth of 200 km [*Reusch et al., 2010*].

The mean fast direction in this area 44.4 ± 20°, and the mean splitting time is 0.91 ± 0.29 s. Area B lies on the northern edge of the Congo craton and includes stations CM07, 11, 12, 17, and YNDE, possessing 34 pairs of SWS measurements. The mean fast direction is 14 ±32°, and the mean splitting time is 1.31 ± 0.38 s. This area also includes stations CM08 and CM14, but data from these stations cannot be used for SWS analysis due to the lack of high-quality waveforms. Area C, the area along the Cameroon shoreline, consists of stations CM01 and 05 and contains 10 pairs of SWS measurements

with a mean fast direction of 44 ± 22° and a mean splitting time of 0.7 ± 0.2 s. Area D is the main part of the CVL and spans from southern Cameroon to the Chad border, and includes stations EKNA, CM09, 10, 13, 15, 16, and CM19-CM32 with 163 pairs of SWS measurements. Within Area D, we observed a mean fast direction of 52.8 ± 20.7°, which is parallel to the general strike of the CVL, and a mean splitting time of 1.0 ± 0.32 s. Area E consists of stations IFE, TORO, and CM18 (Figures 2 and 3). These stations are located in Nigeria and western Cameroon, wherein we observed a mean fast direction of -55.9 ±15.9° and a mean splitting time of 1.3 ± 0.39 s from 17 pairs of SWS measurements. The fast directions observed in Area E are mostly sub-parallel to the African coastline.

We then examined azimuthal variations of the observed splitting parameters, which are diagnostics of complex anisotropy [Silver and Savage, 1994]. None of the stations shows periodic variations, suggesting that a single layer of anisotropy with a horizontal axis of symmetry is sufficient to explain the observations. There is, however, piercing-point dependence of the splitting parameters. For instance, at CM12, two events with a BAZ of 117° and 152°, respectively, shows a fast direction of -50° and 14°, respectively (Figure 6), and nearly N-S fast directions were obtained from events with a BAZ of 26° and 66°, respectively. Similarly, at CM20, we observed fast directions of 15° and 62° for events with a BAZ of 28° and 81°, respectively. In general, measurements with ray-piercing points (at 200 km depth) beneath the CVL have a fast direction that is parallel to the CVL.

5.2. Comparison with previous results

To compare results from this study with station-averaged results of previous studies, we calculate the circular mean of the fast direction and the simple mean of the splitting times for each of the stations. The major difference between our and previous results is that our splitting times are about twice as large as those obtained by previous studies at almost all of the stations (Figure 7).

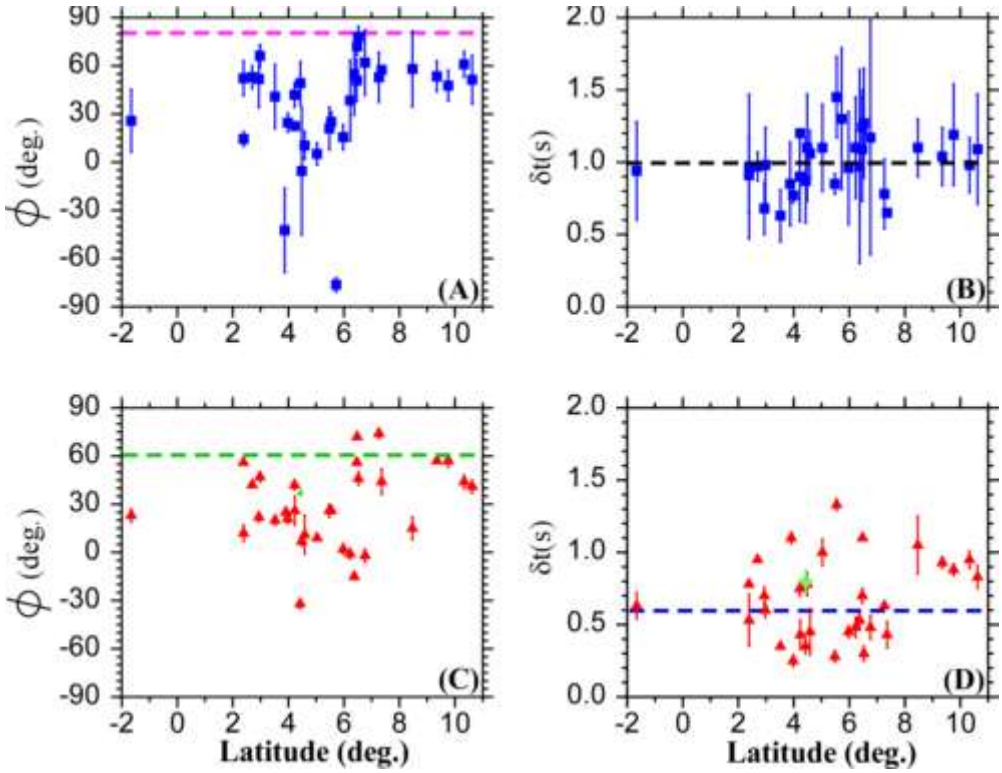

Figure 7. Comparison between our station-averaged measurements and those from previous studies. (A). Fast directions from this study plotted against the latitude. The dashed line shows the APM direction from the model of *Gripp and Gordon* [2012]. (B). Splitting times from this study plotted against the latitude. The dashed line represents the average splitting time. (C). Fast directions from Barruol and Ben Ismail [2001] (green diamond) and *Koch et al*. [2012] (red triangles) plotted against the latitude. The dashed line indicates the APM direction from the model of *Doubrovine et al.* [2012]. (D). Splitting times obtained by Barruol and Ben Ismail [2001] (green diamond) and *Koch et al.* [2012] (red triangles) plotted against the latitude. The dashed line shows the average splitting time observed by *Koch et al.* [2012].

In addition to the obvious differences in most of the splitting time measurements between this and previous studies (Figure 7), there are several other notable discrepancies. The first is that we did not use data from stations CM08 and CM14 due to equipment failures. CM08 did not yield sufficient data for our SWS analysis, while the N-S component at CM14 was not working [*Tokam et al., 2010; Gallacher and Bastow, 2012*], resulting in a nearly linear particle motion pattern [*Liu and Gao, 2013*]. Using data from this station, *Koch et al.* [2012] obtained a fast direction of 25° and a splitting time of 1.1 s at station CM08. At CM14, they obtained a fast direction of -32° and a splitting time of 0.35 s.

The second disagreement is that *Koch et al.* [2012] obtained null results at stations CM07 and CM18, but this study observed a mean fast direction of -42.3° and a mean splitting time of 0.9± 0.30 s at station CM07, and a fast direction of -76.2° and a splitting time of 1.3 ± 0.5 s at CM18. Third, at station CM20, we obtained a fast direction of 38° and a splitting time of 1.1 s while *Koch et al.* [2012] reported a fast direction of -1° and a splitting time of 0.48 s. Also, at station CM23, we observed a fast direction of 54.9° and a splitting time of 0.9 s while *Koch et al.* [2012] obtained a fast direction of -15° and a splitting time of 0.53 s. These discrepancies were mostly caused by the differences in the standards for data selection and result ranking, and the techniques used to obtain the results.

6. Discussion

In the cratonic environment, seismic anisotropy detectable by XKS splitting occurs either by LPO of crystallographic axes of anisotropic minerals (mainly olivine)

developed under axis compression and simple shear, or shape-preferred orientation (SPO) formed by preferably aligned vertical magmatic dikes. The former can either be resulted from shortening of the lithosphere or from flow in the asthenosphere, and the latter is mostly found in areas undergone extension [e.g., *Nicolas and Christensen, 1987; Silver, 1996; Gao et al., 1997, 2010; Savage, 1999; Vauchez et al., 2000; Fouch and Rondenay, 2006; Nowacki et al., 2010; Refayee et al., 2013*]. In the following, we discuss each of the possibilities in light of the observed anisotropy and propose a model that explains both the SWS observations and the formation and evolution of the CVL.

6.1. Fossil anisotropy due to Precambrian collisional events

Many previous studies attributed observed anisotropy to lithospheric fabrics created by the last significant collisional tectonic events [e.g., *Silver and Chan, 1991; Babuska and Plomerova, 1989; James and Assumpcao, 1996; McNamara et al., 1994; Silver, 1996; Fouch et al., 2004; Fouch and Rondenay, 2006; Bastow et al., 2011*].

The observed anisotropy on the Kaapvaal and Zimbabwe cratons as well as on the Limpopo belt sandwiched between the cratons was considered as mostly the result of lithospheric fabrics [e.g., Silver et al., 2001; Barruol and Ben Ismail, 2001; Fouch et al., 2004]. Most of the study area lies between the Congo and West Africa cratons which consist of several tectonic shields including the Bomu-Kibalian, Nigerian, Gabon-Cameroon, and Man-Leo Shields developed during the Precambrian [e.g., Begg et al., 2009] (Figures 2 and 3).

The N-S fast directions observed in the northern edge of the Congo craton (area B) might originate from Precambrian collision events. These converging events include the collision between the Gabon-Cameroon Shield and the Bomu-Kibalian Shield to form

the northern part of the Congo craton, and the collision between the Congo craton and the Oubanguides mobile belt [e.g., Castaing et al., 1994; Toteu et al., 2004; Begg et al., 2009]. This speculation is in agreement with Koch et al. [2012] who suggested that measurements from the northern edge of the Congo craton represent a fossil anisotropy resulted from Precambrian collisional events. However, most of our fast directions throughout the study area are aligned perpendicular to the suture zones (Figures 3 and 6), and consequently, fossil seismic anisotropy, which has remained in the cratonic lithosphere since the Precambrian, cannot account for the majority of splitting parameters observed in the study.

6.2. Mantle flow field associated with a mantle plume

Continental intraplate flood basalt development uplifts, and bathymetric swells in Africa were often attributed to one or more mantle plumes [e.g., *Morgan, 1972; Burke and Dewey, 1973; Nyblade and Robinson, 1994*]. Similarly, a mantle upwelling was proposed for the formation of the CVL [*Van Houten, 1983; Morgan, 1983; Lee et al., 1994; Ebinger and Sleep, 1998; Burke, 2001*]. *Burke* [2001] suggested that a mantle plume, which is located at latitude 7° N and longitude 11.5° E (Figure 3), could be responsible for the development of the CVL. Due to the upwelling of the plume material and the relative movement between the lithosphere and the asthenosphere, a parabolic flow pattern is expected in the vicinity of the plume, as observed in Hawaii and west-central Europe [*Walker et al., 2001, 2005*]. Such a parabolic pattern is not observed (Figure 6). Directly above a mantle plume, laboratory experiments suggest a complicated pattern of splitting parameters and small splitting times in the case of A-type olivine fabrics [*Karato et al., 2008; Druken et al., 2013*], which is not observed either.

Therefore, our SWS results do not support an active plume beneath the CVL. This conclusion is consistent with the observation that the 3He/4He ratios measured on basaltic rocks along the CVL are lower than those observed at typical hotspots such as Loihi and Iceland [*Aka et al., 2004*]. In addition, if a mantle plume was responsible for the formation of the CVL, the melt generation, as reflected by the expected higher-than-normal crustal Vp/Vs, should be much higher than what was observed beneath the CVL [*Gallacher and Bastow, 2012*]. Thus, the mantle potential temperature beneath the CVL is significantly lower than that observed in Afar, Iceland, and other typical mantle plumes [Gallacher and Bastow, 2012]. Body-wave seismic velocities observed beneath the CVL are also higher than those observed beneath the Ethiopia rift [*Stuart et al., 1985; Bastow and Keir, 2011; Gallacher and Bastow, 2012*]. The absence of a deep mantle plume is also suggested by a nearly normal transition zone thickness (251 ± 10 km) observed beneath the CVL [*Reusch et al., 2011*].

6.3. Edge-driven convective flow

Geodynamic modeling suggests that variations in lithospheric thickness create a lateral contrast in temperature and viscosity near the top of the mantle, and the contrast may induce a small-scale convective mantle flow beneath the cratonic margin and could lead to uplifting, rifting, and formation of flood basalts [e.g., *Anderson, 1994, 2001; King and Anderson, 1995, 1998; King and Ritsema, 2000; King, 2007*].

The CVL is flanked by the Congo craton to the south and an area with thinner lithosphere to the north (Figure 3), and thus is a preferable location for EDC with a flow direction that is approximately perpendicular to the CVL. Several studies [*King and Ritsema, 2000; Reusch et al., 2010; Koch et al., 2012; Milelli et al., 2012*] argued that

this small-scale convection system is responsible for the formation of the CVL. This model can explain the lack of age progression along the CVL. However, the anticipated fast directions associated with the proposed EDC should mostly be NW-SE, which is almost orthogonal to the observed fast directions which are dominantly NE-SW along the northern edge of the craton and in the CVL (Figure 6).

Another possible locale for EDC is the boundary between the Congo craton and the Atlantic Ocean basin, with a nearly E-W flow direction [Reusch et al., 2010; Koch et al., 2012; Milelli et al., 2012]. This EDC system if exists, should produce a volcanic line in the Atlantic Ocean that is parallel to the western edge of the Congo craton, with an N-S strike, which is not observed. Thus EDC cannot be responsible for the continental or the oceanic section of the CVL.

6.4. APM induced anisotropy

Numerous studies have suggested that simple shear at the base of the plate can lead to LPO oriented in the direction of shear [e.g., *Zhang and Karato, 1995; Tommasi et al., 1996; Tommasi, 1998; Walker et al., 2004; Liu, 2009*]. As a result, a model that involves asthenospheric flow induced by a moving plate is used to account for anisotropy with fast directions that are parallel to the APM [e.g., *Vinnik et al., 1989; Walker et al., 2004; Marone and Romanowicz, 2007; Liu, 2009*]. The APM for the African plate is small, which is partially responsible for the poorly constrained plate motion directions [e.g., *Walker et al., 2004; Barruol and Fontaine, 2013*]. The current APM direction of the study area based on the HS3-NUVEL1A hotspot model [*Gripp and Gordon, 2002*] is approximately toward the west (260°) (Figure 1), with a rate of 1.7 cm/yr. The majority of the observed fast directions in the vicinity of the CVL (Figures 1 and 6) are at a high

angle (> 30°) with the APM direction predicted by the HS3-NUVEL1A model. The GMHRF model [*Doubrovine et al., 2012*] predicts that the present-day motion of Africa is ENE (68°) at a rate of 1.3 cm/yr (Figure 1). The spatially varying fast directions and the large angle between the fast directions and the APM direction from either of the models at central and southern Cameroon and in Nigeria (Figures 1 and 6) suggest that APM-induced fabrics beneath slow-moving plates such as Africa may not be a major contribution to the observed anisotropy.

6.5. Mantle flow in a lithospheric channel

The dominantly CVL-parallel fast directions can be explained by NE-ward (relative to the lithosphere) mantle flow along a lithospheric channel beneath the CVL (Figure 8A). Recent mantle flow models suggest that the lithosphere in the study areas is underlain by a NE (relative to the lithosphere) directed flow [*Conrad and Behn, 2010; Forte et al., 2010*]. *Forte et al.* [2010] studied the mantle flow field at the depth of 250 km using the joint inversion of mantle rheological structure and density perturbations. Forte et al. [2010] suggested that the asthenosphere is moving toward the NE with a velocity of 5.0 cm/yr beneath the CVL and the neighboring regions (Figure 1). In addition, most seismic tomographic studies of the upper mantle clearly show the existence of low-velocity anomalies beneath the CVL relative to the bordering cratons/shields [e.g., *King and Ritsema, 2000; Reusch et al., 2010*]. *Reusch et al.* [2010] used data recorded by the CBSE network to study the upper mantle structure beneath the CVL. They found a tabular, low-velocity anomaly underlying both the continental and oceanic sections of the CVL with a depth that extends to ~300 km (Figure 6).

We propose that the flow is driven by the SW movements of the lithosphere relative to the asthenosphere, and the direction of the flow is modulated by the geometry of the channel (Figure 8), resulting in fast directions that are dominantly parallel to the CVL for measurements with ray-piercing points beneath the CVL. Under this model, stations adjacent to the CVL but with non-CVL-parallel fast directions such as CM20 (Figure 2) and those in Area B (Figure 3) could be interpreted as being located near the northern and southern boundaries, respectively, of the lithospheric channel (Figure 6). Additionally, the coast-parallel fast directions observed at stations on the Nigerian shield could be explained as reflecting the flow deflected by the keel of the African continent. Such a deflection was suggested beneath the western [*Refayee et al., 2013*] and southern [*Fouch et al., 2000; Gao et al., 2008*] edges of the North American craton.

6.6. Implications on the formation of the CVL

As detailed above, in spite of numerous geochemical, geophysical, and geodynamic investigations, the formation of the CVL remains enigmatic. The lack of a clear age progression of the volcanoes in the CVL and the isotopic signatures ruled out a plume origin of both the continental and oceanic sections of the CVL. Edge-driven small-scale mantle convection cannot explain the orientation of the CVL or the formation of its oceanic section. Viable hypotheses for its formation should be able to explain the linearity, orientation, location, lack of age progression, and possibly its upper-mantle origin (as indicated by isotopic studies) of the volcanic line. In this section, we propose a hypothesis for the formation of the CVL that can explain most, if not all, of previous observations as well as our new shear-wave splitting measurements.

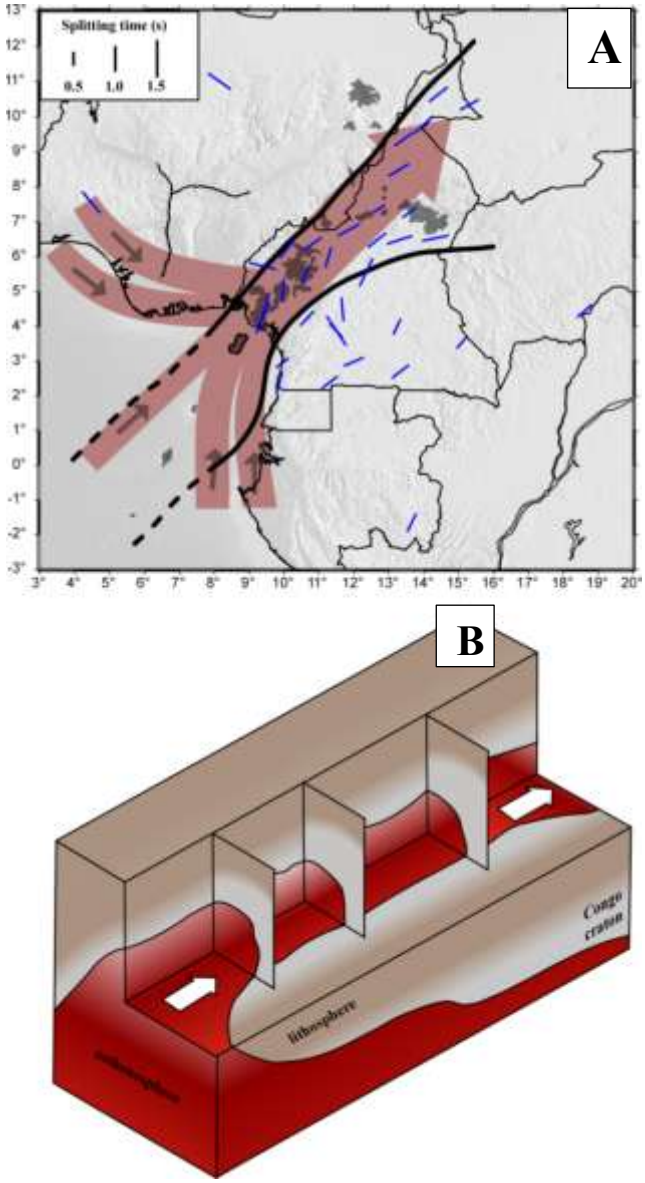

Figure 8. (A) Map view of the study area showing station-averaged XKS splitting parameters (blue bars), and proposed mantle flow lines (brown bands with arrows). (B) Schematic 3-D view of the land portion of the model.

This hypothesis is based on recent geodynamic modeling results suggesting the possibility of thermal-mechanical erosion of the base of the lithosphere by concentrated asthenospheric flow [*Davies, 1994; Ribe and Christensen, 1994; Sleep, 1994; Artemieva and Mooney, 2002; Conrad et al., 2011*]. We propose that the CVL was developed by

gradual basal erosion of the underlying lithosphere, along a line with the maximum flow intensity originated from the 90° sharp change in the orientation of the western margin of central Africa, from E-W north of the CVL to N-S south of the CVL (Figure 2).

This hypothesis can explain one of the puzzling features of the CVL, i.e., it intercepts the African coastline exactly at the joint point between the E-W and N-S segments of the coastline, and forms a nearly 45° angle with both segments (Figure 8). We suggest that the 90° turn of the continental margin creates a perfect locale for the concentration of mantle flow that originates from the SW-ward movement (relative to the asthenosphere) of the African lithosphere and is deflected by the cratonic keel (Figure 8A). Such a relative movement is suggested by geodynamic modeling [*Forte et al., 2010*] (Figure 1). Beneath the Atlantic Ocean, the flow concentration extends toward the SW with a gradually decreasing intensity and produces the oceanic section of the CVL. This interpretation is consistent with the SW-ward decrease of the size of the volcanoes on the ocean floor (Figure 8A). It is also consistent with the suggestion that there is a low-velocity zone beneath the Prinncipe Island [*Meyers et al., 1998*] and beneath the rest of the oceanic section of the CVL [*Reusch et al., 2010*].

This model suggests that the source of magma is at the base of the thinned lithosphere which is consistent with isotopic observations [e.g., *Aka et al., 2004*]. According to this hypothesis, the lack of age progression of the eruptions can be explained by the fact that volcanic eruptions took place in areas with the maximum lithospheric thinning, which is controlled by pre-existing zones of weakness and the distribution of mechanical strength in the lithosphere.

7. Conclusions

The CVL and the adjacent areas are tectonically complex regions which includes cratons, mobile belts, and shear zones, and active magmatism. Our SWS results suggest that the anisotropy beneath the CVL and surrounding areas is mostly located in the asthenosphere, although fossilized anisotropy in the northern part of the Congo craton cannot be ruled out. Spatial distribution of the splitting parameters in the study area does not support the small-scale mantle convection hypothesis nor the mantle plume and APM models as a cause for the observed anisotropy. We suggest that the predominant NE oriented anisotropy beneath the CVL is from a NE-ward (relative to the lithosphere) mantle flow along a lithospheric channel beneath the CVL. This channel is developed due to the differential movement of the African plate relative to the underlying asthenosphere as suggested by several geodynamic modeling studies. The model attributes coast-parallel fast directions north of the CVL to mantle flow deflected by the edge of the Africa continent keel. We suggest that the flood basalts along the CVL were formed by gradual basal erosion of the lithosphere, as a result of concentration of mantle flow associated with the sharp change in the orientation of the continental margin of western Africa. Additional shear-wave splitting and other measurements in the coastal areas and on the ocean floor in the vicinity of the CVL should be able to test and refine the proposed hypothesis.

II. SEISMIC ANISOTROPY AND SUBDUCTION-INDUCED MANTLE FABRICS BENEATH THE ARABIAN AND NUBIAN PLATES ADJACENT TO THE RED SEA

Abstract

For most continental areas, the mechanisms leading to mantle fabrics responsible for the observed anisotropy remain ambiguous, partially due to the lack of sufficient spatial coverage of reliable seismological observations. Here we report the first joint analysis of shear-wave splitting measurements obtained at stations on the Arabian and Nubian plates adjacent to the Red Sea. More than 1100 pairs of high-quality splitting parameters show dominantly N-S fast orientations at all 47 stations and larger-than-normal splitting times beneath the Afro-Arabian Dome (AAD). The uniformly N-S fast orientations and large splitting times up to 1.5 s are inconsistent with significant contributions from the lithosphere, which is about 50-80 km thick beneath the AAD and even thinner beneath the Red Sea. The results can best be explained by simple shear between the lithosphere and the asthenosphere associated with northward subduction of the African/Arabian plates over the past 150 Ma.

1. Introduction

In spite of numerous shear-wave splitting (SWS) studies, the mechanisms leading to observed seismic anisotropy in a given study area are usually ambiguous, and reliable interpretation of SWS measurements requires understanding tectonic history, mantle structure, plate motions, and results of geodynamic modeling of mantle flow. It is not clear whether anisotropy reflects a fossil lithospheric fabric or asthenospheric flow. The

region around the Red Sea is well-suited for examining what are the important controls, because this is a region with well-characterized plate motions, mantle plume effects, a nascent ocean basin, and deformed lithosphere. These competing effects have been evaluated using data from Arabia [e.g., *Wolfe et al., 1999; Hansen et al., 2006*] but without constraints from NE Africa, especially Egypt. The recent availability of broadband seismic data from Egypt (Figure 1) provides a new opportunity to investigate mantle dynamics and anisotropy-forming mechanisms.

The study area includes most of the Arabian plate and the NE part of the Nubian plate. The Red Sea and the Afro-Arabian Dome [AAD; *Camp and Roobol, 1992*] occupy the central part of the study area, and the Arabian-Nubian Shield (ANS) comprises the core of the AAD (Figure 1). The basement fabrics of Arabia and northern Nubia formed as a single lithospheric tract in Neoproterozoic time associated with accretion of juvenile arcs and back arc basins to form the ANS at ~900-630 Ma followed by collision of E and W Gondwana about 630-600 Ma, through mostly east-west convergence. In the study area (Figure 1), the dominant strike of basement structures including that of the suture zones ranges from NE-SW to NW-SE and is mostly N-S on the ANS but is largely unknown beneath Egypt due to limited exposure [*Berhe, 1990; Stern and Johnson, 2010*]. The crust of Africa west of the Nile is thought to be reworked older crust of the Saharan metacraton [*Abdelsalam et al., 2002*], followed by orogenic collapse, delamination, and north-directed tectonic escape ~600-580 Ma [*Stoeser and Camp, 1985; Avigad and Gvirtzman, 2009; Stern and Johnson, 2010*]. Mantle fabrics formed by Neoproterozoic tectonics and magmatism were likely modified by opening of the Red Sea and the uplift of flanking regions beginning~30 Ma [*Bosworth et al., 2005; Lazar et al., 2012*].

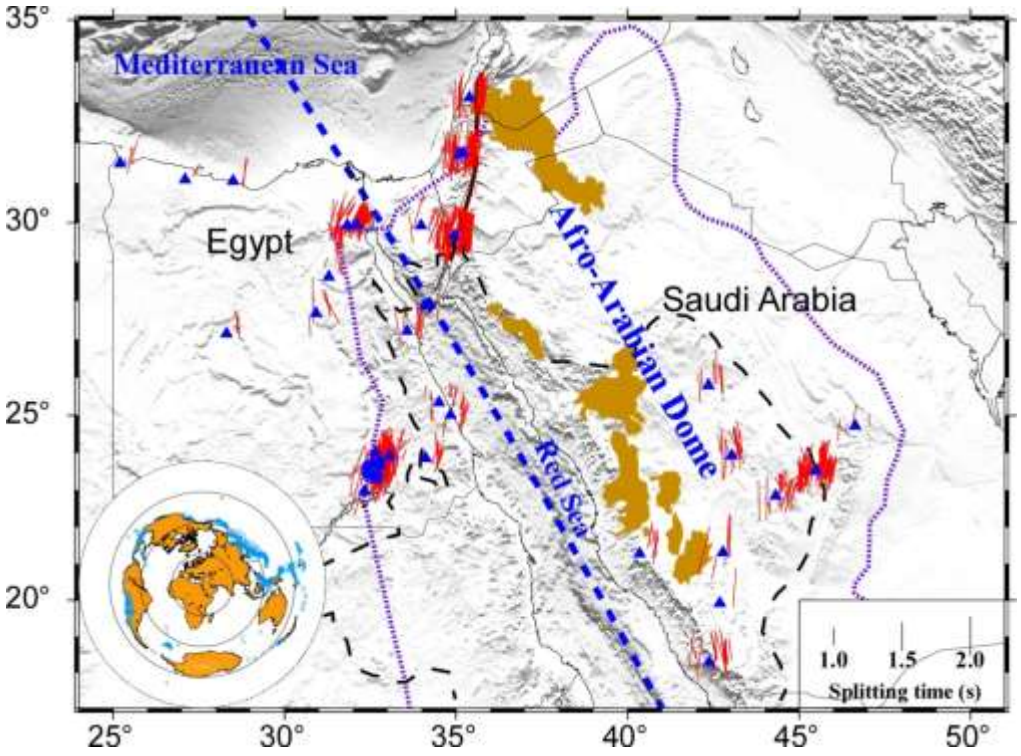

Figure 1. A topographic relief map of the study area showing the seismic stations (triangles) used in the study, and shear-wave splitting measurements (red bars) plotted above ray-piercing points at the depth of 200 km. The orientation of the bars represents the fast orientation, and the length of the bar indicates the splitting time. Brown color show areas covered by Cenozoic volcanic rocks. The dashed blue line is a great-circle arc approximately along the Red Sea axis, the dashed purple line outlines the northern part of Afro-Arabian Dome, and the dashed black line outlines the Arabian-Nubian Shield [*Camp and Roobol, 1992*]. The inset shows distribution of earthquakes (blue circles) used in the study.

We have some idea of how thick the lithosphere is beneath western Arabia but not NE Africa. *Hansen et al.* [2007] used S-wave receiver functions and GRACE gravity data and concluded that the lithosphere thickens from ~50-80 km near the coast and thickens to ~120 km beneath the eastern edge of the ANS (see Figures 5 and 6 in *Hansen et al.,* 2007), which is at a distance of about 500 km from the Red Sea.

The direction and strength of mantle flow beneath the Red Sea and adjacent Arabian and Nubian plates were investigated by a number of seismic anisotropy [*Wolfe et*

al., 1999; Levin and Park, 2000; Schmid et al., 2004; Hansen et al., 2006; Levin et al., 2006; Kaviani et al., 2011, 2013] and geodynamic modeling [*Conrad and Behn, 2010; Forte et al., 2010; Faccenna et al., 2013*] studies. Figure 2 shows results from the previous studies. Except for a few studies [*Wolfe et al., 1999; Hansen et al., 2006*], most previous SWS studies focused on the vicinity of the Dead Sea Transform Fault separating the Nubian and Arabian plates. Based on SWS measurements at 8 stations in southern Saudi Arabia, *Wolfe et al.* [1999] reported dominantly N-S fast orientations (measured clockwise from the North) with larger-than-normal splitting times. The models that they proposed include N-S trending lithospheric fabrics formed by E-W Neoproterozoic convergence, northward absolute plate motion (APM) of the Arabian plate, and northward asthenospheric flow from a mantle plume beneath Afar. *Hansen et al.* [2006] measured SWS parameters at about 20 stations in Arabia (Figure 2). Similar to *Wolfe et al.* [1999], they found dominantly N-S fast orientations and attributed the observed seismic anisotropy to a combined effect of two flow systems: a NE-ward flow from GPS-determined APM of the Arabian plate [*Reilinger et al., 1997*], and a NW-oriented flow along the strike of the Red Sea from the Afar plume.

Using SWS parameters and geodetic measurements as constraints, *Faccenna et al.* [2013] investigated mantle flow beneath Arabia and northern Nubia. The model that fits the observed seismic anisotropy in Arabia the best invokes slab-pull, upwelling from the lower mantle beneath southern Africa, and a N-S oriented zone of thinned lithosphere ("lithospheric channel") beneath the AAD that directs flow from a mantle plume beneath Afar. Other models proposed by *Faccenna et al.* [2013] use different assumptions about the relative roles of slab pull and mantle heterogeneities. Most of these models and others

from geodynamic modeling studies [*Forte et al., 2010; Conrad and Behn, 2010; Kreemer, 2009*] predicted that the flow direction beneath southern Arabia is more northeasterly than that beneath the northern part, due to the influence of radial flow from the Afar mantle flow to the south and the stronger influence of northward subduction in the north. In addition, most models predict that the flow direction beneath Arabia is more northeasterly than that beneath Nubia, due to the ENE-ward movement of Arabia relative to Nubia [*DeMets et al., 1994*]. Until now, the predictions for mantle flow beneath NE Africa could not be tested due to the unavailability of broadband seismic data for Egypt.

2. Data and Methods

The study uses three seismic phases: SKS which leaves the source as an S-wave, converts to a P-wave at the boundary between the mantle and the liquid outer core, and converts to an S-wave at the core-mantle boundary on the receiver side; SKKS which is similar to SKS but the P-wave bounces back to the outer core; and PKS which leaves the source and travels through the outer core as a P-wave and converts to an S-wave at the core-mantle-boundary. Hereafter the three phases are collectively called XKS. Data from stations located east of the Red Sea were obtained from the IRIS (Incorporated Research Institutions for Seismology) DMC (Data Management Center) for the recording period of early 1990 to middle 2013. The Egyptian National Seismic Network (ENSN) recorded the rest of the data for the period of late 2010 to the end of 2012. The epicentral distance used for PKS, 120 SKKS and SKS is 120°-180°, 95°-180°, and 84°-180°, respectively [*Liu and Gao, 2013*]. The splitting parameters were measured and ranked using the

procedure developed by *Liu* [2009] and *Liu and Gao* [2013] based on the transverse component energy minimization technique [*Silver and Chan, 1991*].

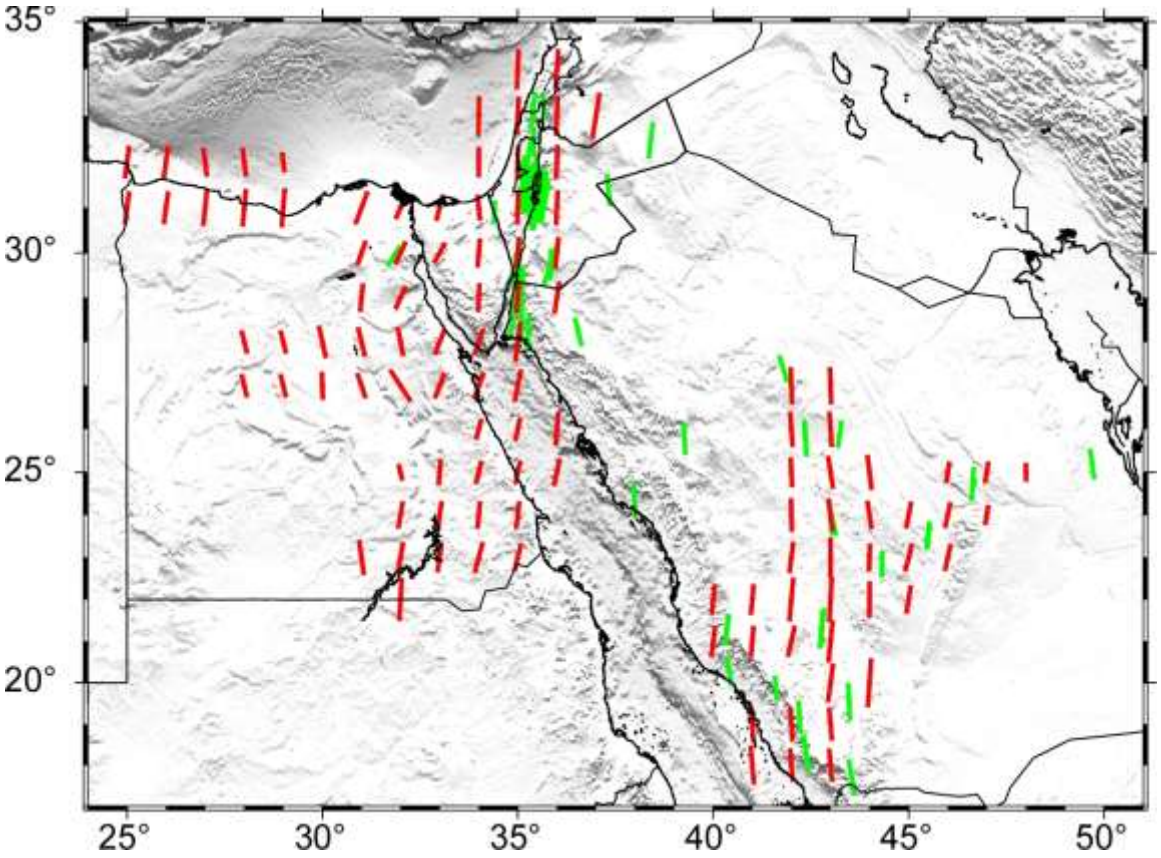

Figure 2. Spatially averaged shear-wave splitting parameters from this study (red bars). Green bars show station averaged splitting parameters from previous studies [*Wolfe et al., 1999; Levin and Park, 2000; Schmid et al., 2004; Hansen et al., 2006; Levin et al., 2006; Kaviani et al.,2011, 2013*]. Station averaged splitting parameters to the southeast of the gray dashed line are plotted in Figures 3D and 3E.

The seismograms were filtered in the frequency band of 0.04-0.5 Hz, and the XKS time window used to compute the splitting parameters starts at 5 s before and ends at 20 s after the predicted XKS arrival times. A manual check was applied to adjust the XKS window and to verify the automatic-ranking results to ensure that no high quality events were ignored and no low quality results were selected [*Liu and Gao, 2013*].

3. Results

A total of 1144 well-defined non-null SWS measurements are obtained at 47 stations (Figure 1). Null measurements are characterized by the lack of observable energy on the transverse component as a result of the backazimuth (BAZ) directions being either parallel or perpendicular to the fast orientation, or the medium traveled by the XKS phase is isotropic [e.g., *Silver and Chan, 1991*]. Two or more null events with non-parallel or orthogonal back-azimuths indicate the paucity of anisotropy. We observed clear splitting at all stations in the study area, and thus the null measurements are not used in the discussions below. In addition, we do not observe clear systematic variations of the splitting parameters as a function of back-azimuth, suggesting that a single layer of anisotropy with a horizontal axis of symmetry is adequate to represent the SWS measurements. To better visualize the measurements, we compute the coordinates of ray-piercing points at 150 km depth, and spatially average the SWS parameters in consecutive circles with a radius of 1°. The distance between the center of neighboring circles is 1°. The resulting spatial distribution of the measurements is shown in Figure 2, in which station-average measurements from previous studies are also plotted.

The station-averaged results are also displayed against the perpendicular distance to the Red Sea axis (Figure 3), for the purpose of identifying subtle spatial variations of the splitting parameters. The most remarkable feature of the measurements (Figures 2 and 3) is the almost consistently N-S fast orientations in the entire study area. This is especially true for the areas to the NE and SW of the Red Sea (Figure 3d). The splitting times are the largest (about 1.5 s) in the study area along the axial region of the AAD

(which is centered approximately along the 42° E longitudinal line), and decrease gradually toward the NE and SW.

4. Discussion

The uniform N-S fast orientations and the systematic spatial variation of the splitting times have several important implications on mantle flow models and on the formation mechanisms of seismic anisotropy beneath the study area.

1). The uniform N-S fast orientations, large splitting times observed in areas with thin lithosphere, and apparently spatially varying dominant orientations of basement fabrics [*Berhe, 1990; Stern and Johnson, 2010*] make it unlikely for the lithosphere to be the main source of the observed anisotropy. A lithosphere origin predicts that areas with thin lithosphere such as the area between the Red Sea and the axial area of the AAD [*Hansen et al., 2007; Chang and van der Lee, 2011*] should have small splitting times, not the observed large splitting times. To produce the 1.5 s splitting time observed on the AAD with a commonly-accepted mantle anisotropy of 4% [*Mainprice and Silver, 1993*], the required layer thickness is about 170 km, which is more than 2 times of the thickness of the lithosphere beneath the AAD [*Hansen et al., 2007*]. If we use the shear-wave anisotropy value of 2.64% measured from upper mantle kimberlite nodules acquired on the Kaapvaal craton [*Ben-Ismail et al., 2001*], the required thickness is as large as 255 km. Additionally, spatially varying fast orientations and reduction in splitting times are expected beneath the Sahara Metacraton due to disturbance of the accretion related lithospheric fabrics by the tectonic reactivation events and lithospheric delamination. Such expected changes are not observed. Because fabric directions on a lithospheric scale

beneath the study area especially beneath Egypt are poorly known, our data cannot completely exclude contributions from the lithosphere to the N-S directed anisotropy.

2) Magmatic dikes parallel to the Red Sea contribute insignificantly to the observed anisotropy. The dikes should lead to Red Sea-parallel fast orientations and large splitting times in the Red Sea basin, neither of which is observed (Figure 2). The lack of a significant amount of dikes in the lithosphere is consistent with the notion that the Red Sea was the product of passive rifting, probably because of slab-pull along the subduction zones to the north and northeast [*Stern and Johnson, 2010*].

3) Neither the fast orientations nor the splitting times support the existence of a flow system along a lithospheric channel beneath the Red Sea. It has been proposed that such a channeled flow, when combined with the NE-ward APM of Arabia, could give rise to the N-S fast orientations observed on Arabia [*Hansen et al., 2006*]. In order to produce the N-S fast orientations on the AAD, the Red Sea parallel flow system must extend beyond the surface expression of the Red Sea, probably on both sides of it. If this is the case, one would expect that the fast orientations observed on the Egyptian side would be parallel to the strike of the Red Sea, due to a lack of a NE-directed APM-driven flow system. Additionally, if the two flow systems produce LPO at different depths, azimuthally varying splitting parameters are expected [*Silver and Savage, 1994*]. None of these predictions are consistent with the observed splitting parameters.

4) Anisotropy with a uniform N-S fast orientation observed beneath the AAD is unlikely the result of channeled flow beneath the AAD. The co-existence of N-S directed anisotropy and a zone of low-seismic velocity was proposed to be the result of mantle flow beneath the thinned AAD lithosphere [*Wolfe et al., 1999; Chang and van der Lee,*

2011]. The fact that N-S fast orientations are also observed outside the AAD in Egypt places doubts on this interpretation (unless the off-AAD N-S fast orientations are coincidental). In the absence of an existing model that can satisfactorily explain the spatial distribution of the SWS parameters, we search for other anisotropy-forming mechanisms in the study area that can lead to the observed distribution. Numerous studies demonstrated that relative to Eurasia, the African plate has been moving northward since at least 150 Ma, most probably driven by the subduction of the Neotethys oceanic slab [*Dercourt et al., 1986; Reilinger and McClusky, 2011*].

From 59 to 0 Ma, the African plate moved more than 1200 km toward Eurasia without significant changes in the direction of motion but with variable plate velocities [*McQuarrie et al., 2003; Reilinger and McClusky, 2011*]. From 59 to 25 Ma, the Nubia-Arabian plate moved northward at about 32 mm/yr. The rate for Nubia reduced by more than 50% since 25 Ma, probably due to the collision of Africa and Eurasia which increased resistance to subduction [*Jolivet and Faccenna, 2000*], or the rifting along the Red Sea which reduced the north-northeastward pull on Nubia from the Arabian section of the subducting Neotethys slab [*Reilinger and McClusky, 2011*]. Numerical [e.g., *Lithgow-Bertelloni and Richards, 1998; Conrad and Hager, 2001; Behn et al., 2004*] and laboratory [e.g., *Funiciello et al., 2006*] studies suggest the existence of subduction parallel LPO beneath the horizontal portion of subducting plates.

The LPO is induced by the relative movement between the partially coupled lithosphere and asthenosphere, as well as by trench rollback [*Conrad and Hager, 2001*]. We propose that the observed seismic anisotropy with N-S fast orientations in Arabia and northern Nubia represents mantle fabrics induced in the boundary layer by the long-term

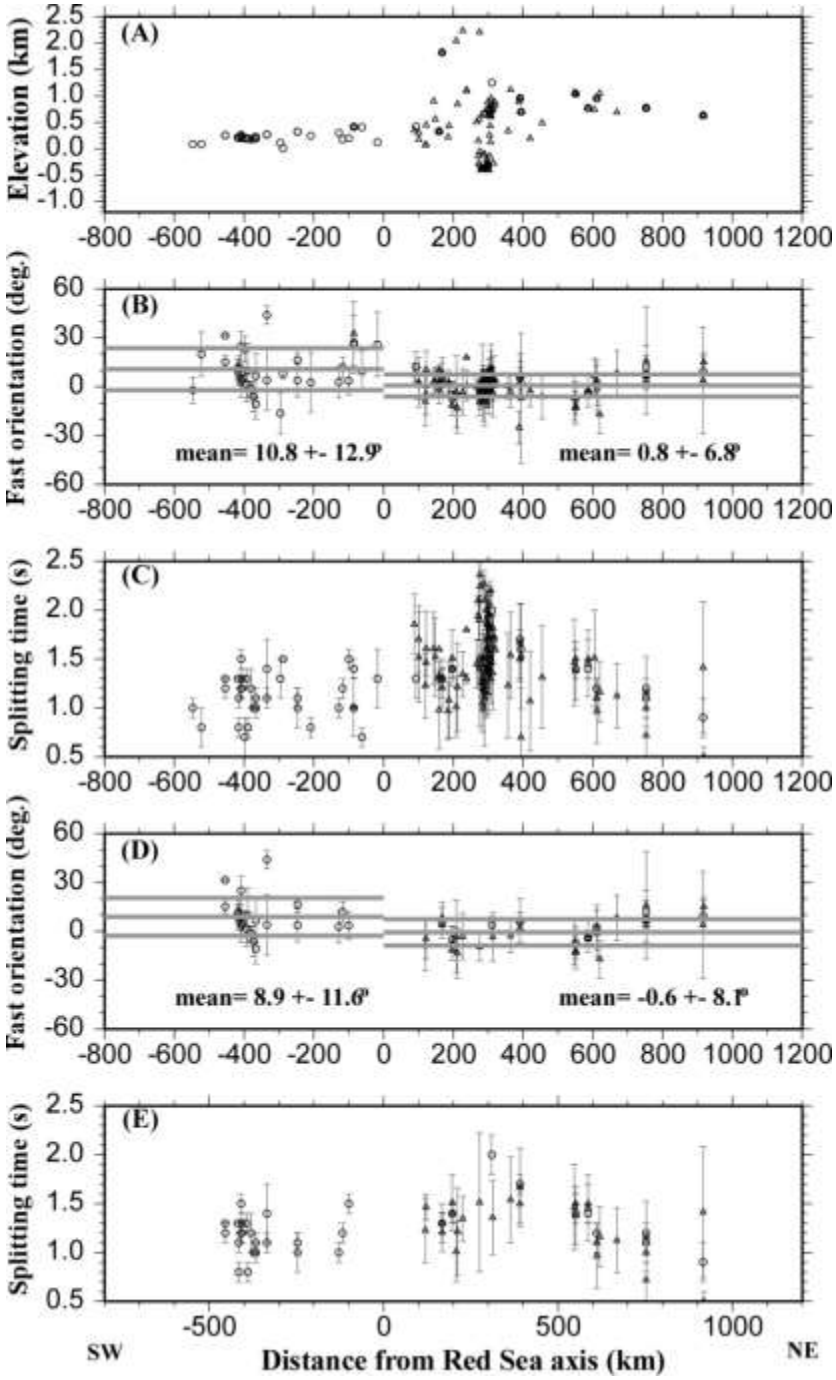

Figure 3. Cross-section views of surface elevation (A) and station-averaged shear-wave splitting parameters (B-E). (B) and (C) are fast orientations and splitting times, respectively, of all the measurements, and (D) and (E) are measurements beyond the Red Sea, located in the area to the southeast of the Red-Sea-perpendicular line in Figure 2. Circles represent data from this study, and triangles from previous studies shown in the previous figure. The horizontal lines in (B) and (D) show the mean (central lines) and mean plus/minus the standard deviation.

northward subduction of the African (before 24 Ma) and Nubian and Arabian plates (after 24 Ma) beneath Eurasia. Under this model, the large splitting times observed beneath the axial area of the AAD can be explained by concentration of LPO associated with lithospheric thinning. Such thinning was suggested from numerous seismic tomography studies [e.g., *Chang and van der Lee, 2011*]. The fact that the fast orientations are almost perfectly parallel to the direction of subduction implies that beneath the study area, subduction- induced LPO is much stronger than that produced by other processes, such as westward drift of the Earth's lithosphere [*Doglioni et al., 2007*], and the opening of the Red Sea, which would lead to a more northeasterly fast orientation on Arabia.

5. Conclusions

For the first time, shear-wave splitting parameters are measured on both the Nubian and Arabian plates adjacent to the Red Sea. Consistently N-S fast orientations are observed at virtually all the 47 stations, which, when combined with the systematic spatial variation of splitting times, are inconsistent with previously proposed anisotropy-forming models invoking lithospheric fabrics, radial flow from an active mantle plume beneath Afar, or channeled flow from Afar beneath the Red Sea or the Afro-Arabian Dome. Conversely, the observations can best be explained by olivine LPO developed at the boundary layer between the lithosphere and the asthenosphere induced by the northward movement of the African plate since at least 150 Ma.

SECTION

2. CONCLUSIONS

The CVL and the adjacent areas are tectonically complex regions, which includes cratons, mobile belts, shear zones, and active magmatism. Our SWS results suggest that the anisotropy beneath the CVL and surrounding areas is mostly located in the asthenosphere, although fossilized anisotropy in the northern part of the Congo craton cannot be ruled out. Spatial distribution of the splitting parameters in the study area does not support the small-scale mantle convection hypothesis nor the mantle plume and APM models as a cause for the observed anisotropy. We suggest that the predominant NE oriented anisotropy beneath the CVL is from a NE-ward (relative to the lithosphere) mantle flow along a lithospheric channel beneath the CVL. This channel is developed due to the differential movement of the African plate relative to the underlying asthenosphere as suggested by several geodynamic modeling studies. The model attributes coast-parallel fast directions north of the CVL to mantle flow deflected by the edge of the Africa continent keel. We suggest that the flood basalts along the CVL were formed by gradual basal erosion of the lithosphere, as a result of concentration of mantle flow associated with the sharp change in the orientation of the continental margin of western Africa. Additional shear-wave splitting and other measurements in the coastal areas and on the ocean floor in the vicinity of the CVL should be able to test and refine the proposed hypothesis.

For the first time, shear-wave splitting parameters are measured on both the Nubian and Arabian plates adjacent to the Red Sea. Consistently N-S fast orientations are observed at virtually all the 47 stations, which, when combined with the systematic spatial variation of splitting times, are inconsistent with previously proposed anisotropy-forming models invoking lithospheric fabrics, radial flow from an active mantle plume beneath Afar, or channeled flow from Afar beneath the Red Sea or the Afro-Arabian Dome. Conversely, the observations can best be explained by olivine LPO developed at the boundary layer between the lithosphere and the asthenosphere induced by the northward movement of the African plate since at least 150 Ma.

APPENDIX (A)

STATION LOCATIONS AND AVERAGED SPLITTING PARAMETERS RESULTS

Station	Lat.	Long.	Φ	STD Φ	δt	STD δt	Number of measurements
BGCA	5.18	18.42	25.85	19.53	0.95	0.04	73
CM01	2.39	9.83	14.50	4.51	0.98	0.38	2
CM02	2.70	13.29	53.04	7.05	0.98	0.02	17
CM03	3.52	15.03	40.94	19.93	0.63	0.09	5
CM04	2.98	11.96	66.23	7.05	0.99	0.06	18
CM05	2.94	9.91	51.89	17.69	0.69	0.06	8
CM06	2.38	11.27	52.32	10.84	0.91	0.04	43
CM07	3.87	11.46	-42.32	26.36	0.85	0.15	4
CM09	4.23	9.33	22.50	2.50	1.23	0.03	2
CM10	4.22	10.62	42.03	7.69	0.91	0.13	6
CM11	3.98	13.19	24.69	5.86	0.78	0.02	6
CM12	4.48	11.63	-5.42	39.88	1.13	0.15	6
CM13	4.59	9.46	10.50	8.78	1.06	0.07	5
CM15	5.03	9.93	5.22	6.99	1.10	0.15	5
CM16	5.48	10.57	21.00	13.23	0.85	0.05	2
CM17	5.55	12.31	25.24	6.00	1.46	0.07	16
CM18	5.72	9.35	-76.22	4.36	1.32	0.22	5
CM19	5.97	11.23	15.65	7.81	0.96	0.20	4
CM20	6.22	10.05	38.50	25.06	1.15	0.25	2
CM21	6.47	12.62	50.90	13.09	1.10	0.10	13
CM22	6.48	13.27	72.15	5.83	1.24	0.08	13
CM23	6.37	10.79	55.00	25.68	0.98	0.48	2
CM24	6.52	14.29	78.21	6.34	1.27	0.11	13
CM25	6.76	11.81	62.00	20.92	1.18	0.58	2
CM26	7.26	13.55	52.91	15.50	0.78	0.06	15
CM27	7.36	12.67	57.50	2.50	0.65	0.00	2
CM28	8.47	13.24	58.15	23.56	1.10	0.12	3
CM29	9.35	13.39	53.57	9.28	1.04	0.05	19
CM30	9.76	13.95	47.67	9.59	1.20	0.09	16
CM31	10.33	15.26	61.06	8.01	0.98	0.05	19
CM32	10.62	14.37	51.44	15.18	1.09	0.09	19
EKNA	4.23	9.33	19.00	5.00	1.50	0.28	1
IFE	7.55	4.46	-45.12	9.52	1.27	0.12	9
MSKU	-1.66	13.61	49.30	13.43	0.88	0.04	52
TORO	10.99	8.12	-54.95	7.10	1.32	0.27	3
YNDE	3.87	11.46	-33.50	0.50	1.70	0.25	2

AFIFxx_XI	23.93	43.04	172.956	10.019	1.369	0.076	18
AMDAxx_HL	22.97	32.33	15.192	4.093	1.156	0.071	16
BISHxx_XI	19.92	42.69	4	5	2	0.23	1
BGIOxx_GE	31.72	35.09	1.342	8.99	1.449	0.057	36
BRNSxx_HL	23.86	34.11	3.871	10.151	1.059	0.066	11
BRSxxx_HL	23.86	34.11	16.5	4.509	0.975	0.175	2
DB2xxx_HL	31.05	28.5	8	3.003	1.5	0.05	2
DRWAxx_HL	23.29	32.66	4.918	6.842	1.312	0.064	12
EILxxx_GE	29.67	34.95	5.062	8.164	1.271	0.017	288
FRFxxx_HL	27.15	28.31	178.034	7.933	1.01	0.139	5
GMRxxx_HL	23.52	32.41	7.301	7.995	1.115	0.053	24
GRWxxx_HL	23.67	32.79	173.842	9.199	1.016	0.048	25
HAGxxx_HL	29.95	32.1	9.548	12.586	0.675	0.083	4
HALMxx_XI	22.85	44.32	2.358	13.729	1.157	0.09	22
HRGxxx_HL	27.22	33.57	3.608	8.468	1.511	0.084	9
JERxxx_GE	31.77	35.2	1.618	7.047	1.362	0.033	87
KEGxxx_MN	29.93	31.83	25.822	17.666	1.021	0.023	159
KOTxxx_HL	29.93	31.83	26.998	2.946	1.4	0.1	3
KURxxx_HL	24	32.65	6.84	13.3	0.972	0.092	9
MADxxx_HL	22.97	32.33	31.5	0.5	1.275	0.025	2
MANxxx_HL	23.92	33.07	4.121	18.564	1.08	0.12	10
MATxxx_HL	31.09	27.1	23	8.053	0.7	0.15	2
MRNIxx_GE	33.12	35.39	2.474	6.002	1.631	0.05	36
MRSxxx_HL	25.01	34.84	12.028	6.174	1.188	0.103	8
NADBxx_HL	25.34	34.5	2.896	9.644	1.006	0.135	9
NAHDxx_HL	23.8	32.78	169.437	9.217	1.127	0.056	22
NBNSxx_HL	28.62	31.29	2.654	18.437	0.838	0.066	4
NGALxx_HL	23.42	32.73	1.471	10.832	1.317	0.057	15
NGMRxx_HL	23.52	32.41	12	7	0.8	0.1	1
NKLxxx_HL	29.93	33.98	12.258	9.076	1.269	0.183	8
NKRLxx_HL	23.66	32.72	178.748	4.61	1.212	0.225	4
NMANxx_HL	23.92	33.07	44	5.5	1.4	0.35	1
NNALxx_HL	23.29	32.66	8	4.5	1.2	0.12	1
NNMRxx_HL	23.74	32.56	9.856	16.9	0.787	0.095	12
NSKDxx_HL	23.66	32.39	23.293	12.763	1.164	0.069	18
NWKLxx_HL	23.41	32.45	10.801	6.146	1.257	0.041	23
RAYNxx_II	23.52	45.5	12.069	13.289	1.133	0.023	158
RAYNxx_XI	23.52	45.5	7.4	2.245	1.16	0.062	5
RIYDxx_XI	24.72	46.64	9.409	9.443	0.9	0.158	4
SH2xxx_HL	27.88	34.08	26	19.775	1.325	0.325	2
SLMxxx_HL	31.49	25.21	19.984	13.636	0.79	0.25	5
TAMRxx_HL	27.68	30.92	163.65	12.785	1.256	0.179	8
UOSSxx_II	24.95	56.2	153.553	10.281	1.019	0.024	120
UQSKxx_XI	25.79	42.36	176.142	1.884	1.45	0.058	7
WALxxx_HL	23.38	32.58	2.911	9.336	1.495	0.09	11
YAFxxx_YR	13.87	45.25	63.76	10.333	0.979	0.044	17

APPENDIX (B)

EVENTS AND PHASES FOR SPLITTING ANALYSIS

Station	Phase	Event time	Lat	Long	Phi	STD phi	δt	STD δt	BAZ	Event lat	Event long	Event depth	quality
AMDAxx_HL	SKS	EQ110411441	22.97	32.33	17	1.5	1.3	0.1	85.99	4.08	123.04	525	A
AMDAxx_HL	SKS	EQ112521941	22.97	32.33	11	13	0.9	0.4	346.12	49.53	-126.89	22	B
AMDAxx_HL	SKS	EQ112940802	22.97	32.33	12	6.5	1.3	0.3	42.78	43.89	142.48	187	B
AMDAxx_HL	SKS	EQ113180405	22.97	32.33	20	5.5	1.1	0.2	89.09	-0.95	126.91	17	B
AMDAxx_HL	SKS	EQ113531112	22.97	32.33	18	5.5	1.3	0.4	209.2	-55.99	-27.73	113	B
AMDAxx_HL	SKS	EQ120450622	22.97	32.33	16	5.5	1.1	0.2	49.86	36.21	141.39	28	B
AMDAxx_HL	SKS	EQ120931736	22.97	32.33	15	13	1.9	0.7	304.53	16.4	-98.32	9	B
AMDAxx_HL	SKS	EQ121571931	22.97	32.33	14	7	1.1	0.2	51.07	34.94	141.13	15	B
AMDAxx_HL	SKS	EQ121901133	22.97	32.33	12	11.5	0.9	0.3	38.01	45.5	151.29	20	B
AMDAxx_HL	SKS	EQ122270259	22.97	32.33	16	15	1.4	0.8	36.79	49.8	145.06	583.2	B
AMDAxx_HL	SKS	EQ122391505	22.97	32.33	17	6	1.4	0.2	86.24	2.19	126.84	91.1	B
AMDAxx_HL	SKS	EQ122970853	22.97	32.33	5	14	0.8	0.2	56.99	29.06	139.25	436	A
BRNSxx_HL	SKS	EQ112940802	23.86	34.11	177	15.5	0.9	0.3	43.46	43.89	142.48	187	B
BRNSxx_HL	SKS	EQ113180405	23.86	34.11	17	3.5	1.1	0.2	89.74	-0.95	126.91	17	B
BRNSxx_HL	SKS	EQ120921404	23.86	34.11	173	9.5	1.4	0.3	49.94	37.12	140.96	48	B
BRNSxx_HL	SKS	EQ121120116	23.86	34.11	10	5	1	0.2	87.36	-1.62	134.28	16	B
BRNSxx_HL	SKS	EQ121571931	23.86	34.11	175	9.5	0.9	0.2	51.77	34.94	141.13	15	B
BRNSxx_HL	SKS	EQ121670114	23.86	34.11	17	9.5	1.2	0.3	83.9	5.72	126.35	41.4	B
BRNSxx_HL	SKS	EQ122752221	23.86	34.11	177	8	0.9	0.1	46.77	39.81	143.1	15	A
BRNSxx_HL	SKS	EQ122970853	23.86	34.11	177	8.5	0.9	0.2	57.7	29.06	139.25	436	A
BRNSxx_HL	SKS	EQ123451653	23.86	34.11	14	2	1.5	0.2	93.69	-6.53	129.82	155	B
BRSxxx_HL	SKS	EQ103340324	23.86	34.11	12	11	0.8	0.2	58.35	28.35	139.19	470	B
DB2xxx_HL	SKS	EQ103340324	31.05	28.5	11	4	1.5	0.2	55.57	28.35	139.19	470	B
DB2xxx_HL	SKS	EQ110122132	31.05	28.5	5	3	1.5	0.1	56.3	26.97	139.88	512	B
DRWAxx_HL	SKS	EQ110122132	23.29	32.66	10	4.5	1.1	0.1	58.68	26.97	139.88	512	A
DRWAxx_HL	SKS	EQ110411441	23.29	32.66	14	10.5	1	0.3	86.13	4.08	123.04	525	B
DRWAxx_HL	SKS	EQ113281025	23.29	32.66	179	8.5	1.5	0.3	44.58	41.9	142.64	38	B
DRWAxx_HL	SKS	EQ120010527	23.29	32.66	8	9.5	1.3	0.3	55.47	31.46	138.07	365.3	B
DRWAxx_HL	SKS	EQ120211847	23.29	32.66	2	5	1.5	0.2	300.14	14.87	-93	45	B
DRWAxx_HL	SKS	EQ121571931	23.29	32.66	5	6	1.1	0.2	51.2	34.94	141.13	15	B
DRWAxx_HL	SKS	EQ121692032	23.29	32.66	178	9.5	1.4	0.3	47.47	38.92	141.83	36	B
DRWAxx_HL	SKS	EQ121901133	23.29	32.66	178	4	1.8	0.2	38.14	45.5	151.29	20	B
DRWAxx_HL	SKS	EQ122110920	23.29	32.66	173	8.5	1.4	0.3	41	47.38	139.07	502.3	B
DRWAxx_HL	SKS	EQ123451653	23.29	32.66	16	12	1	0.4	93.2	-6.53	129.82	155	B
FRFxxx_HL	SKS	EQ103340324	27.15	28.31	172	3	1.5	0.2	55.62	28.35	139.19	470	B
FRFxxx_HL	SKS	EQ110122132	27.15	28.31	8	5	0.9	0.1	56.42	26.97	139.88	512	A
FRFxxx_HL	SKS	EQ112940802	27.15	28.31	166	10	1	0.2	41.33	43.89	142.48	187	B
FRFxxx_HL	SKS	EQ120010527	27.15	28.31	2	5.5	0.9	0.1	53.56	31.46	138.07	365.3	B
FRFxxx_HL	SKS	EQ120450622	27.15	28.31	2	15.5	0.6	0.3	48.08	36.21	141.39	28	B
GMRxxx_HL	SKS	EQ103340324	23.52	32.41	12	7	0.8	0.1	57.65	28.35	139.19	470	A
GMRxxx_HL	SKS	EQ110122132	23.52	32.41	22	4	1	0.1	58.56	26.97	139.88	512	A
GMRxxx_HL	SKS	EQ112940802	23.52	32.41	179	7.5	0.9	0.2	42.83	43.89	142.48	187	B
GMRxxx_HL	SKS	EQ113180405	23.52	32.41	11	8	1.3	0.4	89.08	-0.95	126.91	17	B
GMRxxx_HL	SKS	EQ120010527	23.52	32.41	8	17.5	0.8	0.4	55.37	31.46	138.07	365.3	B
GMRxxx_HL	SKS	EQ120120320	23.52	32.41	3	11	0.9	0.2	49.34	36.99	141.07	16	B

GMRxxx_HL	SKS	EQ120450622	23.52	32.41	178	9	0.8	0.2	49.89	36.21	141.39	28	A
GMRxxx_HL	SKS	EQ121120116	23.52	32.41	16	5	1.2	0.2	86.73	-1.62	134.28	16	B
GMRxxx_HL	SKS	EQ121201028	23.52	32.41	6	9	0.9	0.2	50.84	35.6	140.35	44	B
GMRxxx_HL	SKS	EQ121571931	23.52	32.41	0	6	0.9	0.2	51.09	34.94	141.13	15	B
GMRxxx_HL	SKS	EQ121670114	23.52	32.41	8	3.5	1.4	0.2	83.22	5.72	126.35	41.4	B
GMRxxx_HL	SKS	EQ121901133	23.52	32.41	16	6	1.2	0.2	38.04	45.5	151.29	20	B
GMRxxx_HL	SKS	EQ122020610	23.52	32.41	10	9	1.1	0.3	33.02	49.41	155.91	19	B
GMRxxx_HL	SKS	EQ122110920	23.52	32.41	176	4.5	1	0.1	40.94	47.38	139.07	502.3	B
GMRxxx_HL	SKS	EQ122270259	23.52	32.41	7	8.5	1	0.2	36.84	49.8	145.06	583.2	A
GMRxxx_HL	SKS	EQ122311531	23.52	32.41	8	3	1.5	0.3	85.08	2.64	128.7	10	B
GMRxxx_HL	SKS	EQ122391505	23.52	32.41	8	2	1.5	0.2	86.24	2.19	126.84	91.1	B
GMRxxx_HL	SKS	EQ122970853	23.52	32.41	18	8	0.8	0.2	57	29.06	139.25	436	B
GMRxxx_HL	SKS	EQ123451653	23.52	32.41	17	2.5	1.1	0.2	93.07	-6.53	129.82	155	B
GRWxxx_HL	SKS	EQ103340324	23.67	32.79	174	14.5	0.8	0.2	57.8	28.35	139.19	470	B
GRWxxx_HL	SKS	EQ110010956	23.67	32.79	5	11	0.9	0.3	247.16	-26.8	-63.14	576.8	B
GRWxxx_HL	SKS	EQ110122132	23.67	32.79	0	14.5	0.8	0.2	58.71	26.97	139.88	512	A
GRWxxx_HL	SKS	EQ112521941	23.67	32.79	8	7	1	0.3	346.46	49.53	-126.89	22	B
GRWxxx_HL	SKS	EQ112940802	23.67	32.79	166	4.5	1.1	0.1	42.97	43.89	142.48	187	B
GRWxxx_HL	SKS	EQ113281025	23.67	32.79	169	11.5	1	0.2	44.64	41.9	142.64	38	B
GRWxxx_HL	SKS	EQ120010527	23.67	32.79	169	17	1	0.3	55.53	31.46	138.07	365.3	A
GRWxxx_HL	SKS	EQ120211847	23.67	32.79	7	7.5	1.8	0.4	300.37	14.87	-93	45	B
GRWxxx_HL	SKS	EQ120450622	23.67	32.79	168	5.5	1	0.2	50.04	36.21	141.39	28	A
GRWxxx_HL	SKS	EQ120921404	23.67	32.79	175	15.5	1.2	0.4	49.43	37.12	140.96	48	B
GRWxxx_HL	SKS	EQ121201028	23.67	32.79	162	9	1.1	0.4	50.99	35.6	140.35	44	B
GRWxxx_HL	SKS	EQ121410719	23.67	32.79	1	16	0.9	0.3	46.42	39.55	143.25	11	B
GRWxxx_HL	SKS	EQ121571931	23.67	32.79	173	7	0.8	0.1	51.24	34.94	141.13	15	B
GRWxxx_HL	SKS	EQ121760315	23.67	32.79	178	17	1	0.5	24.21	57.6	163.2	10	B
GRWxxx_HL	SKS	EQ121941251	23.67	32.79	168	15.5	0.9	0.3	38.07	45.45	151.66	12	B
GRWxxx_HL	SKS	EQ122020610	23.67	32.79	165	5	1.1	0.1	33.18	49.41	155.91	19	B
GRWxxx_HL	SKS	EQ122752221	23.67	32.79	178	5.5	0.9	0.1	46.26	39.81	143.1	15	B
GRWxxx_HL	SKS	EQ122970853	23.67	32.79	168	18.5	0.8	0.3	57.15	29.06	139.25	436	B
HAGxxx_HL	SKS	EQ103340324	29.95	32.1	4	8	0.6	0.1	57.41	28.35	139.19	470	B
HAGxxx_HL	SKS	EQ110010956	29.95	32.1	29	15	0.5	0.2	248.6	-26.8	-63.14	576.8	B
HAGxxx_HL	SKS	EQ110122132	29.95	32.1	11	5.5	0.6	0.1	58.2	26.97	139.88	512	A
HAGxxx_HL	SKS	EQ110450340	29.95	32.1	175	14.5	0.9	0.4	243.38	-35.38	-72.83	21	B
HRGxxx_HL	SKS	EQ103340324	27.22	33.57	12	2.5	1.5	0.1	58.09	28.35	139.19	470	B
HRGxxx_HL	SKS	EQ112521941	27.22	33.57	4	4.5	1.1	0.2	347.15	49.53	-126.89	22	B
HRGxxx_HL	SKS	EQ113112235	27.22	33.57	171	9	2	0.4	294.91	11.56	-85.86	177	B
HRGxxx_HL	SKS	EQ113180405	27.22	33.57	12	3.5	1.4	0.3	89.32	-0.95	126.91	17	B
HRGxxx_HL	SKS	EQ113281025	27.22	33.57	173	16	1.6	0.5	45.09	41.9	142.64	38	B
HRGxxx_HL	SKS	EQ120010527	27.22	33.57	10	3.5	1.5	0.1	55.92	31.46	138.07	365.3	B
HRGxxx_HL	SKS	EQ120450622	27.22	33.57	5	7.5	1.2	0.2	50.42	36.21	141.39	28	A
HRGxxx_HL	SKS	EQ120740908	27.22	33.57	173	8.5	1.8	0.3	44.99	40.89	144.94	12	B
HRGxxx_HL	SKS	EQ121410719	27.22	33.57	12	13.5	1.5	0.4	46.82	39.55	143.25	11	B
KOTxxx_HL	SKS	EQ103340324	29.93	31.83	31	4.5	1.6	0.2	57.28	28.35	139.19	470	B
KOTxxx_HL	SKS	EQ110122132	29.93	31.83	26	9	1.3	0.5	58.06	26.97	139.88	512	B

KOTxxx_HL	SKS	EQ120450622	29.93	31.83	24	7.5	1.3	0.3	49.76	36.21	141.39	28	B
KURxxx_HL	SKS	EQ103340324	24	32.65	172	7.5	1	0.3	57.73	28.35	139.19	470	B
KURxxx_HL	SKS	EQ120231604	24	32.65	16	15	1	0.3	239.79	-36.41	-73.03	20	B
KURxxx_HL	SKS	EQ120721232	24	32.65	13	16.5	1.1	0.4	39.84	45.24	147.61	110.4	B
KURxxx_HL	SKS	EQ121930231	24	32.65	22	3.5	1.5	0.3	38.15	45.4	151.42	10	B
KURxxx_HL	SKS	EQ121960430	24	32.65	177	15	1.1	0.4	38.1	45.52	151.32	10	B
KURxxx_HL	SKS	EQ122020610	24	32.65	179	7	0.8	0.1	33.12	49.41	155.91	19	B
KURxxx_HL	SKS	EQ122270259	24	32.65	4	10.5	0.7	0.2	36.95	49.8	145.06	583.2	B
MADxxx_HL	SKS	EQ103340324	22.97	32.33	31	6	1.2	0.2	57.64	28.35	139.19	470	B
MADxxx_HL	SKS	EQ110122132	22.97	32.33	32	5.5	1.3	0.2	58.56	26.97	139.88	512	B
MANxxx_HL	SKS	EQ110450340	23.92	33.07	5	11.5	1.4	0.3	240.91	-35.38	-72.83	21	B
MANxxx_HL	SKS	EQ120211847	23.92	33.07	4	6	1.5	0.3	300.64	14.87	-93	45	B
MANxxx_HL	SKS	EQ120220600	23.92	33.07	170	11	1.5	0.3	207.99	-56.65	-24.9	10	B
MANxxx_HL	SKS	EQ120241631	23.92	33.07	154	3.5	1	0.1	209.2	-56.34	-27.72	7.6	B
MANxxx_HL	SKS	EQ121571931	23.92	33.07	34	10	0.9	0.3	51.36	34.94	141.13	15	B
MANxxx_HL	SKS	EQ121901133	23.92	33.07	165	16	0.7	0.3	38.3	45.5	151.29	20	B
MANxxx_HL	SKS	EQ121941251	23.92	33.07	23	6.5	1.6	0.4	38.18	45.45	151.66	12	B
MANxxx_HL	SKS	EQ122391505	23.92	33.07	19	17.5	0.8	0.3	86.49	2.19	126.84	91.1	B
MATxxx_HL	SKS	EQ103340324	31.09	27.1	15	4	0.6	0.1	54.83	28.35	139.19	470	B
MATxxx_HL	SKS	EQ110122132	31.09	27.1	31	8	0.9	0.2	55.54	26.97	139.88	512	B
MRSxxx_HL	SKS	EQ103340324	25.01	34.84	9	6.5	1	0.2	58.64	28.35	139.19	470	B
MRSxxx_HL	SKS	EQ112940802	25.01	34.84	16	4.5	0.9	0.2	43.78	43.89	142.48	187	B
MRSxxx_HL	SKS	EQ120241631	25.01	34.84	9	10.5	1.1	0.3	209.84	-56.34	-27.72	7.6	B
MRSxxx_HL	SKS	EQ122860031	25.01	34.84	19	7	1.4	0.4	90.58	-4.89	134.03	13	B
MRSxxx_HL	SKS	EQ122970853	25.01	34.84	0	5.5	1.4	0.2	57.99	29.06	139.25	436	B
MRSxxx_HL	SKS	EQ123420818	25.01	34.84	8	15	0.8	0.2	48.4	37.89	143.95	31	B
MRSxxx_HL	SKS	EQ123451653	25.01	34.84	17	2.5	1.6	0.2	93.83	-6.53	129.82	155	B
NADBxx_HL	SKS	EQ113180405	25.34	34.5	12	2	1.7	0.3	89.83	-0.95	126.91	17	B
NADBxx_HL	SKS	EQ113281025	25.34	34.5	178	15	0.8	0.3	45.34	41.9	142.64	38	B
NADBxx_HL	SKS	EQ120231604	25.34	34.5	179	4	1.5	0.2	240.72	-36.41	-73.03	20	B
NADBxx_HL	SKS	EQ120241631	25.34	34.5	176	10	0.8	0.2	209.75	-56.34	-27.72	7.6	A
NADBxx_HL	SKS	EQ120450622	25.34	34.5	14	9.5	0.8	0.2	50.75	36.21	141.39	28	B
NADBxx_HL	SKS	EQ120931736	25.34	34.5	168	18	0.6	0.4	307.05	16.4	-98.32	9	B
NADBxx_HL	SKS	EQ121670114	25.34	34.5	15	4.5	1.5	0.3	84.07	5.72	126.35	41.4	B
NADBxx_HL	SKS	EQ122752221	25.34	34.5	173	15	0.8	0.2	46.97	39.81	143.1	15	B
NAHDxx_HL	SKS	EQ103340324	23.8	32.78	167	3	1.1	0.2	57.79	28.35	139.19	470	B
NAHDxx_HL	SKS	EQ110122132	23.8	32.78	167	13.5	1	0.4	58.7	26.97	139.88	512	B
NAHDxx_HL	SKS	EQ112940802	23.8	32.78	164	4.5	1	0.2	42.97	43.89	142.48	187	B
NAHDxx_HL	SKS	EQ120231604	23.8	32.78	4	18	0.6	0.2	239.73	-36.41	-73.03	20	B
NAHDxx_HL	SKS	EQ120450622	23.8	32.78	158	3.5	1.4	0.2	50.03	36.21	141.39	28	B
NAHDxx_HL	SKS	EQ120721232	23.8	32.78	163	10	1.2	0.3	39.89	45.24	147.61	110.4	B
NAHDxx_HL	SKS	EQ120740908	23.8	32.78	169	10.5	1.4	0.3	44.6	40.89	144.94	12	B
NAHDxx_HL	SKS	EQ120931736	23.8	32.78	17	10.5	1.6	0.6	305.19	16.4	-98.32	9	B
NAHDxx_HL	SKS	EQ121571931	23.8	32.78	174	5	1	0.2	51.24	34.94	141.13	15	B
NAHDxx_HL	SKS	EQ121901133	23.8	32.78	170	4	1.1	0.1	38.19	45.5	151.29	20	B
NAHDxx_HL	SKS	EQ121910720	23.8	32.78	165	10	0.9	0.2	36.71	49.21	147.26	558	B

NAHDxx_HL	SKS	EQ121930231	23.8	32.78	171	9	1.2	0.2	38.21	45.4	151.42	10	B
NAHDxx_HL	SKS	EQ122020610	23.8	32.78	171	4.5	0.9	0.1	33.17	49.41	155.91	19	B
NAHDxx_HL	SKS	EQ122270259	23.8	32.78	169	9	0.9	0.2	36.98	49.8	145.06	583.2	B
NAHDxx_HL	SKS	EQ122752221	23.8	32.78	159	7.5	1.1	0.3	46.25	39.81	143.1	15	B
NAHDxx_HL	SKS	EQ122970853	23.8	32.78	169	4.5	0.9	0.2	57.15	29.06	139.25	436	A
NBNSxx_HL	SKS	EQ103340324	28.62	31.29	160	7.5	0.9	0.3	57.02	28.35	139.19	470	B
NBNSxx_HL	SKS	EQ110122132	28.62	31.29	170	14.5	0.8	0.3	57.82	26.97	139.88	512	B
NBNSxx_HL	SKS	EQ112521941	28.62	31.29	20	16	0.7	0.3	345.78	49.53	-126.89	22	B
NBNSxx_HL	SKS	EQ120450622	28.62	31.29	20	16	0.9	0.4	49.46	36.21	141.39	28	B
NGALxx_HL	SKS	EQ121070217	23.42	32.73	20	7	1.5	0.4	92.75	-2.64	121.86	13	B
NGALxx_HL	SKS	EQ121201028	23.42	32.73	3	7.5	1.1	0.2	50.96	35.6	140.35	44	B
NGALxx_HL	SKS	EQ121692032	23.42	32.73	2	17	1.3	0.9	47.49	38.92	141.83	36	B
NGALxx_HL	SKS	EQ121901133	23.42	32.73	179	6.5	1.6	0.3	38.17	45.5	151.29	20	B
NGALxx_HL	SKS	EQ121930231	23.42	32.73	175	5	1.8	0.2	38.19	45.4	151.42	10	B
NGALxx_HL	SKS	EQ121941251	23.42	32.73	0	7	1.2	0.2	38.05	45.45	151.66	12	B
NGALxx_HL	SKS	EQ122020610	23.42	32.73	0	7	1.4	0.3	33.16	49.41	155.91	19	B
NGALxx_HL	SKS	EQ122270259	23.42	32.73	175	5.5	1.2	0.2	36.95	49.8	145.06	583.2	B
NGALxx_HL	SKS	EQ122311531	23.42	32.73	11	14	1.2	0.6	85.22	2.64	128.7	10	B
NGALxx_HL	SKS	EQ122391505	23.42	32.73	19	3.5	1.2	0.2	86.37	2.19	126.84	91.1	B
NGALxx_HL	SKS	EQ122752221	23.42	32.73	176	3.5	1.4	0.2	46.23	39.81	143.1	15	B
NGALxx_HL	SKS	EQ122970853	23.42	32.73	4	6.5	1	0.2	57.14	29.06	139.25	436	B
NGMRxx_HL	SKS	EQ103340324	23.52	32.41	12	7	0.8	0.1	57.65	28.35	139.19	470	A
NKLxxx_HL	SKS	EQ110010956	29.93	33.98	173	6.5	1.5	0.6	249.34	-26.8	-63.14	576.8	B
NKLxxx_HL	SKS	EQ110122132	29.93	33.98	18	7.5	1	0.2	59.13	26.97	139.88	512	B
NKLxxx_HL	SKS	EQ112521941	29.93	33.98	16	5	1.9	0.3	347.52	49.53	-126.89	22	B
NKLxxx_HL	SKS	EQ113180405	29.93	33.98	19	3.5	2	0.3	89.36	-0.95	126.91	17	B
NKLxxx_HL	SKS	EQ120450622	29.93	33.98	12	12.5	0.6	0.2	50.74	36.21	141.39	28	B
NKLxxx_HL	SKS	EQ121201028	29.93	33.98	5	16	0.8	0.3	51.72	35.6	140.35	44	B
NKRLxx_HL	SKS	EQ103340324	23.66	32.72	176	9	0.9	0.2	57.77	28.35	139.19	470	B
NKRLxx_HL	SKS	EQ110010956	23.66	32.72	173	5	1.5	0.3	247.14	-26.8	-63.14	576.8	B
NKRLxx_HL	SKS	EQ110122132	23.66	32.72	1	12.5	0.8	0.2	58.69	26.97	139.88	512	A
NKRLxx_HL	SKS	EQ110411441	23.66	32.72	5	1.5	1.6	0.3	86.16	4.08	123.04	525	B
NMANxx_HL	SKS	EQ103340324	23.92	33.07	44	5.5	1.4	0.3	57.91	28.35	139.19	470	B
NNALxx_HL	SKS	EQ103340324	23.29	32.66	8	4.5	1.2	0.1	57.76	28.35	139.19	470	A
NNMRxx_HL	SKS	EQ121120116	23.74	32.56	45	16.5	0.8	0.4	86.75	-1.62	134.28	16	B
NNMRxx_HL	SKS	EQ121571931	23.74	32.56	8	16.5	0.3	0.2	51.15	34.94	141.13	15	B
NNMRxx_HL	SKS	EQ121692032	23.74	32.56	165	14.5	0.5	0.2	47.43	38.92	141.83	36	B
NNMRxx_HL	SKS	EQ121901133	23.74	32.56	18	14.5	0.9	0.4	38.09	45.5	151.29	20	B
NNMRxx_HL	SKS	EQ122020610	23.74	32.56	6	8.5	0.8	0.2	33.08	49.41	155.91	19	B
NNMRxx_HL	SKS	EQ122110920	23.74	32.56	8	16	0.6	0.2	41	47.38	139.07	502.3	B
NNMRxx_HL	SKS	EQ122270259	23.74	32.56	5	9	0.6	0.1	36.9	49.8	145.06	583.2	B
NNMRxx_HL	SKS	EQ122391505	23.74	32.56	40	12	0.8	0.2	86.29	2.19	126.84	91.1	B
NSKDxx_HL	SKS	EQ103340324	23.66	32.39	37	8.5	1.2	0.3	57.63	28.35	139.19	470	B
NSKDxx_HL	SKS	EQ110010956	23.66	32.39	42	12	1.2	0.4	247.04	-26.8	-63.14	576.8	B
NSKDxx_HL	SKS	EQ110122132	23.66	32.39	37	2.5	1.6	0.2	58.54	26.97	139.88	512	B
NSKDxx_HL	SKS	EQ110411441	23.66	32.39	11	5	1.1	0.3	86.03	4.08	123.04	525	B

NSKDxx_HL	SKS	EQ112940802	23.66	32.39	16	4.5	0.9	0.2	42.83	43.89	142.48	187	A
NSKDxx_HL	SKS	EQ120141636	23.66	32.39	30	14	1	0.3	72.85	19.2	121.16	17	B
NSKDxx_HL	SKS	EQ120450622	23.66	32.39	26	6	1.2	0.3	49.88	36.21	141.39	28	B
NSKDxx_HL	SKS	EQ120931736	23.66	32.39	19	5.5	1.5	0.3	304.87	16.4	-98.32	9	B
NSKDxx_HL	SKS	EQ121120116	23.66	32.39	22	12	0.8	0.2	86.7	-1.62	134.28	16	B
NSKDxx_HL	SKS	EQ121571931	23.66	32.39	28	17	0.8	0.3	51.08	34.94	141.13	15	B
NSKDxx_HL	SKS	EQ121960430	23.66	32.39	17	13	1.3	0.8	38	45.52	151.32	10	B
NSKDxx_HL	SKS	EQ122110920	23.66	32.39	18	12	1	0.4	40.94	47.38	139.07	502.3	B
NSKDxx_HL	SKS	EQ122270259	23.66	32.39	20	2.5	1.3	0.2	36.84	49.8	145.06	583.2	B
NSKDxx_HL	SKS	EQ122391505	23.66	32.39	26	16.5	0.8	0.2	86.23	2.19	126.84	91.1	B
NSKDxx_HL	SKS	EQ122970853	23.66	32.39	39	9	1.2	0.6	56.99	29.06	139.25	436	B
NSKDxx_HL	SKS	EQ123451653	23.66	32.39	21	5.5	1	0.2	93.04	-6.53	129.82	155	B
NWKLxx_HL	SKS	EQ113180405	23.41	32.45	18	2	1.5	0.2	89.1	-0.95	126.91	17	B
NWKLxx_HL	SKS	EQ120010527	23.41	32.45	15	7	1	0.2	55.39	31.46	138.07	365.3	B
NWKLxx_HL	SKS	EQ120450622	23.41	32.45	6	5	1.2	0.2	49.9	36.21	141.39	28	B
NWKLxx_HL	SKS	EQ121120116	23.41	32.45	17	3.5	1.4	0.2	86.77	-1.62	134.28	16	B
NWKLxx_HL	SKS	EQ121410719	23.41	32.45	12	11.5	1	0.2	46.29	39.55	143.25	11	B
NWKLxx_HL	SKS	EQ121571931	23.41	32.45	14	6	1.1	0.2	51.11	34.94	141.13	15	B
NWKLxx_HL	SKS	EQ121670114	23.41	32.45	15	9	1	0.3	83.24	5.72	126.35	41.4	B
NWKLxx_HL	SKS	EQ121692032	23.41	32.45	7	4.5	1.2	0.2	47.38	38.92	141.83	36	B
NWKLxx_HL	SKS	EQ121901133	23.41	32.45	14	7.5	1.4	0.3	38.05	45.5	151.29	20	B
NWKLxx_HL	SKS	EQ121930231	23.41	32.45	13	6	1.2	0.2	38.07	45.4	151.42	10	B
NWKLxx_HL	SKS	EQ121941251	23.41	32.45	172	7	1.4	0.2	37.93	45.45	151.66	12	B
NWKLxx_HL	SKS	EQ122020610	23.41	32.45	10	2.5	1.4	0.1	33.04	49.41	155.91	19	B
NWKLxx_HL	SKS	EQ122110920	23.41	32.45	6	8.5	1.1	0.2	40.94	47.38	139.07	502.3	B
NWKLxx_HL	SKS	EQ122270259	23.41	32.45	6	6	1.2	0.2	36.85	49.8	145.06	583.2	B
NWKLxx_HL	SKS	EQ122311531	23.41	32.45	13	2	1.6	0.1	85.1	2.64	128.7	10	B
NWKLxx_HL	SKS	EQ122391505	23.41	32.45	11	3	1.5	0.2	86.26	2.19	126.84	91.1	B
NWKLxx_HL	SKS	EQ122970853	23.41	32.45	15	6	0.9	0.1	57.02	29.06	139.25	436	B
NWKLxx_HL	SKS	EQ123451653	23.41	32.45	16	4	1.3	0.3	93.1	-6.53	129.82	155	B
SH2xxx_HL	SKS	EQ113180405	27.88	34.08	7	3.5	1.6	0.5	89.52	-0.95	126.91	17	B
SLMxxx_HL	SKS	EQ110122132	31.49	25.21	18	9	0.8	0.2	54.47	26.97	139.88	512	A
SLMxxx_HL	SKS	EQ112940802	31.49	25.21	3	16.5	0.4	0.1	40.13	43.89	142.48	187	A
TAMRxx_HL	SKS	EQ103340324	27.68	30.92	170	12.5	0.9	0.3	56.85	28.35	139.19	470	B
TAMRxx_HL	SKS	EQ110122132	27.68	30.92	167	5	1.2	0.2	57.67	26.97	139.88	512	B
TAMRxx_HL	SKS	EQ112521941	27.68	30.92	179	2	2.3	0.3	345.5	49.53	-126.89	22	B
TAMRxx_HL	SKS	EQ112940802	27.68	30.92	169	15	1	0.3	42.44	43.89	142.48	187	B
TAMRxx_HL	SKS	EQ113281025	27.68	30.92	154	13.5	1.2	0.5	44.02	41.9	142.64	38	B
TAMRxx_HL	SKS	EQ120241631	27.68	30.92	178	17	1.1	0.4	208.65	-56.34	-27.72	7.6	A
WALxxx_HL	SKS	EQ113180405	23.38	32.58	9	1	2.1	0.2	89.16	-0.95	126.91	17	B
WALxxx_HL	SKS	EQ120931736	23.38	32.58	21	5	1.3	0.3	304.88	16.4	-98.32	9	B
WALxxx_HL	SKS	EQ121070217	23.38	32.58	12	3	2	0.6	92.7	-2.64	121.86	13	B
WALxxx_HL	SKS	EQ121571931	23.38	32.58	0	4	1.4	0.2	51.16	34.94	141.13	15	B
WALxxx_HL	SKS	EQ121901133	23.38	32.58	6	13	1.5	0.6	38.11	45.5	151.29	20	B
WALxxx_HL	SKS	EQ122020610	23.38	32.58	3	4.5	1.5	0.2	33.1	49.41	155.91	19	B
WALxxx_HL	SKS	EQ122110920	23.38	32.58	165	9	1.1	0.2	40.98	47.38	139.07	502.3	B

WALxxx_HL	SKS	EQ122270259	23.38	32.58	176	4.5	1.4	0.2	36.89	49.8	145.06	583.2	B
WALxxx_HL	SKS	EQ122752221	23.38	32.58	7	10.5	1.4	0.3	46.17	39.81	143.1	15	B
AMDAxx_HL	PKS	EQ120090407	22.97	32.33	24	10	0.9	0.2	82.84	-10.62	165.16	28	B
BRNSxx_HL	PKS	EQ120090407	23.86	34.11	15	7	0.9	0.2	82.92	-10.62	165.16	28	B
DRWAxx_HL	PKS	EQ120090407	23.29	32.66	11	10.5	1.2	0.4	82.7	-10.62	165.16	28	B
GRWxxx_HL	PKS	EQ120090407	23.67	32.79	17	13	0.6	0.2	82.42	-10.62	165.16	28	A
NAHDxx_HL	PKS	EQ120090407	23.8	32.78	1	5	1.5	0.5	82.3	-10.62	165.16	28	B
NKLxxx_HL	PKS	EQ120090407	29.93	33.98	10	8	0.9	0.2	77.62	-10.62	165.16	28	B
NWKLxx_HL	PKS	EQ120090407	23.41	32.45	13	5.5	1.8	0.3	82.49	-10.62	165.16	28	B
SLMxxx_HL	PKS	EQ120340346	31.49	25.21	18	17.5	0.6	0.2	76.78	-17.38	167.28	8	B
TAMRxx_HL	PKS	EQ120281745	27.68	30.92	144	13.5	0.6	0.2	100.73	-29.43	-177.17	10	B
AMDAxx_HL	SKK	EQ121571931	22.97	32.33	16	15	1.3	0.6	51.07	34.94	141.13	15	B
AMDAxx_HL	SKK	EQ121890335	22.97	32.33	13	7	1.2	0.3	81.69	-4.65	153.3	35	B
AMDAxx_HL	SKK	EQ121901133	22.97	32.33	17	13.5	0.7	0.2	38.01	45.5	151.29	20	B
BRNSxx_HL	SKK	EQ121142240	23.86	34.11	171	9.5	1	0.3	35	48.4	154.74	31	B
BRSxxx_HL	SKK	EQ110521057	23.86	34.11	21	2	1.1	0.2	101.59	-26.14	178.39	558.1	B
DRWAxx_HL	SKK	EQ121571931	23.29	32.66	5	8.5	1.3	0.3	51.2	34.94	141.13	15	B
GMRxxx_HL	SKK	EQ120231604	23.52	32.41	8	4.5	1.7	0.2	239.54	-36.41	-73.03	20	B
GMRxxx_HL	SKK	EQ121571931	23.52	32.41	176	14.5	1.1	0.4	51.09	34.94	141.13	15	B
GMRxxx_HL	SKK	EQ121901133	23.52	32.41	9	5.5	1.1	0.2	38.04	45.5	151.29	20	B
GMRxxx_HL	SKK	EQ122020610	23.52	32.41	11	8.5	1.1	0.3	33.02	49.41	155.91	19	B
GRWxxx_HL	SKK	EQ120450622	23.67	32.79	163	16.5	1	0.5	50.04	36.21	141.39	28	B
GRWxxx_HL	SKK	EQ121142240	23.67	32.79	172	5	0.9	0.1	34.45	48.4	154.74	31	B
GRWxxx_HL	SKK	EQ121571931	23.67	32.79	163	6	1	0.2	51.24	34.94	141.13	15	B
GRWxxx_HL	SKK	EQ121890335	23.67	32.79	7	11	1.4	0.5	81.51	-4.65	153.3	35	B
GRWxxx_HL	SKK	EQ121901133	23.67	32.79	166	5.5	1.2	0.2	38.19	45.5	151.29	20	B
GRWxxx_HL	SKK	EQ122020610	23.67	32.79	167	4.5	1	0.1	33.18	49.41	155.91	19	B
KURxxx_HL	SKK	EQ121571931	24	32.65	30	16.5	0.8	0.2	51.18	34.94	141.13	15	B
KURxxx_HL	SKK	EQ122020610	24	32.65	170	12	0.6	0.2	33.12	49.41	155.91	19	B
MANxxx_HL	SKK	EQ121901133	23.92	33.07	170	16	0.5	0.2	38.3	45.5	151.29	20	B
MANxxx_HL	SKK	EQ122020610	23.92	33.07	17	6	1.1	0.3	33.29	49.41	155.91	19	B
MRSxxx_HL	SKK	EQ110521057	25.01	34.84	18	4.5	1.5	0.5	99.94	-26.14	178.39	558.1	B
NADBxx_HL	SKK	EQ120931736	25.34	34.5	11	17	0.7	0.3	307.05	16.4	-98.32	9	B
NAHDxx_HL	SKK	EQ120931736	23.8	32.78	167	18.5	0.7	0.4	305.19	16.4	-98.32	9	B
NAHDxx_HL	SKK	EQ121142240	23.8	32.78	3	11.5	1.5	0.3	34.44	48.4	154.74	31	B
NAHDxx_HL	SKK	EQ121571931	23.8	32.78	162	6.5	1.4	0.3	51.24	34.94	141.13	15	B
NAHDxx_HL	SKK	EQ121901133	23.8	32.78	165	14	1.1	0.3	38.19	45.5	151.29	20	B
NAHDxx_HL	SKK	EQ122020610	23.8	32.78	157	7.5	1	0.2	33.17	49.41	155.91	19	B
NGALxx_HL	SKK	EQ121142240	23.42	32.73	151	9.5	0.9	0.3	34.43	48.4	154.74	31	B
NGALxx_HL	SKK	EQ121571931	23.42	32.73	1	6	1.5	0.2	51.22	34.94	141.13	15	B
NGALxx_HL	SKK	EQ122020610	23.42	32.73	3	4.5	1.4	0.2	33.16	49.41	155.91	19	B
NKLxxx_HL	SKK	EQ110521057	29.93	33.98	24	4.5	1.5	0.3	91.92	-26.14	178.39	558.1	B
NNMRxx_HL	SKK	EQ121571931	23.74	32.56	175	13	0.6	0.1	51.15	34.94	141.13	15	B
NNMRxx_HL	SKK	EQ121901133	23.74	32.56	13	15	0.9	0.3	38.09	45.5	151.29	20	A
NNMRxx_HL	SKK	EQ121941251	23.74	32.56	172	6.5	1.6	0.2	37.97	45.45	151.66	12	B
NNMRxx_HL	SKK	EQ122020610	23.74	32.56	12	5	0.9	0.2	33.08	49.41	155.91	19	B

NSKDxx_HL	SKK	EQ122020610	23.66	32.39	18	2	1.8	0.3	33.01	49.41	155.91	19	B
NWKLxx_HL	SKK	EQ120450622	23.41	32.45	19	9.5	1.2	0.3	49.9	36.21	141.39	28	B
NWKLxx_HL	SKK	EQ121571931	23.41	32.45	6	12	1.2	0.3	51.11	34.94	141.13	15	B
NWKLxx_HL	SKK	EQ121901133	23.41	32.45	179	10.5	1.1	0.3	38.05	45.5	151.29	20	B
NWKLxx_HL	SKK	EQ122020610	23.41	32.45	10	7	1.2	0.2	33.04	49.41	155.91	19	B
SH2xxx_HL	SKK	EQ113061459	27.88	34.08	45	8.5	1	0.3	199.59	-55.29	-128.84	10	B
SLMxxx_HL	SKK	EQ110231915	31.49	25.21	18	10.5	1.8	0.4	65.23	-20.33	-176.29	236.1	B
SLMxxx_HL	SKK	EQ110521057	31.49	25.21	45	18	0.4	0.2	84	-26.14	178.39	558.1	B
TAMRxx_HL	SKK	EQ120090407	27.68	30.92	147	9	1.5	0.4	77.62	-10.62	165.16	28	B
WALxxx_HL	SKK	EQ121901133	23.38	32.58	173	5.5	1.4	0.2	38.11	45.5	151.29	20	B
WALxxx_HL	SKK	EQ122020610	23.38	32.58	0	5.5	1.5	0.2	33.1	49.41	155.91	19	B
AFIFxx_XI	SKS	EQ953280618	23.93	43.04	14	5.5	1.6	0.3	127.33	-42.98	171.79	10	B
AFIFxx_XI	SKS	EQ953350520	23.93	43.04	164	9	1.4	0.3	312.66	10.16	-104	10	B
AFIFxx_XI	SKS	EQ953640207	23.93	43.04	153	8	1	0.2	6.14	63.21	-150.6	137.3	B
AFIFxx_XI	SKS	EQ960820324	23.93	43.04	169	3	1.5	0.2	26.21	51.22	178.7	20.4	A
AFIFxx_XI	SKS	EQ960881951	23.93	43.04	169	4.5	1.2	0.2	19.14	52.31	-168.78	33	B
AFIFxx_XI	SKS	EQ960901305	23.93	43.04	169	2.5	1.5	0.1	19.16	52.21	-168.73	33	A
AFIFxx_XI	SKS	EQ961510304	23.93	43.04	7	4	1.3	0.2	211.5	-56.72	-26.31	84	B
AFIFxx_XI	SKS	EQ961621524	23.93	43.04	169	3	1.6	0.2	23.84	51.48	-176.85	26.3	A
AFIFxx_XI	SKS	EQ961821132	23.93	43.04	177	5.5	1.3	0.2	33.8	51.73	159.81	33	B
AFIFxx_XI	SKS	EQ961920548	23.93	43.04	169	4	1.6	0.2	20.48	52.17	-171.15	33	B
AFIFxx_XI	SKS	EQ962320419	23.93	43.04	165	6.5	1	0.2	24.62	51.45	-178.37	33	B
AFIFxx_XI	SKS	EQ970230215	23.93	43.04	179	1	2.2	0.2	255.92	-22	-65.72	276.2	B
BGIOxx_GE	SKS	EQ941300636	31.72	35.09	0	10.5	1.5	0.4	248.74	-28.5	-63.1	600.5	B
BGIOxx_GE	SKS	EQ950981745	31.72	35.09	1	2	1.5	0.1	62.45	21.83	142.69	267.4	A
BGIOxx_GE	SKS	EQ951651111	31.72	35.09	169	13	0.7	0.1	299.41	12.13	-88.36	25	A
BGIOxx_GE	SKS	EQ951750658	31.72	35.09	4	1.5	1.6	0.1	77.53	-3.96	153.93	386	A
BGIOxx_GE	SKS	EQ951781009	31.72	35.09	0	9	1	0.2	300.45	18.83	-81.72	10	A
BGIOxx_GE	SKS	EQ952260437	31.72	35.09	3	2.5	1.6	0.3	79.79	-4.84	151.51	127.9	B
BGIOxx_GE	SKS	EQ952300216	31.72	35.09	163	3	1	0.1	211.22	-55.93	-28.83	41.9	A
BGIOxx_GE	SKS	EQ952350706	31.72	35.09	6	2	1.6	0.1	63.45	18.86	145.22	594.9	B
BGIOxx_GE	SKS	EQ952360754	31.72	35.09	2	1.5	1.8	0.1	63.58	18.82	145.04	612.4	B
BGIOxx_GE	SKS	EQ952360755	31.72	35.09	1	4	1.7	0.2	63.53	18.85	145.09	585.8	A
BGIOxx_GE	SKS	EQ952410725	31.72	35.09	22	6.5	1.1	0.2	142.25	-47.94	99.47	10	B
BGIOxx_GE	SKS	EQ952741706	31.72	35.09	173	4.5	1.4	0.2	58.22	29.31	139.04	430.8	B
BGIOxx_GE	SKS	EQ952931921	31.72	35.09	169	3.5	1.8	0.3	63.39	18.71	145.54	224.8	B
BGIOxx_GE	SKS	EQ953050035	31.72	35.09	0	3.5	1.8	0.3	251.61	-28.91	-71.42	19.9	B
BGIOxx_GE	SKS	EQ953532328	31.72	35.09	4	1.5	1.9	0.2	85.15	-3.7	140.23	63.4	A
BGIOxx_GE	SKS	EQ960222319	31.72	35.09	161	5.5	0.8	0.1	206.46	-60.61	-25.9	10.1	B
EILxxx_GE	SKS	EQ000021258	29.67	34.95	3	8.5	1	0.3	18.59	51.45	-175.56	33	A
EILxxx_GE	SKS	EQ000722221	29.67	34.95	6	11.5	1.1	0.3	303.72	14.98	-92.44	62	B
EILxxx_GE	SKS	EQ000881100	29.67	34.95	3	1.5	1.3	0.1	61.51	22.34	143.73	126.5	B
EILxxx_GE	SKS	EQ001231503	29.67	34.95	0	4	1.5	0.2	63.49	17.44	147.52	55	B
EILxxx_GE	SKS	EQ001612331	29.67	34.95	3	5	1.2	0.2	57.64	30.49	137.73	485.3	B
EILxxx_GE	SKS	EQ001661700	29.67	34.95	11	16	1	0.6	84.71	4.54	127.72	89.5	B
EILxxx_GE	SKS	EQ001680755	29.67	34.95	174	4.5	1.5	0.3	244.89	-33.88	-70.09	120.2	B

EILxxx_GE	SKS	EQ002401719	29.67	34.95	0	4	1.5	0.2	61.6	22.22	143.76	99.6	B
EILxxx_GE	SKS	EQ003560101	29.67	34.95	32	17	0.6	0.3	81.71	-5.71	151.12	33	B
EILxxx_GE	SKS	EQ010020730	29.67	34.95	7	5.5	1.8	0.6	83.25	6.75	126.81	33	B
EILxxx_GE	SKS	EQ010140858	29.67	34.95	2	1.5	1.4	0.1	61.7	22.09	143.75	87.3	A
EILxxx_GE	SKS	EQ010591854	29.67	34.95	18	5.5	1.4	0.2	344.69	47.15	-122.73	51.9	B
EILxxx_GE	SKS	EQ011031533	29.67	34.95	176	16.5	0.9	0.3	206.81	-59.72	-25.59	26	B
EILxxx_GE	SKS	EQ011660617	29.67	34.95	12	9	1.4	0.3	62.64	18.83	146.98	33	B
EILxxx_GE	SKS	EQ011700932	29.67	34.95	3	4	1.4	0.2	255.46	-22.74	-67.88	146.6	B
EILxxx_GE	SKS	EQ011801835	29.67	34.95	3	3.5	1.6	0.4	257.87	-19.52	-66.25	273.9	B
EILxxx_GE	SKS	EQ011841310	29.67	34.95	1	3.5	1.4	0.2	62.48	21.64	142.98	290	A
EILxxx_GE	SKS	EQ012851502	29.67	34.95	7	3	1.1	0.1	68.86	12.69	144.98	37	A
EILxxx_GE	SKS	EQ012940340	29.67	34.95	13	4.5	1.8	0.4	87.65	1.83	126.51	33	B
EILxxx_GE	SKS	EQ013321432	29.67	34.95	5	4.5	0.9	0.1	304.66	15.57	-93.11	84.9	A
EILxxx_GE	SKS	EQ020162309	29.67	34.95	4	4.5	1	0.1	304.63	15.5	-93.13	80.2	B
EILxxx_GE	SKS	EQ020410147	29.67	34.95	3	5	1.2	0.2	211.03	-55.91	-29	193.4	B
EILxxx_GE	SKS	EQ020501233	29.67	34.95	171	13	0.6	0.2	209.11	-56.74	-25.44	33	B
EILxxx_GE	SKS	EQ021161606	29.67	34.95	179	1.5	1.5	0.1	68.72	13.09	144.62	85.7	B
EILxxx_GE	SKS	EQ022110655	29.67	34.95	11	12.5	1.4	0.6	207.43	-57.89	-23.24	33	B
EILxxx_GE	SKS	EQ022142311	29.67	34.95	179	11	1	0.3	58.09	29.28	138.97	426.1	B
EILxxx_GE	SKS	EQ022261357	29.67	34.95	0	3	1.5	0.2	67	14.1	146.2	30	B
EILxxx_GE	SKS	EQ022600358	29.67	34.95	179	11.5	1.1	0.3	55.34	31	141.77	33	B
EILxxx_GE	SKS	EQ023160146	29.67	34.95	3	4.5	1	0.2	210	-56.55	-27.54	120	A
EILxxx_GE	SKS	EQ023191958	29.67	34.95	171	15.5	0.9	0.3	213.32	-56.05	-36.4	10	B
EILxxx_GE	SKS	EQ023510432	29.67	34.95	178	5.5	1	0.1	208.72	-56.95	-24.83	10	B
EILxxx_GE	SKS	EQ023521412	29.67	34.95	3	11.5	1.1	0.3	208.67	-57.09	-24.98	10	B
EILxxx_GE	SKS	EQ030700727	29.67	34.95	9	7	0.9	0.2	79.55	-4.69	153.24	40.2	A
EILxxx_GE	SKS	EQ031141056	29.67	34.95	2	8.5	1.1	0.2	35.08	48.76	154.99	43.8	B
EILxxx_GE	SKS	EQ031461923	29.67	34.95	9	10.5	1.2	0.4	86.04	2.35	128.85	31	B
EILxxx_GE	SKS	EQ031661924	29.67	34.95	4	5	0.9	0.2	22.64	51.55	176.92	20	B
EILxxx_GE	SKS	EQ031820552	29.67	34.95	6	2	2	0.3	87.28	4.53	122.51	635.4	B
EILxxx_GE	SKS	EQ032650445	29.67	34.95	175	16.5	0.6	0.2	294.73	19.78	-70.67	10	B
EILxxx_GE	SKS	EQ032961054	29.67	34.95	3	11.5	1.2	0.4	22.85	51.4	176.69	33	B
EILxxx_GE	SKS	EQ033151848	29.67	34.95	178	3	1.5	0.2	61.78	22.32	143.25	101	A
EILxxx_GE	SKS	EQ033220750	29.67	34.95	1	5.5	1.4	0.3	21.86	51.04	178.89	33	B
EILxxx_GE	SKS	EQ040770321	29.67	34.95	1	4	1.3	0.3	256.07	-21.12	-65.59	289.8	B
EILxxx_GE	SKS	EQ042552152	29.67	34.95	2	9.5	0.9	0.2	208.11	-57.98	-25.34	63.9	A
EILxxx_GE	SKS	EQ043002048	29.67	34.95	161	17	0.8	0.3	208.64	-57.07	-24.83	10	B
EILxxx_GE	SKS	EQ043002253	29.67	34.95	166	7	0.9	0.1	208.58	-57.07	-24.68	10	B
EILxxx_GE	SKS	EQ043071002	29.67	34.95	16	4.5	1.7	0.2	349.25	49.28	-128.77	10	B
EILxxx_GE	SKS	EQ043080831	29.67	34.95	176	3.5	1.4	0.2	66.33	14.47	146.84	10	B
EILxxx_GE	SKS	EQ043492320	29.67	34.95	2	14.5	0.8	0.2	299.92	18.96	-81.41	10	B
EILxxx_GE	SKS	EQ050211758	29.67	34.95	164	3.5	1.5	0.2	53.02	34	141.37	10	B
EILxxx_GE	SKS	EQ050401846	29.67	34.95	4	6.5	1.2	0.2	58.29	26.09	144	24	B
EILxxx_GE	SKS	EQ050461442	29.67	34.95	12	5	1.4	0.3	85.16	4.76	126.42	39.7	B
EILxxx_GE	SKS	EQ051090146	29.67	34.95	174	4.5	1.4	0.2	57.83	29.64	138.89	425.8	B
EILxxx_GE	SKS	EQ051380910	29.67	34.95	175	11.5	1	0.2	209.87	-56.41	-26.86	102.2	B

EILxxx_GE	SKS	EQ051631926	29.67	34.95	1	3.5	1.1	0.1	210.04	-56.29	-27.08	94.1	A
EILxxx_GE	SKS	EQ051640702	29.67	34.95	12	5	1.8	0.4	87.4	2.09	126.57	10	B
EILxxx_GE	SKS	EQ051680621	29.67	34.95	14	6	1.4	0.2	345.35	40.77	-126.57	12	B
EILxxx_GE	SKS	EQ051901007	29.67	34.95	15	3.5	1.5	0.2	86.85	2.75	126.53	22.3	B
EILxxx_GE	SKS	EQ051902337	29.67	34.95	178	3	1.2	0.1	53.75	33.42	140.82	55.2	B
EILxxx_GE	SKS	EQ061780239	29.67	34.95	167	11	0.6	0.2	22.67	52.23	176.16	17	B
EILxxx_GE	SKS	EQ062370044	29.67	34.95	3	7	1.6	0.5	253.49	-24.4	-67.03	184	B
EILxxx_GE	SKS	EQ062710136	29.67	34.95	160	4.5	1.2	0.1	37.55	46.46	153.36	11	B
EILxxx_GE	SKS	EQ062861347	29.67	34.95	2	14.5	0.9	0.3	37.76	46.24	153.28	4	B
EILxxx_GE	SKS	EQ062900125	29.67	34.95	8	3.5	1.2	0.2	81.95	-5.88	150.98	32	B
EILxxx_GE	SKS	EQ063192122	29.67	34.95	173	1.5	1	0.1	36.58	47.28	154.15	12	B
EILxxx_GE	SKS	EQ063461548	29.67	34.95	10	2	1.9	0.3	86.9	3.73	124.68	213.5	B
EILxxx_GE	SKS	EQ070200621	29.67	34.95	170	8.5	1.1	0.2	211.61	-55.42	-29.53	10	B
EILxxx_GE	SKS	EQ070302137	29.67	34.95	3	2.5	1.2	0.1	62.12	20.98	144.71	20	A
EILxxx_GE	SKS	EQ070592313	29.67	34.95	154	11.5	0.9	0.2	211.62	-55.24	-29.14	10	B
EILxxx_GE	SKS	EQ070670503	29.67	34.95	8	10	1.4	0.3	56.99	29.91	140.2	139.6	B
EILxxx_GE	SKS	EQ071111753	29.67	34.95	4	8.5	1.3	0.2	232.82	-45.24	-72.65	36.7	B
EILxxx_GE	SKS	EQ071191241	29.67	34.95	6	7	1.1	0.3	20.75	52.01	-179.97	117	B
EILxxx_GE	SKS	EQ072021534	29.67	34.95	2	3	1.8	0.2	255.16	-22.15	-65.78	289.5	B
EILxxx_GE	SKS	EQ072120242	29.67	34.95	172	11	1.4	0.3	210.46	-56.06	-27.73	104	B
EILxxx_GE	SKS	EQ072791238	29.67	34.95	1	16	1.2	0.5	62.64	18.73	147.15	20	B
EILxxx_GE	SKS	EQ072821503	29.67	34.95	8	2.5	1.3	0.2	79.86	-4.81	152.89	39	B
EILxxx_GE	SKS	EQ073040330	29.67	34.95	8	17.5	1	0.3	63.46	18.9	145.39	207	B
EILxxx_GE	SKS	EQ073220540	29.67	34.95	3	3.5	1.5	0.2	254.92	-22.64	-66.32	246.4	B
EILxxx_GE	SKS	EQ073500809	29.67	34.95	4	2.5	1.8	0.2	256.17	-22.95	-70.18	45	B
EILxxx_GE	SKS	EQ081461918	29.67	34.95	24	4	1.3	0.2	4.77	55.9	-153.51	20	B
EILxxx_GE	SKS	EQ081510725	29.67	34.95	8	10	1.4	0.3	55.62	30.8	141.52	16	B
EILxxx_GE	SKS	EQ081751232	29.67	34.95	2	7	1.1	0.2	37.58	46.48	153.27	10	B
EILxxx_GE	SKS	EQ081820617	29.67	34.95	7	5.5	1.6	0.4	206.77	-58.23	-22.1	8	B
EILxxx_GE	SKS	EQ082851040	29.67	34.95	9	3.5	1.2	0.3	291.29	19.16	-64.83	23	B
EILxxx_GE	SKS	EQ083431839	29.67	34.95	15	14	1.2	0.4	143.84	-53.01	106.82	11	B
EILxxx_GE	SKS	EQ090421734	29.67	34.95	13	6	1.3	0.3	85.93	3.89	126.39	20	B
EILxxx_GE	SKS	EQ090431315	29.67	34.95	8	3	1.4	0.3	85.72	4.04	126.55	27	B
EILxxx_GE	SKS	EQ090940531	29.67	34.95	6	1	1.9	0.2	84.44	5.15	127.2	48	B
EILxxx_GE	SKS	EQ091061457	29.67	34.95	13	11.5	1.5	0.6	206.83	-60.2	-26.86	20	B
EILxxx_GE	SKS	EQ091090523	29.67	34.95	5	1.5	1.8	0.2	85.57	4.14	126.68	25	B
EILxxx_GE	SKS	EQ091361822	29.67	34.95	19	8.5	1.3	0.4	3.87	56.23	-151.97	10	B
EILxxx_GE	SKS	EQ092242004	29.67	34.95	36	10.5	1	0.2	84.08	6.04	126.38	95.7	B
EILxxx_GE	SKS	EQ092242248	29.67	34.95	5	16	1.4	0.5	54.45	32.82	140.4	53	B
EILxxx_GE	SKS	EQ092530246	29.67	34.95	174	3.5	1.1	0.1	35.76	48.32	154.19	36	B
EILxxx_GE	SKS	EQ092611153	29.67	34.95	6	12.5	1.3	0.5	84.48	6.51	124.71	10	B
EILxxx_GE	SKS	EQ092771058	29.67	34.95	8	4	1.4	0.3	84.93	6.74	123.38	620	B
EILxxx_GE	SKS	EQ093211530	29.67	34.95	12	12	1.6	0.6	351.55	52.12	-131.4	17	B
EILxxx_GE	SKS	EQ100122153	29.67	34.95	9	8.5	1.2	0.4	294.6	18.44	-72.57	13	B
EILxxx_GE	SKS	EQ100141403	29.67	34.95	10	11	0.9	0.2	71.43	11.51	142.08	37	B
EILxxx_GE	SKS	EQ100171200	29.67	34.95	4	8.5	1.2	0.3	217.65	-57.66	-65.88	5	B

EILxxx_GE	SKS	EQ100632239	29.67	34.95	3	5.5	1.4	0.3	256.14	-22.23	-68.33	114	B
EILxxx_GE	SKS	EQ100791400	29.67	34.95	10	8	1.3	0.4	78.85	-3.36	152.24	414.6	B
EILxxx_GE	SKS	EQ101152109	29.67	34.95	177	5	1.2	0.2	210.83	-55.61	-27.73	7	B
EILxxx_GE	SKS	EQ101530149	29.67	34.95	5	4.5	1.2	0.2	208.97	-57.37	-26.45	127.4	A
EILxxx_GE	SKS	EQ101621637	29.67	34.95	10	6	1.1	0.2	58.55	26.69	142.5	7	B
EILxxx_GE	SKS	EQ101911143	29.67	34.95	178	7	1	0.3	69.6	11.14	146	13	A
EILxxx_GE	SKS	EQ102100731	29.67	34.95	9	6.5	1.1	0.3	85.17	6.55	123.22	618	B
EILxxx_GE	SKS	EQ102151208	29.67	34.95	9	7	1.4	0.4	88.31	1.24	126.21	41	B
EILxxx_GE	SKS	EQ102810326	29.67	34.95	7	3.5	1.3	0.3	18.51	51.37	-175.36	19	B
EILxxx_GE	SKS	EQ102810349	29.67	34.95	7	4	1.2	0.3	18.45	51.29	-175.18	27.7	B
EILxxx_GE	SKS	EQ103111926	29.67	34.95	0	3.5	1.5	0.2	60.92	24.38	141.59	113	B
EILxxx_GE	SKS	EQ103420524	29.67	34.95	178	4.5	1	0.1	209.47	-56.41	-25.74	29.4	B
EILxxx_GE	SKS	EQ103551719	29.67	34.95	11	6	1.5	0.2	57.78	26.9	143.7	14	B
EILxxx_GE	SKS	EQ110050057	29.67	34.95	16	8.5	1.7	0.3	54.69	31.55	142.18	21.4	B
EILxxx_GE	SKS	EQ110101024	29.67	34.95	12	5.5	1.1	0.2	61.19	23.08	143.17	86.6	B
EILxxx_GE	SKS	EQ110122132	29.67	34.95	0	5.5	1.2	0.2	59.6	26.97	139.88	512	A
EILxxx_GE	SKS	EQ110381953	29.67	34.95	28	13	0.7	0.2	80.83	-7.15	155.18	415	B
EILxxx_GE	SKS	EQ110411441	29.67	34.95	5	2.5	1.7	0.4	87.41	4.08	123.04	525	B
EILxxx_GE	SKS	EQ110531409	29.67	34.95	0	3.5	1.4	0.2	61.64	22.11	143.84	112.8	B
EILxxx_GE	SKS	EQ110651432	29.67	34.95	3	5.5	1.1	0.2	209.94	-56.42	-27.06	87.7	A
EILxxx_GE	SKS	EQ110711253	29.67	34.95	3	10	1.6	0.4	48.94	37.73	143.51	34.1	B
EILxxx_GE	SKS	EQ110742029	29.67	34.95	177	2.5	1.3	0.1	52.17	35.21	140.99	19.4	B
EILxxx_GE	SKS	EQ110810718	29.67	34.95	177	9	1.5	0.3	49.13	37.24	144	11	B
EILxxx_GE	SKS	EQ110971311	29.67	34.95	13	10.5	1.3	0.4	306.83	17.21	-94.34	166.2	B
EILxxx_GE	SKS	EQ111251324	29.67	34.95	6	14	0.9	0.4	309.64	16.78	-98.62	24	B
EILxxx_GE	SKS	EQ111410016	29.67	34.95	1	14	1.1	0.3	210.23	-56.07	-27.11	48	B
EILxxx_GE	SKS	EQ111711636	29.67	34.95	2	6	1.5	0.3	256.61	-21.7	-68.23	128	B
EILxxx_GE	SKS	EQ112451347	29.67	34.95	7	6.5	1.5	0.3	248.05	-28.4	-63.03	578.9	B
EILxxx_GE	SKS	EQ112460448	29.67	34.95	5	4.5	1.2	0.2	209.84	-56.45	-26.85	84	A
EILxxx_GE	SKS	EQ112521941	29.67	34.95	11	3.5	1.9	0.2	348.12	49.53	-126.89	22	B
EILxxx_GE	SKS	EQ113261848	29.67	34.95	2	3	1.4	0.3	261.24	-15.36	-65.09	549.9	A
EILxxx_GE	SKS	EQ113450954	29.67	34.95	160	11.5	0.9	0.2	210.66	-56.01	-28.18	116	B
EILxxx_GE	SKS	EQ113491512	29.67	34.95	2	10	1.5	0.3	54.8	31.72	141.63	34.8	B
EILxxx_GE	SKS	EQ120010527	29.67	34.95	2	6	1.1	0.2	56.66	31.46	138.07	365.3	B
EILxxx_GE	SKS	EQ120931736	29.67	34.95	7	2	1.5	0.1	309.11	16.4	-98.32	9	B
EILxxx_GE	SKS	EQ121051513	29.67	34.95	3	10	1.2	0.3	34.32	49.38	155.65	90.3	B
EILxxx_GE	SKS	EQ121472148	29.67	34.95	179	4.5	1.3	0.2	59.57	26.91	140.05	487.4	B
EILxxx_GE	SKS	EQ121490507	29.67	34.95	7	2.5	1.3	0.1	248.42	-28.04	-63.09	586.9	B
EILxxx_GE	SKS	EQ121930231	29.67	34.95	175	8	1	0.2	39.23	45.4	151.42	10	B
EILxxx_GE	SKS	EQ122550128	29.67	34.95	6	3.5	1	0.1	39.42	45.33	151.11	14	B
EILxxx_GE	SKS	EQ122692345	29.67	34.95	10	6	1.7	0.2	324.48	24.67	-110.17	10	B
EILxxx_GE	SKS	EQ122880941	29.67	34.95	3	8.5	1.2	0.3	35.67	48.31	154.43	35	B
EILxxx_GE	SKS	EQ122970853	29.67	34.95	172	7	1.6	0.3	58.15	29.06	139.25	436	B
EILxxx_GE	SKS	EQ122980045	29.67	34.95	9	8	1.9	0.8	294.95	10.09	-85.3	17	B
EILxxx_GE	SKS	EQ123021854	29.67	34.95	28	13	0.9	0.3	352.4	52.67	-132.6	9	B
EILxxx_GE	SKS	EQ123040249	29.67	34.95	16	11	1.5	0.4	351.91	52.37	-131.9	9	B

EILxxx_GE	SKS	EQ123172042	29.67	34.95	17	9.5	1.4	0.3	358.83	57.59	-142.88	10.9	B
EILxxx_GE	SKS	EQ123191902	29.67	34.95	6	9.5	1.5	0.3	250.26	-29.12	-71.19	63	B
EILxxx_GE	SKS	EQ123271307	29.67	34.95	5	6.5	1.5	0.3	253.69	-22.74	-63.57	516.6	B
EILxxx_GE	SKS	EQ130830418	29.67	34.95	3	8	1.2	0.2	31.35	50.73	160.16	8	B
EILxxx_GE	SKS	EQ132072132	29.67	34.95	4	4	1.2	0.2	207.77	-57.79	-23.96	10	B
EILxxx_GE	SKS	EQ970850208	29.67	34.95	8	16	0.9	0.3	21.39	51.28	179.53	33	B
EILxxx_GE	SKS	EQ970911833	29.67	34.95	15	6	1.6	0.3	260.46	-18.3	-69.53	113.8	B
EILxxx_GE	SKS	EQ971131944	29.67	34.95	3	9	1.2	0.3	67.81	13.99	144.9	100.8	A
EILxxx_GE	SKS	EQ971890224	29.67	34.95	5	5	1.4	0.2	60.84	23.8	142.7	33	B
EILxxx_GE	SKS	EQ972601450	29.67	34.95	10	5.5	1.8	0.5	87.37	2.11	126.6	33	B
EILxxx_GE	SKS	EQ973092345	29.67	34.95	0	3.5	1.6	0.2	57.53	27.86	142.61	10	B
EILxxx_GE	SKS	EQ973142306	29.67	34.95	2	4	1.3	0.1	55.78	31.19	140.49	86	A
EILxxx_GE	SKS	EQ980010611	29.67	34.95	3	2	1.5	0.1	61.15	23.91	141.91	95.6	A
EILxxx_GE	SKS	EQ980100820	29.67	34.95	4	7.5	0.9	0.2	302.57	14.37	-91.47	33	B
EILxxx_GE	SKS	EQ980380118	29.67	34.95	3	1.5	1.4	0.1	60.48	24.82	141.75	525.3	B
EILxxx_GE	SKS	EQ982320640	29.67	34.95	179	3.5	1.1	0.2	58.22	28.93	139.33	440.5	B
EILxxx_GE	SKS	EQ982410830	29.67	34.95	1	5	1	0.1	210.48	-55.74	-27.05	33	A
EILxxx_GE	SKS	EQ982420148	29.67	34.95	178	3.5	1.6	0.2	63.43	17.09	148.13	33	B
EILxxx_GE	SKS	EQ982441029	29.67	34.95	164	12	0.9	0.2	208.33	-58.21	-26.53	151.7	B
EILxxx_GE	SKS	EQ982450837	29.67	34.95	10	8.5	1.2	0.3	84.43	5.41	126.76	50	B
EILxxx_GE	SKS	EQ982572316	29.67	34.95	1	16	0.8	0.3	17.15	51.62	-173.15	33	B
EILxxx_GE	SKS	EQ982650116	29.67	34.95	3	14.5	1.2	0.6	70.59	11.82	143.15	9.2	B
EILxxx_GE	SKS	EQ982711923	29.67	34.95	6	4	1.4	0.4	85.96	3.84	126.41	30.1	B
EILxxx_GE	SKS	EQ982760648	29.67	34.95	15	9	1.4	0.4	209.17	-56.62	-25.35	33	B
EILxxx_GE	SKS	EQ982761512	29.67	34.95	169	10	0.8	0.2	209.18	-56.71	-25.57	33	B
EILxxx_GE	SKS	EQ983002116	29.67	34.95	9	6	1.1	0.3	85.66	2.92	128.62	60.7	B
EILxxx_GE	SKS	EQ983400047	29.67	34.95	10	3	1.7	0.3	88.3	1.25	126.2	33	B
EILxxx_GE	SKS	EQ990120232	29.67	34.95	2	2.5	1.3	0.1	59.66	26.74	140.17	440.6	B
EILxxx_GE	SKS	EQ991131856	29.67	34.95	178	6	1.4	0.4	68.4	13.12	145.14	52.5	B
EILxxx_GE	SKS	EQ991691055	29.67	34.95	7	4.5	1.5	0.4	84.4	5.51	126.64	33	B
EILxxx_GE	SKS	EQ991840530	29.67	34.95	0	3.5	1.5	0.2	59.85	26.32	140.48	430.6	B
EILxxx_GE	SKS	EQ992910243	29.67	34.95	174	8	0.9	0.2	210	-56.12	-26.58	33	A
EILxxx_GE	SKS	EQ993250351	29.67	34.95	17	4.5	1.7	0.2	256.79	-21.75	-68.78	101.2	B
HALMxx_XI	SKS	EQ953532328	22.85	44.32	12	3.5	1.7	0.4	91.12	-3.7	140.23	63.4	B
HALMxx_XI	SKS	EQ953590443	22.85	44.32	18	4	0.8	0.2	98.32	-6.9	129.15	141.9	B
HALMxx_XI	SKS	EQ960222319	22.85	44.32	0	7	0.8	0.2	208.16	-60.61	-25.9	10.1	B
HALMxx_XI	SKS	EQ960382119	22.85	44.32	144	12	0.6	0.2	11.91	54.91	-156.25	33	B
HALMxx_XI	SKS	EQ960820324	22.85	44.32	175	13.5	1	0.4	26.87	51.22	178.7	20.4	A
HALMxx_XI	SKS	EQ960881951	22.85	44.32	3	9	0.9	0.3	19.89	52.31	-168.78	33	B
HALMxx_XI	SKS	EQ960901305	22.85	44.32	174	9.5	0.9	0.2	19.92	52.21	-168.73	33	A
HALMxx_XI	SKS	EQ961231334	22.85	44.32	28	18	1.4	0.4	86.19	-4.55	154.83	500	B
HALMxx_XI	SKS	EQ961251613	22.85	44.32	15	9.5	1.1	0.3	72.63	13.85	146.31	33	B
HALMxx_XI	SKS	EQ961510304	22.85	44.32	162	4.5	0.6	0.1	211.76	-56.72	-26.31	84	A
HALMxx_XI	SKS	EQ961602319	22.85	44.32	10	3.5	1.4	0.3	25.17	51.49	-178.13	33	B
HALMxx_XI	SKS	EQ961621524	22.85	44.32	173	13.5	1	0.3	24.54	51.48	-176.85	26.3	B
HALMxx_XI	SKS	EQ961741450	22.85	44.32	163	10.5	0.8	0.1	34.69	51.4	159.24	33	B

HALMxx_XI	SKS	EQ961821132	22.85	44.32	10	7	1.1	0.2	34.21	51.73	159.81	33	B
HALMxx_XI	SKS	EQ961861550	22.85	44.32	8	8.5	1.4	0.3	79.41	8.49	141.56	33	B
HALMxx_XI	SKS	EQ961882136	22.85	44.32	9	7	1.1	0.2	66.66	21.97	142.83	241.1	B
HALMxx_XI	SKS	EQ962981931	22.85	44.32	170	11	0.6	0.2	13.9	66.99	-173.23	19.9	A
HALMxx_XI	SKS	EQ970230215	22.85	44.32	1	2	2.2	0.3	255.79	-22	-65.72	276.2	B
JERxxx_GE	SKS	EQ000371133	31.77	35.2	9	5.5	1.1	0.2	81.14	-5.84	150.88	33	B
JERxxx_GE	SKS	EQ000571824	31.77	35.2	0	13	0.8	0.2	290.98	9.41	-78.53	65	A
JERxxx_GE	SKS	EQ000881100	31.77	35.2	177	3	1.4	0.2	61.53	22.34	143.73	126.5	A
JERxxx_GE	SKS	EQ001140927	31.77	35.2	3	2.5	1.3	0.1	248.94	-28.31	-62.99	608.5	A
JERxxx_GE	SKS	EQ001141701	31.77	35.2	1	6.5	1.1	0.2	248.85	-28.38	-62.94	609.8	B
JERxxx_GE	SKS	EQ001231503	31.77	35.2	1	2	1.5	0.1	63.33	17.44	147.52	55	B
JERxxx_GE	SKS	EQ001470030	31.77	35.2	179	15	1.4	0.6	72.97	11.36	139.24	33	B
JERxxx_GE	SKS	EQ001680755	31.77	35.2	9	6	1.1	0.2	245.98	-33.88	-70.09	120.2	A
JERxxx_GE	SKS	EQ003041201	31.77	35.2	158	16	0.5	0.2	101.41	-9.71	119.07	33	B
JERxxx_GE	SKS	EQ003412257	31.77	35.2	3	2	1.5	0.2	78.54	-4.22	152.73	31	B
JERxxx_GE	SKS	EQ003541311	31.77	35.2	179	2.5	1.5	0.2	69.54	11.77	144.76	33	B
JERxxx_GE	SKS	EQ010140858	31.77	35.2	0	2	1.3	0.1	61.72	22.09	143.75	87.3	A
JERxxx_GE	SKS	EQ010591854	31.77	35.2	8	3.5	1.6	0.2	344.95	47.15	-122.73	51.9	B
JERxxx_GE	SKS	EQ010802047	31.77	35.2	5	3.5	1.5	0.3	78.59	-4.53	153.11	33	B
JERxxx_GE	SKS	EQ011031533	31.77	35.2	179	16	0.8	0.3	207.11	-59.72	-25.59	26	A
JERxxx_GE	SKS	EQ011072154	31.77	35.2	0	16	1.4	0.6	21.13	51.24	-179.78	33	B
JERxxx_GE	SKS	EQ011700932	31.77	35.2	179	2.5	1.6	0.2	256.38	-22.74	-67.88	146.6	B
JERxxx_GE	SKS	EQ011801835	31.77	35.2	2	1.5	1.8	0.2	258.7	-19.52	-66.25	273.9	B
JERxxx_GE	SKS	EQ011820146	31.77	35.2	2	1.5	1.7	0.2	78.49	-4.31	152.96	28	B
JERxxx_GE	SKS	EQ011841310	31.77	35.2	0	3	1.5	0.1	62.5	21.64	142.98	290	A
JERxxx_GE	SKS	EQ011861353	31.77	35.2	8	3	2.1	0.4	265.65	-16.09	-73.99	62	B
JERxxx_GE	SKS	EQ021161606	31.77	35.2	2	1	1.5	0.1	68.53	13.09	144.62	85.7	B
JERxxx_GE	SKS	EQ023160146	31.77	35.2	162	8	1	0.2	210.31	-56.55	-27.54	120	A
JERxxx_GE	SKS	EQ023460830	31.77	35.2	6	2.5	1.5	0.2	78.73	-4.79	153.27	34	B
JERxxx_GE	SKS	EQ023510432	31.77	35.2	179	5	1	0.1	209.01	-56.95	-24.83	10	B
JERxxx_GE	SKS	EQ963661241	31.77	35.2	1	8	1.2	0.2	305.64	15.83	-92.97	99.5	A
JERxxx_GE	SKS	EQ970112028	31.77	35.2	3	8.5	1	0.2	314.91	18.22	-102.76	33	B
JERxxx_GE	SKS	EQ970911842	31.77	35.2	10	3	1.4	0.2	261.25	-18.35	-69.35	115.6	B
JERxxx_GE	SKS	EQ971131944	31.77	35.2	4	2.5	1.5	0.1	67.64	13.99	144.9	100.8	A
JERxxx_GE	SKS	EQ971290906	31.77	35.2	5	2	1.5	0.1	68.39	13.2	144.7	29	A
JERxxx_GE	SKS	EQ971420750	31.77	35.2	0	4	1	0.1	314.3	18.68	-101.6	70	A
JERxxx_GE	SKS	EQ971532124	31.77	35.2	164	5.5	0.9	0.1	208.6	-57.78	-25.47	33	B
JERxxx_GE	SKS	EQ971890224	31.77	35.2	5	2.5	1.5	0.1	60.91	23.8	142.7	33	B
JERxxx_GE	SKS	EQ973092345	31.77	35.2	174	9.5	1.3	0.4	57.67	27.86	142.61	10	B
JERxxx_GE	SKS	EQ973142306	31.77	35.2	177	13	1.3	0.4	56.02	31.19	140.49	86	B
JERxxx_GE	SKS	EQ980100820	31.77	35.2	5	3	1.2	0.1	303.44	14.37	-91.47	33	B
JERxxx_GE	SKS	EQ980380118	31.77	35.2	2	3	1.2	0.1	60.58	24.82	141.75	525.3	B
JERxxx_GE	SKS	EQ981192332	31.77	35.2	1	14	1.2	0.5	55.62	30.78	141.96	33	B
JERxxx_GE	SKS	EQ981582320	31.77	35.2	167	11	1.4	0.3	306.32	15.96	-93.78	86.6	B
JERxxx_GE	SKS	EQ982410830	31.77	35.2	163	5	0.8	0.1	210.78	-55.74	-27.05	33	A
JERxxx_GE	SKS	EQ982650116	31.77	35.2	2	10.5	1.5	0.4	70.41	11.82	143.15	9.2	B

JERxxx_GE	SKS	EQ982760648	31.77	35.2	175	9	0.9	0.2	209.46	-56.62	-25.35	33	B
JERxxx_GE	SKS	EQ982761512	31.77	35.2	171	6	0.8	0.1	209.47	-56.71	-25.57	33	B
JERxxx_GE	SKS	EQ990930617	31.77	35.2	9	8	1.5	0.6	264.45	-16.66	-72.66	87.2	B
JERxxx_GE	SKS	EQ991131856	31.77	35.2	179	4.5	1.4	0.3	68.2	13.12	145.14	52.5	B
JERxxx_GE	SKS	EQ991662042	31.77	35.2	178	6.5	1.1	0.2	310.85	18.39	-97.44	70	B
JERxxx_GE	SKS	EQ991840530	31.77	35.2	179	7	1.4	0.3	60.01	26.32	140.48	430.6	B
JERxxx_GE	SKS	EQ992580301	31.77	35.2	3	2	1.4	0.1	257.84	-20.93	-67.28	218	B
JERxxx_GE	SKS	EQ992910243	31.77	35.2	174	4.5	0.9	0.1	210.3	-56.12	-26.58	33	A
JERxxx_GE	SKS	EQ992960212	31.77	35.2	8	5	1.6	0.3	78.67	-4.81	153.41	83.3	B
JERxxx_GE	SKS	EQ993250351	31.77	35.2	0	1.5	1.5	0.2	257.73	-21.75	-68.78	101.2	B
KEGxxx_MN	SKS	EQ903641914	29.93	31.83	23	18.5	1	0.4	79.32	-5.1	150.97	178.6	B
KEGxxx_MN	SKS	EQ911191812	29.93	31.83	30	4.5	1.8	0.2	269.64	-11.26	-77.67	58.3	B
KEGxxx_MN	SKS	EQ911230214	29.93	31.83	23	13	0.9	0.3	57.3	28.08	139.59	433.1	B
KEGxxx_MN	SKS	EQ921502152	29.93	31.83	22	8	0.9	0.2	53.71	31.17	141.73	18.6	B
KEGxxx_MN	SKS	EQ921511242	29.93	31.83	17	13.5	0.8	0.2	54.16	30.69	141.59	20.2	B
KEGxxx_MN	SKS	EQ921520620	29.93	31.83	24	10.5	1	0.3	54.2	30.64	141.6	31.6	B
KEGxxx_MN	SKS	EQ921531829	29.93	31.83	9	7	0.7	0.1	55.38	29.74	140.7	133.8	B
KEGxxx_MN	SKS	EQ922070253	29.93	31.83	24	16	0.8	0.2	46.95	38.73	143.01	17.4	B
KEGxxx_MN	SKS	EQ922110227	29.93	31.83	27	7.5	1.4	0.3	46.12	39.61	143.28	26.5	B
KEGxxx_MN	SKS	EQ922110430	29.93	31.83	32	12	1	0.6	46.11	39.49	143.5	15.9	B
KEGxxx_MN	SKS	EQ922241514	29.93	31.83	21	3.5	0.9	0.1	52.64	32.54	141.64	15.5	B
KEGxxx_MN	SKS	EQ922320057	29.93	31.83	28	6	1	0.3	16.82	50.5	-174.92	9.9	B
KEGxxx_MN	SKS	EQ922371940	29.93	31.83	6	3.5	1	0.2	208.49	-56.62	-26.55	106.6	B
KEGxxx_MN	SKS	EQ922421919	29.93	31.83	25	6.5	0.7	0.1	53.84	33.19	137.98	289.4	A
KEGxxx_MN	SKS	EQ932050201	29.93	31.83	6	9.5	1.9	0.7	82.7	5.07	127.71	116.2	B
KEGxxx_MN	SKS	EQ932200834	29.93	31.83	23	7.5	1	0.2	66.91	12.98	144.8	59.3	A
KEGxxx_MN	SKS	EQ932202003	29.93	31.83	35	11.5	1	0.3	66	13.48	145.66	56.1	B
KEGxxx_MN	SKS	EQ932231417	29.93	31.83	11	6	1	0.2	66.26	13.18	145.65	21.6	A
KEGxxx_MN	SKS	EQ932280433	29.93	31.83	20	7	0.9	0.1	66.83	12.97	144.97	18.3	A
KEGxxx_MN	SKS	EQ932490356	29.93	31.83	30	6.5	0.8	0.1	77.54	-4.64	153.23	49	A
KEGxxx_MN	SKS	EQ932522152	29.93	31.83	11	3	1.3	0.2	209.09	-56.21	-27.33	110	B
KEGxxx_MN	SKS	EQ932531912	29.93	31.83	13	3.5	1.8	0.3	301.62	14.72	-92.64	34.1	A
KEGxxx_MN	SKS	EQ932690331	29.93	31.83	46	14.5	0.7	0.3	73.07	10	138.22	10	B
KEGxxx_MN	SKS	EQ932691155	29.93	31.83	22	7.5	0.9	0.2	66.76	13.01	145.02	63.7	B
KEGxxx_MN	SKS	EQ932721826	29.93	31.83	14	14	1.2	0.6	214.63	-42.68	-18.39	10	B
KEGxxx_MN	SKS	EQ932841554	29.93	31.83	21	7.5	0.8	0.1	54.88	32.02	137.83	350.7	B
KEGxxx_MN	SKS	EQ932920402	29.93	31.83	1	11	0.7	0.2	253.81	-22.38	-65.97	272	A
KEGxxx_MN	SKS	EQ933230143	29.93	31.83	35	13	0.8	0.2	9.33	54.29	-164.16	30.3	B
KEGxxx_MN	SKS	EQ940171230	29.93	31.83	29	7.5	1.5	0.2	334.09	34.21	-118.54	18.4	B
KEGxxx_MN	SKS	EQ940732051	29.93	31.83	10	11	0.9	0.3	302.5	15.99	-92.43	164.2	B
KEGxxx_MN	SKS	EQ941032222	29.93	31.83	67	4.5	1.4	0.2	85.64	-3.14	135.97	28.5	B
KEGxxx_MN	SKS	EQ941190711	29.93	31.83	170	12.5	0.9	0.4	247.12	-28.3	-63.25	561.5	B
KEGxxx_MN	SKS	EQ941300636	29.93	31.83	25	13.5	0.6	0.2	246.87	-28.5	-63.1	600.5	A
KEGxxx_MN	SKS	EQ941450403	29.93	31.83	69	9	0.9	0.3	86.82	-4.2	135.49	33	B
KEGxxx_MN	SKS	EQ942062200	29.93	31.83	8	4.5	1.2	0.2	208.99	-56.36	-27.36	81.3	A
KEGxxx_MN	SKS	EQ942100017	29.93	31.83	46	16	0.5	0.2	12.26	52.4	-168.33	11	B

KEGxxx_MN	SKS	EQ942162215	29.93	31.83	73	6.5	1.1	0.3	90.68	-6.34	131.57	33	B
KEGxxx_MN	SKS	EQ942311002	29.93	31.83	19	17	0.6	0.3	248.75	-26.64	-63.42	563.6	B
KEGxxx_MN	SKS	EQ942391603	29.93	31.83	62	3.5	1.9	0.3	81.71	6.8	126.73	100.1	B
KEGxxx_MN	SKS	EQ942582347	29.93	31.83	179	9	1.1	0.3	200.44	-57.8	-8.77	10	B
KEGxxx_MN	SKS	EQ942812144	29.93	31.83	62	17	0.6	0.2	88.03	-1.26	127.98	16.6	B
KEGxxx_MN	SKS	EQ942911712	29.93	31.83	32	7	1	0.4	41.22	43.58	147.1	60.3	B
KEGxxx_MN	SKS	EQ942930115	29.93	31.83	175	2.5	0.9	0.1	238.66	-39.19	-70.81	161.8	A
KEGxxx_MN	SKS	EQ951190943	29.93	31.83	56	10	1.2	0.3	77.73	11.85	125.98	15	B
KEGxxx_MN	SKS	EQ951381431	29.93	31.83	20	6	0.9	0.2	40.43	44.32	147.54	89.4	B
KEGxxx_MN	SKS	EQ951750658	29.93	31.83	19	5	1.1	0.2	76.45	-3.96	153.93	386	B
KEGxxx_MN	SKS	EQ951792114	29.93	31.83	16	13.5	1.2	0.4	88.54	-1.55	127.47	33	B
KEGxxx_MN	SKS	EQ951882115	29.93	31.83	32	10.5	1	0.3	53.57	33.97	137.13	333.3	B
KEGxxx_MN	SKS	EQ952300216	29.93	31.83	8	5	1.3	0.2	209.86	-55.93	-28.83	41.9	A
KEGxxx_MN	SKS	EQ952350706	29.93	31.83	27	4.5	0.9	0.1	61.83	18.86	145.22	594.9	A
KEGxxx_MN	SKS	EQ952360628	29.93	31.83	23	5.5	1	0.1	61.89	18.85	145.12	602.2	B
KEGxxx_MN	SKS	EQ952360754	29.93	31.83	27	8.5	1	0.2	61.96	18.82	145.04	612.4	A
KEGxxx_MN	SKS	EQ952360755	29.93	31.83	28	4	1.1	0.1	61.91	18.85	145.09	585.8	A
KEGxxx_MN	SKS	EQ952440630	29.93	31.83	58	16.5	0.9	0.3	89.27	0.04	123.24	144.4	B
KEGxxx_MN	SKS	EQ952522058	29.93	31.83	9	8.5	1.2	0.3	257.35	-20.14	-69.32	75	B
KEGxxx_MN	SKS	EQ953532328	29.93	31.83	31	18	0.7	0.2	83.93	-3.7	140.23	63.4	B
KEGxxx_MN	SKS	EQ960480559	29.93	31.83	57	5.5	1.9	0.3	83.14	-0.89	136.95	33	B
KEGxxx_MN	SKS	EQ960481421	29.93	31.83	61	7	1	0.2	83.44	-0.57	135.84	19.2	B
KEGxxx_MN	SKS	EQ960482018	29.93	31.83	49	17.5	0.9	0.4	83.54	-0.92	136.23	31.9	B
KEGxxx_MN	SKS	EQ960490225	29.93	31.83	61	11	1.5	0.5	83.79	-1.34	136.46	10	B
KEGxxx_MN	SKS	EQ960551552	29.93	31.83	66	4.5	1.2	0.2	82.92	-0.87	137.35	33	B
KEGxxx_MN	SKS	EQ960590944	29.93	31.83	14	13	0.9	0.3	86.39	1.76	126.05	115.5	B
KEGxxx_MN	SKS	EQ960762204	29.93	31.83	19	15	0.9	0.3	56.87	28.98	138.94	477.2	A
KEGxxx_MN	SKS	EQ960901305	29.93	31.83	31	6.5	0.7	0.2	12.56	52.21	-168.73	33	B
KEGxxx_MN	SKS	EQ961231334	29.93	31.83	22	14	0.9	0.3	76.47	-4.55	154.83	500	B
KEGxxx_MN	SKS	EQ961251613	29.93	31.83	15	5.5	0.9	0.1	65.32	13.85	146.31	33	B
KEGxxx_MN	SKS	EQ961251649	29.93	31.83	26	11	0.8	0.1	65.34	13.86	146.26	33	B
KEGxxx_MN	SKS	EQ961510304	29.93	31.83	6	3	1.2	0.1	208.33	-56.72	-26.31	84	A
KEGxxx_MN	SKS	EQ961562322	29.93	31.83	29	17	1	0.4	61.2	18.47	146.87	59.2	B
KEGxxx_MN	SKS	EQ961610112	29.93	31.83	24	3	0.9	0.1	62.85	17.44	145.46	149	A
KEGxxx_MN	SKS	EQ961661504	29.93	31.83	32	13.5	1	0.3	77.35	12.81	125.06	28.8	B
KEGxxx_MN	SKS	EQ961780322	29.93	31.83	21	7	0.9	0.1	57.51	27.73	139.75	468.5	A
KEGxxx_MN	SKS	EQ961881156	29.93	31.83	28	12	0.9	0.3	63.15	15.51	147.66	33	B
KEGxxx_MN	SKS	EQ961882136	29.93	31.83	20	2	0.9	0.1	60.62	21.97	142.83	241.1	A
KEGxxx_MN	SKS	EQ962212312	29.93	31.83	45	12.5	1	0.3	77.77	11.98	125.68	33	B
KEGxxx_MN	SKS	EQ962260638	29.93	31.83	45	17	0.9	0.5	88.62	-0.24	125.02	27.9	B
KEGxxx_MN	SKS	EQ962462041	29.93	31.83	24	7.5	0.7	0.1	68.03	12.32	143.81	33	B
KEGxxx_MN	SKS	EQ962550237	29.93	31.83	14	14	0.8	0.3	50.52	35.54	140.94	55	B
KEGxxx_MN	SKS	EQ962921644	29.93	31.83	9	18	0.7	0.4	53.68	33.69	137.4	337.5	B
KEGxxx_MN	SKS	EQ963260743	29.93	31.83	47	17.5	0.9	0.4	81.96	6.66	126.46	52.7	B
KEGxxx_MN	SKS	EQ963661241	29.93	31.83	15	8.5	1.7	0.5	302.73	15.83	-92.97	99.5	B
KEGxxx_MN	SKS	EQ970701922	29.93	31.83	39	14	0.6	0.2	80.44	7.74	127.65	10	B

KEGxxx_MN	SKS	EQ970911833	29.93	31.83	11	13	0.8	0.3	259.18	-18.3	-69.53	113.8	B
KEGxxx_MN	SKS	EQ971290906	29.93	31.83	28	5	1	0.1	66.78	13.2	144.7	29	A
KEGxxx_MN	SKS	EQ971420750	29.93	31.83	19	1.5	1.2	0.1	311.07	18.68	-101.6	70	B
KEGxxx_MN	SKS	EQ971471509	29.93	31.83	25	15	0.6	0.2	63.77	16.33	145.44	536.3	B
KEGxxx_MN	SKS	EQ971532124	29.93	31.83	9	7.5	1.1	0.3	207.22	-57.78	-25.47	33	B
KEGxxx_MN	SKS	EQ972601450	29.93	31.83	14	8.5	1.1	0.3	85.81	2.11	126.6	33	B
KEGxxx_MN	SKS	EQ972710138	29.93	31.83	24	9	1	0.3	94.3	-3.78	119.73	33	B
KEGxxx_MN	SKS	EQ972730627	29.93	31.83	5	18	0.6	0.3	52.99	31.96	141.88	10	B
KEGxxx_MN	SKS	EQ973092345	29.93	31.83	18	7	0.9	0.1	55.94	27.86	142.61	10	B
KEGxxx_MN	SKS	EQ973142306	29.93	31.83	26	4	0.9	0.1	54.3	31.19	140.49	86	B
KEGxxx_MN	SKS	EQ980010611	29.93	31.83	19	1.5	0.9	0.1	59.52	23.91	141.91	95.6	A
KEGxxx_MN	SKS	EQ980591738	29.93	31.83	35	14.5	1.1	0.4	53.54	33.46	138.12	291.4	B
KEGxxx_MN	SKS	EQ981501818	29.93	31.83	18	12.5	0.7	0.2	46.52	39.03	143.44	33	A
KEGxxx_MN	SKS	EQ981970618	29.93	31.83	23	10	0.9	0.2	68.58	12.05	143.24	10	B
KEGxxx_MN	SKS	EQ982320640	29.93	31.83	20	3.5	0.8	0.1	56.72	28.93	139.33	440.5	B
KEGxxx_MN	SKS	EQ982351357	29.93	31.83	18	1	1.2	0.2	296.12	11.66	-88.04	54.6	B
KEGxxx_MN	SKS	EQ982410830	29.93	31.83	5	4.5	1	0.2	209.35	-55.74	-27.05	33	B
KEGxxx_MN	SKS	EQ982420148	29.93	31.83	26	10	1	0.2	61.58	17.09	148.13	33	B
KEGxxx_MN	SKS	EQ982510910	29.93	31.83	31	2	1.2	0.1	67.13	13.26	144.01	141	B
KEGxxx_MN	SKS	EQ982711923	29.93	31.83	58	17	0.6	0.2	84.41	3.84	126.41	30.1	B
KEGxxx_MN	SKS	EQ982760648	29.93	31.83	3	7.5	1.1	0.2	208.04	-56.62	-25.35	33	B
KEGxxx_MN	SKS	EQ982761512	29.93	31.83	167	11.5	0.9	0.2	208.06	-56.71	-25.57	33	B
KEGxxx_MN	SKS	EQ982810451	29.93	31.83	71	5	1.7	0.4	262.07	-16.12	-71.4	136.2	B
KEGxxx_MN	SKS	EQ982831629	29.93	31.83	37	17	0.9	0.4	91.31	-0.38	119.86	33	B
KEGxxx_MN	SKS	EQ983001133	29.93	31.83	28	9.5	1.2	0.3	51.98	33.49	141.4	33	B
KEGxxx_MN	SKS	EQ983011625	29.93	31.83	37	15.5	0.6	0.2	87.22	0.84	125.97	33	B
KEGxxx_MN	SKS	EQ990120232	29.93	31.83	20	4.5	0.9	0.1	58.11	26.74	140.17	440.6	A
MRNIxx_GE	SKS	EQ000571824	33.12	35.39	3	6.5	1	0.2	291.42	9.41	-78.53	65	B
MRNIxx_GE	SKS	EQ000881100	33.12	35.39	3	3	1.5	0.2	61.58	22.34	143.73	126.5	A
MRNIxx_GE	SKS	EQ001140927	33.12	35.39	2	1.5	1.8	0.1	249.51	-28.31	-62.99	608.5	B
MRNIxx_GE	SKS	EQ001141701	33.12	35.39	4	1.5	1.7	0.1	249.42	-28.38	-62.94	609.8	B
MRNIxx_GE	SKS	EQ001231503	33.12	35.39	2	8.5	1.5	0.3	63.26	17.44	147.52	55	B
MRNIxx_GE	SKS	EQ001680755	33.12	35.39	177	6	1.7	0.4	246.73	-33.88	-70.09	120.2	B
MRNIxx_GE	SKS	EQ002030153	33.12	35.39	9	4.5	2	0.5	295.82	9.42	-85.33	33	B
MRNIxx_GE	SKS	EQ002251026	33.12	35.39	8	1.5	2	0.2	86.71	-3.07	136.11	33	B
MRNIxx_GE	SKS	EQ002401719	33.12	35.39	5	4.5	1.6	0.2	61.66	22.22	143.76	99.6	B
MRNIxx_GE	SKS	EQ002781437	33.12	35.39	0	6	1.5	0.4	283.57	11.12	-62.56	110.3	B
MRNIxx_GE	SKS	EQ003541311	33.12	35.39	7	2.5	1.8	0.1	69.43	11.77	144.76	33	B
MRNIxx_GE	SKS	EQ010140858	33.12	35.39	3	2.5	1.5	0.1	61.76	22.09	143.75	87.3	A
MRNIxx_GE	SKS	EQ011031533	33.12	35.39	159	13	1.1	0.3	207.33	-59.72	-25.59	26	B
MRNIxx_GE	SKS	EQ011660617	33.12	35.39	3	16	1.5	0.6	62.48	18.83	146.98	33	B
MRNIxx_GE	SKS	EQ011801835	33.12	35.39	0	1.5	2	0.2	259.26	-19.52	-66.25	273.9	A
MRNIxx_GE	SKS	EQ011820146	33.12	35.39	4	3	2	0.2	77.98	-4.31	152.96	28	B
MRNIxx_GE	SKS	EQ011841310	33.12	35.39	2	2.5	1.5	0.1	62.55	21.64	142.98	290	A
MRNIxx_GE	SKS	EQ013321432	33.12	35.39	179	4	1.5	0.2	306.1	15.57	-93.11	84.9	B
MRNIxx_GE	SKS	EQ990120232	33.12	35.39	170	7.5	1	0.3	59.98	26.74	140.17	440.6	B

MRNIxx_GE	SKS	EQ991840530	33.12	35.39	178	8.5	0.9	0.2	60.15	26.32	140.48	430.6	B
MRNIxx_GE	SKS	EQ992010053	33.12	35.39	171	3.5	1.5	0.2	59.17	26.9	141.46	89.5	B
RAYNxx_II	SKS	EQ000021258	23.52	45.5	4	2.5	1.2	0.2	24.47	51.45	-175.56	33	B
RAYNxx_II	SKS	EQ000722221	23.52	45.5	175	15.5	0.9	0.3	308.8	14.98	-92.44	62	B
RAYNxx_II	SKS	EQ001120435	23.52	45.5	179	5.5	1	0.2	25.76	51.42	-178.14	33	B
RAYNxx_II	SKS	EQ001140927	23.52	45.5	11	4	1	0.1	248.94	-28.31	-62.99	608.5	A
RAYNxx_II	SKS	EQ001141701	23.52	45.5	15	7	0.9	0.1	248.84	-28.38	-62.94	609.8	A
RAYNxx_II	SKS	EQ001231503	23.52	45.5	10	5	1	0.1	69.33	17.44	147.52	55	A
RAYNxx_II	SKS	EQ001251424	23.52	45.5	3	3.5	1.4	0.2	25.92	51.44	-178.49	33	B
RAYNxx_II	SKS	EQ001470030	23.52	45.5	53	10.5	0.8	0.2	78.17	11.36	139.24	33	B
RAYNxx_II	SKS	EQ001680755	23.52	45.5	11	10.5	1.3	0.3	243.96	-33.88	-70.09	120.2	B
RAYNxx_II	SKS	EQ002401719	23.52	45.5	5	6.5	0.7	0.1	66.54	22.22	143.76	99.6	B
RAYNxx_II	SKS	EQ003011902	23.52	45.5	176	9.5	1.2	0.4	292.83	17.6	-61.19	37.9	B
RAYNxx_II	SKS	EQ003060427	23.52	45.5	24	16.5	0.9	0.4	274.66	-7.95	-74.42	150.9	B
RAYNxx_II	SKS	EQ003402211	23.52	45.5	3	4	1.1	0.2	19.85	52.58	-167.85	33	B
RAYNxx_II	SKS	EQ003630434	23.52	45.5	25	6.5	1.2	0.2	87	-4.05	152.31	33	B
RAYNxx_II	SKS	EQ010140858	23.52	45.5	0	4.5	0.9	0.2	66.66	22.09	143.75	87.3	A
RAYNxx_II	SKS	EQ011072154	23.52	45.5	179	12	1.2	0.4	26.67	51.24	-179.78	33	B
RAYNxx_II	SKS	EQ011552241	23.52	45.5	55	4.5	1.6	0.3	70.33	17.1	145.83	83	B
RAYNxx_II	SKS	EQ011801835	23.52	45.5	18	7.5	0.9	0.2	259.26	-19.52	-66.25	273.9	B
RAYNxx_II	SKS	EQ011820146	23.52	45.5	12	3.5	1.1	0.2	86.98	-4.31	152.96	28	B
RAYNxx_II	SKS	EQ011861353	23.52	45.5	59	9.5	1.4	0.3	265.56	-16.09	-73.99	62	B
RAYNxx_II	SKS	EQ012851502	23.52	45.5	18	15	0.9	0.3	74.66	12.69	144.98	37	B
RAYNxx_II	SKS	EQ020062207	23.52	45.5	175	7	1.2	0.3	21.82	52.06	-171.07	33	B
RAYNxx_II	SKS	EQ020162309	23.52	45.5	18	7.5	0.9	0.2	309.8	15.5	-93.13	80.2	A
RAYNxx_II	SKS	EQ020870456	23.52	45.5	40	13.5	0.8	0.3	257.56	-21.66	-68.33	125.1	B
RAYNxx_II	SKS	EQ021160715	23.52	45.5	169	7.5	0.9	0.1	32.87	53.51	160.63	62.6	B
RAYNxx_II	SKS	EQ021161606	23.52	45.5	15	5.5	0.9	0.2	74.44	13.09	144.62	85.7	A
RAYNxx_II	SKS	EQ021480404	23.52	45.5	21	12	0.6	0.1	249.09	-28.94	-66.8	22.2	B
RAYNxx_II	SKS	EQ021612248	23.52	45.5	2	13.5	0.9	0.3	77.93	10.98	140.69	33	B
RAYNxx_II	SKS	EQ022261357	23.52	45.5	12	8	0.8	0.2	72.88	14.1	146.2	30	A
RAYNxx_II	SKS	EQ023111514	23.52	45.5	2	9	1	0.3	27.12	51.2	179.33	33	B
RAYNxx_II	SKS	EQ023460830	23.52	45.5	45	18.5	0.6	0.6	87.31	-4.79	153.27	34	B
RAYNxx_II	SKS	EQ023620936	23.52	45.5	8	6	1	0.3	20.81	51.43	-168.53	10	B
RAYNxx_II	SKS	EQ030700727	23.52	45.5	14	15	0.8	0.4	87.23	-4.69	153.24	40.2	B
RAYNxx_II	SKS	EQ030741941	23.52	45.5	15	12	1.4	0.6	34.01	52.25	160.39	30.2	B
RAYNxx_II	SKS	EQ030781443	23.52	45.5	15	7	1.7	0.4	33.93	52.21	160.72	33	B
RAYNxx_II	SKS	EQ031741212	23.52	45.5	11	10	1.1	0.4	28.13	51.44	176.78	20	B
RAYNxx_II	SKS	EQ032081141	23.52	45.5	7	11	0.8	0.2	258.28	-20.13	-65.18	345.3	B
RAYNxx_II	SKS	EQ032650445	23.52	45.5	16	17	1	0.4	299.26	19.78	-70.67	10	B
RAYNxx_II	SKS	EQ032961054	23.52	45.5	178	4.5	1.2	0.2	28.2	51.4	176.69	33	B
RAYNxx_II	SKS	EQ033010233	23.52	45.5	37	11.5	1.3	0.3	88.59	-5.38	151.51	65	B
RAYNxx_II	SKS	EQ033210643	23.52	45.5	1	15	1.1	0.4	27.47	51.15	178.65	33	B
RAYNxx_II	SKS	EQ033310607	23.52	45.5	172	12.5	0.9	0.3	16.89	53.61	-163.26	33	B
RAYNxx_II	SKS	EQ033422012	23.52	45.5	2	4	1.1	0.2	27.69	51.09	178.26	33	B
RAYNxx_II	SKS	EQ040770321	23.52	45.5	12	14.5	1	0.3	257.35	-21.12	-65.59	289.8	B

RAYNxx_II	SKS	EQ041240436	23.52	45.5	36	6	1.6	0.3	239.64	-37.69	-73.41	21	B
RAYNxx_II	SKS	EQ042431223	23.52	45.5	12	12	1.1	0.4	37.36	49.54	157.28	11.5	B
RAYNxx_II	SKS	EQ042781920	23.52	45.5	16	4.5	0.9	0.1	72.15	14.55	146.99	7.2	B
RAYNxx_II	SKS	EQ043080831	23.52	45.5	5	11	1.1	0.4	72.27	14.47	146.84	10	B
RAYNxx_II	SKS	EQ043530646	23.52	45.5	169	8	0.9	0.1	38.3	48.84	156.31	11	B
RAYNxx_II	SKS	EQ050171050	23.52	45.5	5	16.5	0.9	0.4	77.94	10.99	140.68	12	B
RAYNxx_II	SKS	EQ050360334	23.52	45.5	4	3.5	1.1	0.2	71.3	16.01	145.87	142.7	B
RAYNxx_II	SKS	EQ090550558	23.52	45.5	4	16	1.1	0.4	73.12	13.79	146.3	9	B
RAYNxx_II	SKS	EQ091731955	23.52	45.5	2	9.5	0.9	0.2	25.88	51.28	-178.2	35	B
RAYNxx_II	SKS	EQ092860537	23.52	45.5	6	4.5	1.2	0.3	19.3	52.75	-167	24	B
RAYNxx_II	SKS	EQ092862021	23.52	45.5	9	6.5	1.4	0.6	19.44	52.6	-167.12	14	B
RAYNxx_II	SKS	EQ093000004	23.52	45.5	15	5.5	1.6	0.4	213.08	-59.96	-65.16	10	B
RAYNxx_II	SKS	EQ093170727	23.52	45.5	12	13	1	0.4	260.26	-17.92	-64.1	608	B
RAYNxx_II	SKS	EQ093181944	23.52	45.5	11	3.5	1	0.1	255.66	-22.97	-66.64	220.4	A
RAYNxx_II	SKS	EQ100591125	23.52	45.5	19	12.5	1.1	0.3	242.91	-34.9	-71.62	46	B
RAYNxx_II	SKS	EQ100632239	23.52	45.5	12	13	0.9	0.3	256.94	-22.23	-68.33	114	A
RAYNxx_II	SKS	EQ100670947	23.52	45.5	3	3	1	0.1	68.75	19.35	144.74	427	A
RAYNxx_II	SKS	EQ100681406	23.52	45.5	8	4.5	1.1	0.3	23.42	51.49	-173.53	35	B
RAYNxx_II	SKS	EQ100701439	23.52	45.5	28	10	1.4	0.3	243.68	-34.29	-71.89	11	B
RAYNxx_II	SKS	EQ100791400	23.52	45.5	9	7.5	1.2	0.3	86.37	-3.36	152.24	414.6	A
RAYNxx_II	SKS	EQ101072315	23.52	45.5	16	17	1	0.4	91.49	-6.67	147.29	53	B
RAYNxx_II	SKS	EQ101911143	23.52	45.5	23	10.5	0.8	0.2	75.63	11.14	146	13	B
RAYNxx_II	SKS	EQ101930011	23.52	45.5	24	16.5	0.6	0.2	256.99	-22.15	-68.22	115	B
RAYNxx_II	SKS	EQ101990556	23.52	45.5	7	2	1.9	0.3	20.74	52.88	-169.85	14	B
RAYNxx_II	SKS	EQ102110356	23.52	45.5	178	16	0.7	0.3	33.98	52.5	159.84	23	B
RAYNxx_II	SKS	EQ102160715	23.52	45.5	12	3.5	1.6	0.4	90.56	-5.49	146.82	220	B
RAYNxx_II	SKS	EQ102161258	23.52	45.5	12	10	1.4	0.6	26	51.42	-178.65	27	B
RAYNxx_II	SKS	EQ102810326	23.52	45.5	3	2.5	1	0.1	24.42	51.37	-175.36	19	B
RAYNxx_II	SKS	EQ110010956	23.52	45.5	12	14.5	1.5	0.5	250.59	-26.8	-63.14	576.8	B
RAYNxx_II	SKS	EQ110531409	23.52	45.5	0	5.5	0.9	0.2	66.61	22.11	143.84	112.8	B
RAYNxx_II	SKS	EQ110921059	23.52	45.5	12	6.5	1.3	0.3	260.07	-19.58	-69.07	84.4	B
RAYNxx_II	SKS	EQ112620814	23.52	45.5	1	2.5	1.1	0.1	22.3	52.04	-171.98	31	B
RAYNxx_II	SKS	EQ112870335	23.52	45.5	13	15.5	0.9	0.5	91.17	-6.57	147.88	37	B
RAYNxx_II	SKS	EQ112980324	23.52	45.5	2	2	0.9	0.1	22.15	52.16	-171.83	38	A
RAYNxx_II	SKS	EQ113040716	23.52	45.5	175	5	1	0.1	26.97	52.37	177.93	159	B
RAYNxx_II	SKS	EQ113261848	23.52	45.5	13	3	1	0.2	263.24	-15.36	-65.09	549.9	B
RAYNxx_II	SKS	EQ120812215	23.52	45.5	17	7	1	0.3	91.61	-6.24	145.96	118	B
RAYNxx_II	SKS	EQ121080713	23.52	45.5	16	13	0.9	0.3	90.43	-5.46	147.12	198	B
RAYNxx_II	SKS	EQ121351000	23.52	45.5	10	13	1.1	0.4	262.31	-17.68	-69.59	105.9	B
RAYNxx_II	SKS	EQ121490507	23.52	45.5	15	5.5	0.9	0.1	249.25	-28.04	-63.09	586.9	B
RAYNxx_II	SKS	EQ122102003	23.52	45.5	16	17.5	1	0.4	87.22	-4.65	153.17	41	B
RAYNxx_II	SKS	EQ122231837	23.52	45.5	5	7.5	1	0.3	19.59	52.63	-167.42	13	B
RAYNxx_II	SKS	EQ122551636	23.52	45.5	8	13	1	0.4	76.15	11.84	143.22	8	B
RAYNxx_II	SKS	EQ123191902	23.52	45.5	48	2.5	1.9	0.2	249.75	-29.12	-71.19	63	B
RAYNxx_II	SKS	EQ123200821	23.52	45.5	40	7	1.4	0.2	87.76	-3.11	148.27	10	B
RAYNxx_II	SKS	EQ123240944	23.52	45.5	13	12.5	1	0.5	88.87	-5.7	151.6	13	B

RAYNxx_II	SKS	EQ123271307	23.52	45.5	9	4	1.5	0.2	255.04	-22.74	-63.57	516.6	B
RAYNxx_II	SKS	EQ123500449	23.52	45.5	12	9.5	1.1	0.5	28.75	52.27	174.04	26	B
RAYNxx_II	SKS	EQ970911833	23.52	45.5	39	18	0.6	0.4	261.61	-18.3	-69.53	113.8	B
RAYNxx_II	SKS	EQ970951223	23.52	45.5	12	7.5	1.1	0.3	91.27	-6.49	147.41	69.1	B
RAYNxx_II	SKS	EQ971281329	23.52	45.5	7	4.5	1.2	0.3	21.87	51.72	-170.8	33	B
RAYNxx_II	SKS	EQ971290906	23.52	45.5	14	10	0.9	0.2	74.31	13.2	144.7	29	B
RAYNxx_II	SKS	EQ971471509	23.52	45.5	5	9.5	1.1	0.3	71.19	16.33	145.44	536.3	B
RAYNxx_II	SKS	EQ971682103	23.52	45.5	2	15	0.9	0.3	26.38	51.35	-179.33	33	B
RAYNxx_II	SKS	EQ973322253	23.52	45.5	31	15.5	0.6	0.2	266.25	-13.74	-68.79	586	B
RAYNxx_II	SKS	EQ973411756	23.52	45.5	1	10	1.2	0.3	31.16	54.66	162.88	33	B
RAYNxx_II	SKS	EQ973510438	23.52	45.5	10	6	1.2	0.4	27.34	51.19	178.87	20	B
RAYNxx_II	SKS	EQ981350558	23.52	45.5	9	4	1	0.1	73.35	14.18	144.88	154.1	A
RAYNxx_II	SKS	EQ981480458	23.52	45.5	173	9.5	0.9	0.2	34.34	52.15	159.64	47	B
RAYNxx_II	SKS	EQ990640033	23.52	45.5	44	9.5	1.1	0.2	259.09	-20.42	-68.9	110.9	B
RAYNxx_II	SKS	EQ990951108	23.52	45.5	26	17	0.9	0.4	89.57	-5.59	149.57	150	B
RAYNxx_II	SKS	EQ990960822	23.52	45.5	13	7	0.9	0.2	91.47	-6.53	147.01	33	B
RAYNxx_II	SKS	EQ991131856	23.52	45.5	10	4.5	0.9	0.1	74.2	13.12	145.14	52.5	B
RAYNxx_II	SKS	EQ992580301	23.52	45.5	17	15	0.8	0.3	258.05	-20.93	-67.28	218	B
RAYNxx_II	SKS	EQ993171931	23.52	45.5	15	5	1.8	0.5	29.04	53.36	171.42	33	B
RAYNxx_II	SKS	EQ993312312	23.52	45.5	176	7	1.1	0.2	29.97	54.95	165.66	33	B
RAYNxx_XI	SKS	EQ960820324	23.52	45.5	7	14.5	1	0.4	27.4	51.22	178.7	20.4	B
RAYNxx_XI	SKS	EQ960881951	23.52	45.5	7	11	1.1	0.5	20.48	52.31	-168.78	33	B
RAYNxx_XI	SKS	EQ960901305	23.52	45.5	8	2.5	1.1	0.2	20.51	52.21	-168.73	33	A
RAYNxx_XI	SKS	EQ961251613	23.52	45.5	4	7	1.4	0.3	73.06	13.85	146.31	33	B
RIYDxx_XI	SKS	EQ961971651	24.72	46.64	179	18.5	0.8	0.3	69.4	18.73	145.63	176.5	B
RIYDxx_XI	SKS	EQ962802013	24.72	46.64	11	11	1.1	0.4	356.24	49.05	-127.88	10	B
RIYDxx_XI	SKS	EQ970230215	24.72	46.64	24	9.5	0.5	0.1	257.4	-22	-65.72	276.2	B
UQSKxx_XI	SKS	EQ961621524	25.79	42.36	176	6.5	1.4	0.2	23.41	51.48	-176.85	26.3	B
UQSKxx_XI	SKS	EQ961881156	25.79	42.36	174	5.5	1.5	0.4	69.39	15.51	147.66	33	B
UQSKxx_XI	SKS	EQ961882136	25.79	42.36	176	4	1.5	0.2	65.9	21.97	142.83	241.1	B
UQSKxx_XI	SKS	EQ961971651	25.79	42.36	174	5	1.5	0.4	67.51	18.73	145.63	176.5	B
UQSKxx_XI	SKS	EQ963661241	25.79	42.36	177	9.5	1.2	0.3	308.62	15.83	-92.97	99.5	A
UQSKxx_XI	SKS	EQ970230215	25.79	42.36	176	3	1.5	0.4	256.54	-22	-65.72	276.2	B
AFIFxx_XI	PKS	EQ953350520	23.93	43.04	5	16.5	1.1	0.4	312.66	10.16	-104	10	B
AFIFxx_XI	PKS	EQ953411004	23.93	43.04	160	15	0.9	0.2	96.73	-20.03	168.81	15.5	B
AFIFxx_XI	PKS	EQ961470143	23.93	43.04	179	5	1.4	0.5	98.71	-22.19	171.48	108.2	B
BGIOxx_GE	PKS	EQ942341726	31.72	35.09	4	1.5	1.6	0.1	76.99	-11.51	166.45	142.1	B
BGIOxx_GE	PKS	EQ942741635	31.72	35.09	8	3.5	1.7	0.3	83.55	-17.75	167.68	16.6	B
BGIOxx_GE	PKS	EQ943070307	31.72	35.09	7	2.5	1.4	0.2	76.49	-10.93	166.25	155.8	B
BGIOxx_GE	PKS	EQ950842244	31.72	35.09	2	2	1.8	0.2	76.65	-11	166.12	79.4	B
BGIOxx_GE	PKS	EQ951030234	31.72	35.09	0	2	1.6	0.2	76.42	-13.45	170.43	637.7	B
BGIOxx_GE	PKS	EQ951252248	31.72	35.09	13	3.5	1.3	0.2	83.9	-18.55	168.78	116.7	B
BGIOxx_GE	PKS	EQ952431710	31.72	35.09	3	2	2	0.4	82.01	-15.84	166.43	16.8	B
BGIOxx_GE	PKS	EQ952691824	31.72	35.09	6	2	1.7	0.2	78.42	-13.1	167	186.4	B
BGIOxx_GE	PKS	EQ952861522	31.72	35.09	5	4.5	1	0.1	143.31	-59.01	158.28	14.4	A
BGIOxx_GE	PKS	EQ952960358	31.72	35.09	6	2.5	1.4	0.2	79.6	-14.28	167.29	199.4	B

BGIOxx_GE	PKS	EQ953411004	31.72	35.09	8	3	1.8	0.3	85.81	-20.03	168.81	15.5	B
EILxxx_GE	PKS	EQ000162319	29.67	34.95	13	5.5	1.2	0.2	78.91	-11.66	166.32	39.5	B
EILxxx_GE	PKS	EQ001271344	29.67	34.95	15	5	1	0.2	79.06	-11.3	165.43	12	B
EILxxx_GE	PKS	EQ001981725	29.67	34.95	6	5	1.2	0.3	79.66	-12.4	166.51	33	B
EILxxx_GE	PKS	EQ002160109	29.67	34.95	24	14	0.9	0.2	79.27	-12.04	166.45	33	B
EILxxx_GE	PKS	EQ002220008	29.67	34.95	10	5	1.2	0.3	82.73	-15.69	167.99	33	B
EILxxx_GE	PKS	EQ002781658	29.67	34.95	7	7.5	1.1	0.5	83.04	-15.42	166.91	23	B
EILxxx_GE	PKS	EQ010091649	29.67	34.95	2	6	1.9	0.7	82.27	-14.93	167.17	103	B
EILxxx_GE	PKS	EQ010190810	29.67	34.95	5	3.5	1.2	0.2	78.87	-11.66	166.38	50	B
EILxxx_GE	PKS	EQ012992305	29.67	34.95	9	5.5	1.4	0.4	86.26	-18.49	168.11	33	B
EILxxx_GE	PKS	EQ020150447	29.67	34.95	14	4	1.2	0.2	84.97	-17.33	167.72	10	B
EILxxx_GE	PKS	EQ021682126	29.67	34.95	9	4.5	1.1	0.2	79.96	-12.59	166.38	33	A
EILxxx_GE	PKS	EQ021800239	29.67	34.95	8	3	1.2	0.2	79.64	-12.4	166.52	33	A
EILxxx_GE	PKS	EQ031332121	29.67	34.95	11	2.5	1.4	0.2	84.9	-17.29	167.74	33	B
EILxxx_GE	PKS	EQ032331212	29.67	34.95	170	11	1	0.2	125.93	-45.1	167.14	28	B
EILxxx_GE	PKS	EQ032731937	29.67	34.95	3	4	1.2	0.2	126.5	-45.49	167.04	10	B
EILxxx_GE	PKS	EQ040510558	29.67	34.95	13	3	1.1	0.2	78.77	-11.61	166.45	84	B
EILxxx_GE	PKS	EQ043041326	29.67	34.95	11	4.5	1.2	0.2	82.4	-15.47	168.08	10	B
EILxxx_GE	PKS	EQ050391448	29.67	34.95	9	3	1.3	0.2	81.39	-14.25	167.26	206.3	B
EILxxx_GE	PKS	EQ060660628	29.67	34.95	19	7	1	0.2	82	-14.81	167.37	136.2	B
EILxxx_GE	PKS	EQ060780436	29.67	34.95	11	8.5	1.2	0.3	76.98	-13.43	172.39	10	B
EILxxx_GE	PKS	EQ062192218	29.67	34.95	8	6	1.3	0.4	82.98	-15.8	167.79	150	B
EILxxx_GE	PKS	EQ070840040	29.67	34.95	13	13.5	1	0.5	88.45	-20.62	169.36	34	B
EILxxx_GE	PKS	EQ070932026	29.67	34.95	10	5.5	1.5	0.4	88.65	-20.63	168.99	12	B
EILxxx_GE	PKS	EQ071151334	29.67	34.95	2	7	1.2	0.4	81.68	-14.28	166.86	55	B
EILxxx_GE	PKS	EQ072730947	29.67	34.95	15	16.5	1.4	0.7	131.6	-49.14	164.11	18	B
EILxxx_GE	PKS	EQ083451315	29.67	34.95	13	7	1	0.2	79.54	-12.34	166.57	51	B
EILxxx_GE	PKS	EQ092220406	29.67	34.95	9	6.5	1.2	0.3	79	-11.61	166.09	35	B
EILxxx_GE	PKS	EQ092812335	29.67	34.95	16	6	1.3	0.2	79.53	-12.4	166.7	35	B
EILxxx_GE	PKS	EQ092850937	29.67	34.95	8	5.5	1.1	0.2	79.67	-12.41	166.5	42	B
EILxxx_GE	PKS	EQ092901318	29.67	34.95	3	6	1.4	0.4	80.43	-13.02	166.42	35	B
EILxxx_GE	PKS	EQ092961514	29.67	34.95	2	10.5	1.5	0.6	79.7	-12.2	166.05	31.1	B
EILxxx_GE	PKS	EQ093041909	29.67	34.95	3	2.5	1.2	0.2	78.55	-11.38	166.38	133.9	A
EILxxx_GE	PKS	EQ093271836	29.67	34.95	7	10	0.8	0.2	80.07	-12.62	166.25	35	B
EILxxx_GE	PKS	EQ100631402	29.67	34.95	0	4.5	1.3	0.4	80.59	-13.57	167.23	176	B
EILxxx_GE	PKS	EQ101010219	29.67	34.95	5	9	1.1	0.4	80.32	-12.97	166.52	10	B
EILxxx_GE	PKS	EQ102222318	29.67	34.95	8	14.5	0.9	0.3	81.59	-14.46	167.35	191.6	B
EILxxx_GE	PKS	EQ110760803	29.67	34.95	9	2.5	1.2	0.2	84.78	-17.27	167.9	10	B
EILxxx_GE	PKS	EQ111720204	29.67	34.95	9	4.5	1.1	0.2	79.19	-11.48	165.55	14	B
EILxxx_GE	PKS	EQ112440614	29.67	34.95	11	5	1.1	0.2	79.51	-12.36	166.66	39	A
EILxxx_GE	PKS	EQ120361640	29.67	34.95	7	4.5	1.1	0.3	86.04	-17.95	167.23	8	B
EILxxx_GE	PKS	EQ121740431	29.67	34.95	14	3.5	1.3	0.1	138.28	-54.36	158.79	14	B
EILxxx_GE	PKS	EQ121880228	29.67	34.95	3	9	1.4	0.6	81.84	-14.66	167.34	160.1	B
EILxxx_GE	PKS	EQ122491309	29.67	34.95	3	2.5	1.5	0.2	79.74	-12.48	166.51	27	B
EILxxx_GE	PKS	EQ122942300	29.67	34.95	5	5	1.2	0.4	80.98	-13.55	166.56	36	B
EILxxx_GE	PKS	EQ123370054	29.67	34.95	8	2	1.4	0.2	84.55	-16.98	167.65	32	B

EILxxx_GE	PKS	EQ123562228	29.67	34.95	8	5	1.1	0.2	81.47	-14.33	167.29	188	A
EILxxx_GE	PKS	EQ130310333	29.67	34.95	7	9	1	0.3	77.68	-10.63	166.38	9.2	B
EILxxx_GE	PKS	EQ130380030	29.67	34.95	2	9	1.2	0.4	79.78	-11.66	164.94	8	B
EILxxx_GE	PKS	EQ130391112	29.67	34.95	8	8	0.9	0.2	78.32	-10.9	165.89	15.9	B
EILxxx_GE	PKS	EQ130402102	29.67	34.95	12	7.5	0.9	0.2	78.41	-10.95	165.84	15.6	B
EILxxx_GE	PKS	EQ130420940	29.67	34.95	7	3.5	1.1	0.2	77.95	-11.06	166.74	34.3	B
EILxxx_GE	PKS	EQ131560447	29.67	34.95	5	4.5	1.3	0.3	78.62	-11.4	166.3	39	B
EILxxx_GE	PKS	EQ970292319	29.67	34.95	13	4	1.1	0.2	80.33	-12.9	166.38	33	B
EILxxx_GE	PKS	EQ971130347	29.67	34.95	7	3.5	1.8	0.3	81.14	-13.6	166.39	33	B
EILxxx_GE	PKS	EQ973191859	29.67	34.95	5	9.5	1.4	0.6	82.42	-15.15	167.38	123.1	B
EILxxx_GE	PKS	EQ980792108	29.67	34.95	6	5	1.3	0.2	132.73	-50.01	163.11	10	B
EILxxx_GE	PKS	EQ982060239	29.67	34.95	9	9	1.1	0.3	80.86	-13.61	166.87	43.5	B
EILxxx_GE	PKS	EQ982260055	29.67	34.95	11	2.5	1.4	0.2	78.71	-11.43	166.22	57.6	B
EILxxx_GE	PKS	EQ982641209	29.67	34.95	6	3.5	1.3	0.2	80.86	-13.57	166.79	33	B
EILxxx_GE	PKS	EQ982730303	29.67	34.95	9	2.5	1.6	0.3	84.74	-17.2	167.83	33	B
EILxxx_GE	PKS	EQ990372147	29.67	34.95	3	3	1.8	0.4	80.07	-12.85	166.7	90.1	B
EILxxx_GE	PKS	EQ990452112	29.67	34.95	10	9	1.1	0.4	82.49	-15.51	168	10	B
EILxxx_GE	PKS	EQ992601454	29.67	34.95	6	2.5	1.5	0.2	80.85	-13.79	167.24	196.8	B
HALMxx_XI	PKS	EQ961470143	22.85	44.32	16	2	1.5	0.3	100	-22.19	171.48	108.2	B
HALMxx_XI	PKS	EQ963100941	22.85	44.32	5	8	1.1	0.3	111.68	-31.16	180	369.4	A
JERxxx_GE	PKS	EQ000162319	31.77	35.2	6	2.5	1.4	0.1	77.28	-11.66	166.32	39.5	B
JERxxx_GE	PKS	EQ000170004	31.77	35.2	1	5.5	1.2	0.3	77.22	-11.59	166.3	33	B
JERxxx_GE	PKS	EQ001620917	31.77	35.2	4	2	1.5	0.2	77.1	-11.45	166.24	33	A
JERxxx_GE	PKS	EQ002781658	31.77	35.2	3	6.5	1.2	0.6	81.22	-15.42	166.91	23	B
JERxxx_GE	PKS	EQ010091649	31.77	35.2	6	3.5	1.3	0.3	80.47	-14.93	167.17	103	B
JERxxx_GE	PKS	EQ010190810	31.77	35.2	4	2.5	1.6	0.2	77.25	-11.66	166.38	50	B
JERxxx_GE	PKS	EQ010591230	31.77	35.2	7	2	1.6	0.2	87.65	-21.99	170.21	10	B
JERxxx_GE	PKS	EQ021012156	31.77	35.2	7	2	1.6	0.2	79.49	-14.39	167.69	10	B
JERxxx_GE	PKS	EQ021682126	31.77	35.2	3	1.5	1.6	0.2	78.29	-12.59	166.38	33	B
JERxxx_GE	PKS	EQ021800239	31.77	35.2	179	1.5	1.8	0.2	77.98	-12.4	166.52	33	B
JERxxx_GE	PKS	EQ023311643	31.77	35.2	3	8.5	1.4	0.4	79.51	-14.49	167.83	33	B
JERxxx_GE	PKS	EQ031332121	31.77	35.2	7	1.5	1.6	0.2	82.96	-17.29	167.74	33	B
JERxxx_GE	PKS	EQ962280733	31.77	35.2	6	1.5	1.5	0.1	78.79	-13.3	166.84	33	B
JERxxx_GE	PKS	EQ962450645	31.77	35.2	6	1.5	1.6	0.1	77.25	-11.81	166.62	187.2	A
JERxxx_GE	PKS	EQ970292319	31.77	35.2	8	3	1.5	0.2	78.65	-12.9	166.38	33	B
JERxxx_GE	PKS	EQ971121651	31.77	35.2	9	2	1.5	0.2	78.96	-13.22	166.45	33	B
JERxxx_GE	PKS	EQ971130347	31.77	35.2	5	2.5	1.7	0.2	79.43	-13.6	166.39	33	B
JERxxx_GE	PKS	EQ972681954	31.77	35.2	9	1.5	1.5	0.1	78.12	-12.5	166.47	33	B
JERxxx_GE	PKS	EQ973041229	31.77	35.2	5	3	1.8	0.2	78.52	-13.11	166.92	182.8	B
JERxxx_GE	PKS	EQ973191859	31.77	35.2	7	2	1.6	0.2	80.59	-15.15	167.38	123.1	A
JERxxx_GE	PKS	EQ980262306	31.77	35.2	161	10.5	0.8	0.2	127.46	-47.51	165.18	33	B
JERxxx_GE	PKS	EQ981971156	31.77	35.2	5	2.5	1.6	0.2	76.71	-11.04	166.16	110.2	A
JERxxx_GE	PKS	EQ982060239	31.77	35.2	5	1.5	1.5	0.1	79.12	-13.61	166.87	43.5	A
JERxxx_GE	PKS	EQ982260055	31.77	35.2	4	3	1.5	0.2	77.1	-11.43	166.22	57.6	B
JERxxx_GE	PKS	EQ982641209	31.77	35.2	0	1.5	1.6	0.2	79.14	-13.57	166.79	33	B
KEGxxx_MN	PKS	EQ903561901	29.93	31.83	30	12	1	0.2	79.51	-14.95	168.04	26.7	B

KEGxxx_MN	PKS	EQ922172108	29.93	31.83	34	9.5	0.8	0.1	76.97	-12.13	166.59	91	B
KEGxxx_MN	PKS	EQ922592103	29.93	31.83	28	5.5	0.7	0.1	78.88	-14.05	167.27	184.2	A
KEGxxx_MN	PKS	EQ931901303	29.93	31.83	30	14	0.8	0.2	82.77	-17.37	167.93	16.8	B
KEGxxx_MN	PKS	EQ941240637	29.93	31.83	17	8.5	0.7	0.2	82.13	-17.05	168.26	206.4	B
KEGxxx_MN	PKS	EQ942341726	29.93	31.83	17	5.5	1.1	0.2	76.33	-11.51	166.45	142.1	B
KEGxxx_MN	PKS	EQ961620104	29.93	31.83	46	12	0.8	0.2	78.26	-13.48	167.13	200.1	B
KEGxxx_MN	PKS	EQ962450645	29.93	31.83	43	6	1.2	0.2	76.57	-11.81	166.62	187.2	B
KEGxxx_MN	PKS	EQ962581310	29.93	31.83	22	10.5	1	0.2	75.9	-10.88	165.99	72.7	B
KEGxxx_MN	PKS	EQ972631611	29.93	31.83	37	16.5	1.2	0.4	94.59	-28.68	-177.62	30	B
KEGxxx_MN	PKS	EQ973191859	29.93	31.83	47	14.5	0.9	0.3	80.2	-15.15	167.38	123.1	B
KEGxxx_MN	PKS	EQ980840312	29.93	31.83	170	8.5	1	0.2	148.64	-62.88	149.53	10	B
KEGxxx_MN	PKS	EQ981971156	29.93	31.83	51	7.5	1.4	0.3	75.98	-11.04	166.16	110.2	B
KEGxxx_MN	PKS	EQ982121240	29.93	31.83	21	13	0.9	0.3	87.67	-21.61	169.82	33	B
KEGxxx_MN	PKS	EQ982641209	29.93	31.83	12	12	1.1	0.3	78.6	-13.57	166.79	33	B
MRNIxx_GE	PKS	EQ001620917	33.12	35.39	6	3.5	1.9	0.2	76.12	-11.45	166.24	33	B
MRNIxx_GE	PKS	EQ001981725	33.12	35.39	5	3	1.9	0.2	76.97	-12.4	166.51	33	B
MRNIxx_GE	PKS	EQ002101238	33.12	35.39	7	2	2	0.2	76.94	-12.36	166.49	37.3	B
MRNIxx_GE	PKS	EQ002132244	33.12	35.39	5	3.5	1.8	0.3	76.14	-16.7	174.54	10	B
MRNIxx_GE	PKS	EQ002670842	33.12	35.39	7	1.5	2	0.1	76.25	-11.67	166.4	125	B
MRNIxx_GE	PKS	EQ002781658	33.12	35.39	3	2.5	1.7	0.4	80.11	-15.42	166.91	23	B
MRNIxx_GE	PKS	EQ010190810	33.12	35.39	8	1.5	1.8	0.1	76.25	-11.66	166.38	50	A
MRNIxx_GE	PKS	EQ013461253	33.12	35.39	7	2.5	2	0.2	81.66	-17.19	167.72	33	B
RAYNxx_II	PKS	EQ002132244	23.52	45.5	18	18	0.9	0.4	91.74	-16.7	174.54	10	B
RAYNxx_II	PKS	EQ091960922	23.52	45.5	21	9	1.2	0.4	130.5	-45.76	166.56	12	B
RAYNxx_II	PKS	EQ092881748	23.52	45.5	179	18.5	0.6	0.3	307.64	3.27	-103.82	10	B
RAYNxx_II	PKS	EQ093131044	23.52	45.5	17	2.5	1.4	0.2	91.03	-17.24	178.33	595	B
RAYNxx_II	PKS	EQ102030503	23.52	45.5	33	10.5	1	0.3	92.2	-15.13	168.16	6	B
RAYNxx_II	PKS	EQ112800858	23.52	45.5	2	11.5	0.9	0.3	113.04	-32.51	-179.04	36	B
RAYNxx_II	PKS	EQ113570058	23.52	45.5	20	4	1.4	0.2	128.13	-43.49	172.8	9.7	B
RAYNxx_II	PKS	EQ113570218	23.52	45.5	22	9	1.4	0.5	128.18	-43.53	172.74	6.9	B
RAYNxx_II	PKS	EQ972921553	23.52	45.5	24	8.5	1	0.3	95.53	-21.8	-175.01	33	B
RAYNxx_II	PKS	EQ980881948	23.52	45.5	18	17	0.9	0.3	90.47	-17.55	-179.09	537.2	B
AFIFxx_XI	SKK	EQ953451409	23.93	43.04	4	6.5	1.4	0.2	321.45	18.93	-105.47	20	B
AFIFxx_XI	SKK	EQ960791712	23.93	43.04	173	15	0.9	0.3	311.7	15.85	-97.31	33	B
AFIFxx_XI	SKK	EQ961620403	23.93	43.04	169	4.5	1.6	0.2	24.18	51.56	-177.63	33	B
BGIOxx_GE	SKK	EQ941852136	31.72	35.09	171	7	1.2	0.2	308.05	14.89	-97.32	14.6	B
BGIOxx_GE	SKK	EQ942401502	31.72	35.09	15	5	1.1	0.2	308.54	17.01	-95.84	68	B
BGIOxx_GE	SKK	EQ950850216	31.72	35.09	164	4.5	0.9	0.1	210.99	-55.95	-28.21	48.4	B
BGIOxx_GE	SKK	EQ951401345	31.72	35.09	169	6	1	0.2	210.75	-56.03	-27.74	100	B
BGIOxx_GE	SKK	EQ951481959	31.72	35.09	175	6	1.5	0.5	251.46	-28.98	-71.22	42	B
BGIOxx_GE	SKK	EQ951750658	31.72	35.09	11	8	1.6	0.4	77.53	-3.96	153.93	386	B
BGIOxx_GE	SKK	EQ952091429	31.72	35.09	5	1.5	1.9	0.1	76.39	-21.18	-175.39	92.4	B
BGIOxx_GE	SKK	EQ953170738	31.72	35.09	6	10	1.1	0.2	64.22	-15.11	-173.47	10	B
BGIOxx_GE	SKK	EQ960771448	31.72	35.09	10	11	1.6	0.5	80.09	-14.7	167.3	164.4	B
EILxxx_GE	SKK	EQ000261326	29.67	34.95	7	8.5	1	0.3	71.48	-17.27	-174	33	B
EILxxx_GE	SKK	EQ002700617	29.67	34.95	177	4	1.6	0.3	71.24	-17.18	-173.93	56	B

EILxxx_GE	SKK	EQ003530119	29.67	34.95	13	6	1.4	0.4	82.58	-21.18	-179.12	628.2	B
EILxxx_GE	SKK	EQ012750048	29.67	34.95	2	7.5	1.1	0.2	69.41	-16.18	-173.82	106.9	B
EILxxx_GE	SKK	EQ012851502	29.67	34.95	179	6	1.3	0.3	68.86	12.69	144.98	37	B
EILxxx_GE	SKK	EQ023460830	29.67	34.95	6	5	1.8	0.4	79.62	-4.79	153.27	34	B
EILxxx_GE	SKK	EQ030700727	29.67	34.95	1	1	1.8	0.1	79.55	-4.69	153.24	40.2	B
EILxxx_GE	SKK	EQ032451828	29.67	34.95	11	10.5	1.2	0.3	67.17	-15.23	-173.22	10	B
EILxxx_GE	SKK	EQ040251143	29.67	34.95	11	9	1.3	0.3	70.9	-16.83	-174.2	129.8	B
EILxxx_GE	SKK	EQ040722213	29.67	34.95	3	16.5	1.2	0.4	69.69	-15.58	-175.1	271.5	B
EILxxx_GE	SKK	EQ042632026	29.67	34.95	156	15	0.6	0.2	23.78	52.21	174.03	25	B
EILxxx_GE	SKK	EQ043080831	29.67	34.95	178	5	1.5	0.2	66.33	14.47	146.84	10	B
EILxxx_GE	SKK	EQ050401846	29.67	34.95	2	5.5	1.4	0.2	58.29	26.09	144	24	B
EILxxx_GE	SKK	EQ060712054	29.67	34.95	4	2	2	0.2	79.68	-5.07	153.66	47.3	B
EILxxx_GE	SKK	EQ061201917	29.67	34.95	3	8	0.8	0.2	252.38	-27.02	-71.02	12	B
EILxxx_GE	SKK	EQ062181816	29.67	34.95	0	7.5	1.4	0.2	58.26	26.12	144.01	20	B
EILxxx_GE	SKK	EQ062192218	29.67	34.95	4	2.5	1.8	0.3	82.98	-15.8	167.79	150	B
EILxxx_GE	SKK	EQ062231430	29.67	34.95	12	6.5	1.2	0.2	312.84	18.54	-101.05	56	B
EILxxx_GE	SKK	EQ070940634	29.67	34.95	8	6.5	1.1	0.3	80.68	-7.76	156.49	17	B
EILxxx_GE	SKK	EQ071210015	29.67	34.95	9	2.5	1.9	0.2	80.83	-7.12	155.13	9	B
EILxxx_GE	SKK	EQ071262111	29.67	34.95	0	2.5	1.6	0.4	79.7	-19.4	-179.35	676.4	B
EILxxx_GE	SKK	EQ071870109	29.67	34.95	14	11	1.4	0.4	305.91	16.35	-93.99	113	B
EILxxx_GE	SKK	EQ072821503	29.67	34.95	5	3.5	1.5	0.3	79.86	-4.81	152.89	39	B
EILxxx_GE	SKK	EQ073220540	29.67	34.95	5	15	0.7	0.3	254.92	-22.64	-66.32	246.4	B
EILxxx_GE	SKK	EQ073500809	29.67	34.95	3	5.5	0.9	0.2	256.17	-22.95	-70.18	45	B
EILxxx_GE	SKK	EQ083240611	29.67	34.95	178	7.5	2	0.4	291.95	8.27	-82.97	32	B
EILxxx_GE	SKK	EQ093181944	29.67	34.95	19	18.5	0.6	0.2	254.73	-22.97	-66.64	220.4	B
EILxxx_GE	SKK	EQ100750221	29.67	34.95	170	3.5	1.4	0.2	243.23	-36.22	-73.26	18	B
EILxxx_GE	SKK	EQ100791400	29.67	34.95	179	6	1.5	0.5	78.85	-3.36	152.24	414.6	B
EILxxx_GE	SKK	EQ101471714	29.67	34.95	10	6.5	1.8	0.4	81.1	-13.7	166.64	31	B
EILxxx_GE	SKK	EQ102810326	29.67	34.95	0	11.5	0.9	0.3	18.51	51.37	-175.36	19	B
EILxxx_GE	SKK	EQ102810349	29.67	34.95	178	15.5	1	0.4	18.45	51.29	-175.18	27.7	B
EILxxx_GE	SKK	EQ110022020	29.67	34.95	170	14	1	0.5	240.85	-38.35	-73.33	24	B
EILxxx_GE	SKK	EQ110651432	29.67	34.95	171	11	1.2	0.2	209.94	-56.42	-27.06	87.7	B
EILxxx_GE	SKK	EQ110921059	29.67	34.95	17	17	0.8	0.3	259.03	-19.58	-69.07	84.4	B
EILxxx_GE	SKK	EQ110931407	29.67	34.95	1	2.5	1.5	0.2	76.21	-17.64	-178.59	551.7	B
EILxxx_GE	SKK	EQ110971311	29.67	34.95	22	3	2	0.3	306.83	17.21	-94.34	166.2	B
EILxxx_GE	SKK	EQ111711636	29.67	34.95	14	17	0.9	0.4	256.61	-21.7	-68.23	128	B
EILxxx_GE	SKK	EQ112480952	29.67	34.95	179	5	1.5	0.4	67.7	-15.3	-173.62	37	B
EILxxx_GE	SKK	EQ121490507	29.67	34.95	23	13.5	0.9	0.2	248.42	-28.04	-63.09	586.9	B
EILxxx_GE	SKK	EQ122071120	29.67	34.95	1	8	1.3	0.4	80.79	-9.69	159.73	20	B
EILxxx_GE	SKK	EQ123191902	29.67	34.95	178	12	1.2	0.4	250.26	-29.12	-71.19	63	B
EILxxx_GE	SKK	EQ131340032	29.67	34.95	17	12	1.1	0.2	63.66	18.73	145.29	602.3	A
EILxxx_GE	SKK	EQ982810451	29.67	34.95	11	7	0.7	0.2	263.39	-16.12	-71.4	136.2	B
EILxxx_GE	SKK	EQ991031038	29.67	34.95	17	14.5	0.9	0.3	81.15	-21.42	-176.46	164.2	B
EILxxx_GE	SKK	EQ992960212	29.67	34.95	2	1.5	1.5	0.2	79.56	-4.81	153.41	83.3	B
EILxxx_GE	SKK	EQ993250351	29.67	34.95	5	6.5	1	0.3	256.79	-21.75	-68.78	101.2	B
HALMxx_XI	SKK	EQ961231334	22.85	44.32	8	9.5	1.4	0.7	86.19	-4.55	154.83	500	B

HALMxx_XI	SKK	EQ970230215	22.85	44.32	179	2	2	0.3	255.79	-22	-65.72	276.2	B
JERxxx_GE	SKK	EQ000081647	31.77	35.2	3	7.5	1.4	0.3	67.98	-16.92	-174.25	183.4	B
JERxxx_GE	SKK	EQ001140927	31.77	35.2	168	3	1.1	0.3	248.94	-28.31	-62.99	608.5	B
JERxxx_GE	SKK	EQ001252036	31.77	35.2	0	3.5	1.1	0.2	73.7	-17.91	-178.52	515.8	B
JERxxx_GE	SKK	EQ002700617	31.77	35.2	1	2	1.4	0.1	68.05	-17.18	-173.93	56	A
JERxxx_GE	SKK	EQ011670213	31.77	35.2	0	7	1.6	0.3	63.77	-14.89	-173.34	10	B
JERxxx_GE	SKK	EQ020870456	31.77	35.2	4	5.5	1.2	0.3	257.62	-21.66	-68.33	125.1	B
JERxxx_GE	SKK	EQ971420750	31.77	35.2	21	4.5	1.4	0.2	314.3	18.68	-101.6	70	A
JERxxx_GE	SKK	EQ971470800	31.77	35.2	16	13.5	0.8	0.3	64.26	-15.21	-173.33	14	B
JERxxx_GE	SKK	EQ981971156	31.77	35.2	9	9	1.9	0.5	76.71	-11.04	166.16	110.2	B
JERxxx_GE	SKK	EQ991161817	31.77	35.2	176	17.5	1	0.4	281.08	-1.65	-77.78	172.6	B
JERxxx_GE	SKK	EQ992960212	31.77	35.2	6	4	2	0.4	78.67	-4.81	153.41	83.3	B
KEGxxx_MN	SKK	EQ910082204	29.93	31.83	34	16.5	0.8	0.3	68.65	-18.06	-173.53	32.9	B
KEGxxx_MN	SKK	EQ912011148	29.93	31.83	32	14.5	1.1	0.4	7.84	54.56	-161.65	32.5	B
KEGxxx_MN	SKK	EQ912022259	29.93	31.83	68	10	0.9	0.3	84.11	3.01	128.43	34.4	B
KEGxxx_MN	SKK	EQ922371940	29.93	31.83	8	3	1.5	0.2	208.49	-56.62	-26.55	106.6	B
KEGxxx_MN	SKK	EQ922931203	29.93	31.83	38	11.5	1.2	0.3	84.55	-19.39	169.59	20.6	B
KEGxxx_MN	SKK	EQ931901537	29.93	31.83	54	7.5	0.9	0.2	75.93	-19.78	-177.49	398.2	B
KEGxxx_MN	SKK	EQ932010738	29.93	31.83	13	17	0.9	0.3	65.14	-16.81	-172.6	30.5	B
KEGxxx_MN	SKK	EQ932200834	29.93	31.83	16	9.5	0.9	0.2	66.91	12.98	144.8	59.3	B
KEGxxx_MN	SKK	EQ932490356	29.93	31.83	22	10	0.9	0.2	77.54	-4.64	153.23	49	B
KEGxxx_MN	SKK	EQ932640328	29.93	31.83	21	12	1.5	0.4	340.3	42.32	-122.03	10.3	B
KEGxxx_MN	SKK	EQ940541800	29.93	31.83	9	13.5	0.9	0.3	68.36	-17.45	-174.29	33	B
KEGxxx_MN	SKK	EQ941032222	29.93	31.83	63	15.5	0.8	0.3	85.64	-3.14	135.97	28.5	B
KEGxxx_MN	SKK	EQ941170923	29.93	31.83	54	5.5	1.3	0.2	75.9	-21.51	-173.67	28.1	B
KEGxxx_MN	SKK	EQ941940235	29.93	31.83	14	10.5	1.9	0.5	82.03	-16.62	167.52	33	B
KEGxxx_MN	SKK	EQ942062200	29.93	31.83	3	18	1	0.5	208.99	-56.36	-27.36	81.3	B
KEGxxx_MN	SKK	EQ942930115	29.93	31.83	161	4	1.5	0.4	238.66	-39.19	-70.81	161.8	B
KEGxxx_MN	SKK	EQ951750658	29.93	31.83	21	10.5	1	0.2	76.45	-3.96	153.93	386	B
KEGxxx_MN	SKK	EQ952260437	29.93	31.83	34	18	0.6	0.4	78.74	-4.84	151.51	127.9	B
KEGxxx_MN	SKK	EQ952281624	29.93	31.83	16	16	0.8	0.2	77.98	-5.43	153.77	18.7	B
KEGxxx_MN	SKK	EQ952291001	29.93	31.83	34	6.5	1	0.2	77.92	-5.17	153.45	21	B
KEGxxx_MN	SKK	EQ952300216	29.93	31.83	0	14.5	0.9	0.3	209.86	-55.93	-28.83	41.9	B
KEGxxx_MN	SKK	EQ952360754	29.93	31.83	30	3.5	1	0.1	61.96	18.82	145.04	612.4	A
KEGxxx_MN	SKK	EQ960561417	29.93	31.83	5	5.5	1.7	0.3	299.14	12.96	-91.06	8	B
KEGxxx_MN	SKK	EQ960771448	29.93	31.83	32	18.5	0.6	0.5	79.69	-14.7	167.3	164.4	B
KEGxxx_MN	SKK	EQ961231334	29.93	31.83	23	17.5	0.8	0.2	76.47	-4.55	154.83	500	B
KEGxxx_MN	SKK	EQ962151255	29.93	31.83	55	17	1.2	0.6	78.8	-10.77	161.45	33	B
KEGxxx_MN	SKK	EQ963381256	29.93	31.83	31	14	0.9	0.3	67.75	-18.35	-172.27	32.7	B
KEGxxx_MN	SKK	EQ970781750	29.93	31.83	20	11	0.9	0.2	66.36	-16.61	-173.9	98.9	B
KEGxxx_MN	SKK	EQ970951223	29.93	31.83	38	13	1.1	0.3	82.65	-6.49	147.41	69.1	B
KEGxxx_MN	SKK	EQ971420750	29.93	31.83	15	7	1.3	0.3	311.07	18.68	-101.6	70	B
KEGxxx_MN	SKK	EQ971890224	29.93	31.83	9	16	0.8	0.2	59.2	23.8	142.7	33	B
KEGxxx_MN	SKK	EQ973072137	29.93	31.83	16	18.5	1.1	0.4	74.31	-19.96	-175.36	151.9	B
KEGxxx_MN	SKK	EQ973560205	29.93	31.83	14	3	1.4	0.2	81.46	-5.49	147.87	179.3	B
KEGxxx_MN	SKK	EQ980881948	29.93	31.83	49	8.5	1.5	0.3	73.41	-17.55	-179.09	537.2	B

KEGxxx_MN	SKK	EQ983610038	29.93	31.83	36	10	1	0.2	78.57	-21.63	-176.38	144.3	B
MRNIxx_GE	SKK	EQ000881100	33.12	35.39	4	15.5	1.5	0.7	61.58	22.34	143.73	126.5	B
MRNIxx_GE	SKK	EQ001680755	33.12	35.39	174	5	1.6	0.3	246.73	-33.88	-70.09	120.2	B
MRNIxx_GE	SKK	EQ002700617	33.12	35.39	4	3	1.7	0.2	66.15	-17.18	-173.93	56	A
MRNIxx_GE	SKK	EQ003530119	33.12	35.39	5	3	1.6	0.3	77.55	-21.18	-179.12	628.2	A
MRNIxx_GE	SKK	EQ010091649	33.12	35.39	9	2.5	1.9	0.2	79.36	-14.93	167.17	103	B
MRNIxx_GE	SKK	EQ011391736	33.12	35.39	10	9.5	1.6	0.5	74.1	-19.9	-177.51	368.7	B
MRNIxx_GE	SKK	EQ013461402	33.12	35.39	3	10.5	1.1	0.3	127.92	-42.81	124.69	10	B
RAYNxx_II	SKK	EQ000021258	23.52	45.5	179	13	1.1	0.5	24.47	51.45	-175.56	33	B
RAYNxx_II	SKK	EQ001140927	23.52	45.5	6	1.5	1.3	0.1	248.94	-28.31	-62.99	608.5	A
RAYNxx_II	SKK	EQ001141701	23.52	45.5	11	9.5	1.4	0.3	248.84	-28.38	-62.94	609.8	B
RAYNxx_II	SKK	EQ001252036	23.52	45.5	13	17	0.6	0.2	90.77	-17.91	-178.52	515.8	B
RAYNxx_II	SKK	EQ001331843	23.52	45.5	61	12.5	2	0.6	254.97	-23.55	-66.45	225	B
RAYNxx_II	SKK	EQ001680755	23.52	45.5	6	8	1.4	0.3	243.96	-33.88	-70.09	120.2	B
RAYNxx_II	SKK	EQ003341025	23.52	45.5	10	6	1.5	0.2	254.63	-24.87	-70.89	58.2	B
RAYNxx_II	SKK	EQ020300842	23.52	45.5	21	7	1.3	0.3	314.35	18.19	-95.91	108.9	B
RAYNxx_II	SKK	EQ020311627	23.52	45.5	11	3	1.4	0.2	88.96	-12.8	169.53	667.1	B
RAYNxx_II	SKK	EQ021480404	23.52	45.5	2	8	1.4	0.4	249.09	-28.94	-66.8	22.2	B
RAYNxx_II	SKK	EQ023111514	23.52	45.5	4	11	1.1	0.3	27.12	51.2	179.33	33	B
RAYNxx_II	SKK	EQ031242008	23.52	45.5	1	5	1.4	0.3	110.04	-30.59	-178.29	45.6	B
RAYNxx_II	SKK	EQ032331212	23.52	45.5	12	12	1.4	0.4	129.7	-45.1	167.14	28	B
RAYNxx_II	SKK	EQ040350518	23.52	45.5	176	4	1.8	0.3	251.39	-26.13	-63.46	558.4	B
RAYNxx_II	SKK	EQ041240436	23.52	45.5	25	15	1.5	0.5	239.64	-37.69	-73.41	21	B
RAYNxx_II	SKK	EQ093181944	23.52	45.5	9	4.5	1.2	0.2	255.66	-22.97	-66.64	220.4	B
RAYNxx_II	SKK	EQ100632239	23.52	45.5	15	15.5	1	0.3	256.94	-22.23	-68.33	114	B
RAYNxx_II	SKK	EQ100640919	23.52	45.5	172	14	1.2	0.5	240.95	-36.63	-73.22	29.9	B
RAYNxx_II	SKK	EQ100681406	23.52	45.5	7	12	0.8	0.4	23.42	51.49	-173.53	35	B
RAYNxx_II	SKK	EQ100750221	23.52	45.5	9	10.5	1.4	0.3	241.46	-36.22	-73.26	18	B
RAYNxx_II	SKK	EQ100851452	23.52	45.5	8	8	1.5	0.3	251.04	-27.95	-70.82	42	B
RAYNxx_II	SKK	EQ100872138	23.52	45.5	20	11	1.4	0.3	242.49	-35.39	-73.39	29.9	B
RAYNxx_II	SKK	EQ100922258	23.52	45.5	12	5.5	1.4	0.2	241.42	-36.23	-72.88	24	B
RAYNxx_II	SKK	EQ102941753	23.52	45.5	24	13.5	1.4	0.5	331.18	24.7	-109.16	13	B
RAYNxx_II	SKK	EQ110900011	23.52	45.5	33	14.5	0.9	0.3	88.38	-16.54	-177.52	15.5	B
RAYNxx_II	SKK	EQ110971311	23.52	45.5	21	17.5	1	0.4	312.24	17.21	-94.34	166.2	B
RAYNxx_II	SKK	EQ113261848	23.52	45.5	4	2.5	1.6	0.3	263.24	-15.36	-65.09	549.9	B
RAYNxx_II	SKK	EQ120190648	23.52	45.5	23	9.5	1.6	0.6	131.61	-46.69	165.78	20	B
RAYNxx_II	SKK	EQ120861812	23.52	45.5	159	3.5	1.4	0.2	314.96	10.07	-104.16	10	B
RAYNxx_II	SKK	EQ121490507	23.52	45.5	8	5.5	1.3	0.2	249.25	-28.04	-63.09	586.9	A
RAYNxx_II	SKK	EQ122692345	23.52	45.5	15	13.5	0.9	0.2	332.17	24.67	-110.17	10	B
RAYNxx_II	SKK	EQ123191902	23.52	45.5	32	6	1.6	0.2	249.75	-29.12	-71.19	63	B
RAYNxx_II	SKK	EQ131881835	23.52	45.5	7	2	1.5	0.3	86.21	-3.92	153.92	386.2	B
RAYNxx_II	SKK	EQ971420750	23.52	45.5	11	12	0.7	0.2	319.75	18.68	-101.6	70	A
RAYNxx_II	SKK	EQ972060647	23.52	45.5	169	4.5	1.6	0.5	248.28	-30.46	-71.91	33	B
RAYNxx_II	SKK	EQ972880103	23.52	45.5	29	5	2	0.2	247.61	-30.93	-71.22	58	B
RAYNxx_II	SKK	EQ983481625	23.52	45.5	6	8.5	1.4	0.3	238.86	-38.21	-71.03	138.4	B
RAYNxx_II	SKK	EQ992580301	23.52	45.5	5	4.5	1.2	0.2	258.05	-20.93	-67.28	218	B

RAYNxx_XI	SKK	EQ961201440	23.52	45.5	11	10.5	1.2	0.5	88.28	-6.52	155	44	B
RIYDxx_XI	SKK	EQ970230215	24.72	46.64	4	4	1.2	0.2	257.4	-22	-65.72	276.2	B
UQSKxx_XI	SKK	EQ962320419	25.79	42.36	0	3	1.7	0.2	24.2	51.45	-178.37	33	B
BISHxx_XI	SKS	EQ953341509	19.92	42.69	4	5	2	0.2	44.63	44.28	145.62	136	B
RANIxx_XI	SKS	EQ960820324	21.31	42.78	2	3.5	2.2	0.3	26.22	51.22	178.7	20	B
RANIxx_XI	SKS	EQ960881951	21.31	42.78	3	3	1.9	0.3	19.16	52.31	-168.78	33	B
RANIxx_XI	SKS	EQ960901256	21.31	42.78	4	2.5	2.3	0.3	19.13	52.21	-168.64	33	B
RANIxx_XI	SKS	EQ960901305	21.31	42.78	3	4.5	1.8	0.3	19.18	52.21	-168.73	33	B
RANIxx_XI	SKS	EQ961510304	21.31	42.78	11	15	1.2	0.7	211.24	-56.72	-26.31	84	B
RANIxx_XI	SKS	EQ961621524	21.31	42.78	177	6	1.8	0.3	23.86	51.48	-176.85	26	B
RANIxx_XI	SKK	EQ960560308	21.31	42.78	11	15.5	1.3	0.5	310.82	15.98	-98.07	21	B
RANIxx_XI	SKK	EQ961100019	21.31	42.78	16	16.5	1.4	0.5	253.62	-23.94	-70.09	49	B
SODAxx_XI	SKS	EQ960312030	18.29	42.38	173	6	2	0.3	43.22	44.47	149.37	20	B
SODAxx_XI	SKS	EQ960531459	18.29	42.38	174	12	1.4	0.4	42.75	45.26	148.54	124	A
SODAxx_XI	SKS	EQ960762204	18.29	42.38	172	12.5	1.4	0.5	60.66	28.98	138.94	477	B
SODAxx_XI	SKS	EQ960820324	18.29	42.38	176	11	1.4	0.4	26.25	51.22	178.7	20	A
SODAxx_XI	SKS	EQ960881951	18.29	42.38	168	4.5	1.5	0.2	19.17	52.31	-168.78	33	B
SODAxx_XI	SKS	EQ960901256	18.29	42.38	169	1.5	1.4	0.1	19.15	52.21	-168.64	33	B
SODAxx_XI	SKS	EQ960901305	18.29	42.38	168	2	1.4	0.1	19.19	52.21	-168.73	33	A
SODAxx_XI	SKS	EQ961780322	18.29	42.38	179	9.5	1.3	0.3	61.6	27.73	139.75	468	A
SODAxx_XI	SKS	EQ961821132	18.29	42.38	165	9	1.6	0.3	33.52	51.73	159.81	33	B
SODAxx_XI	SKS	EQ961881156	18.29	42.38	178	7	1.5	0.4	70.37	15.51	147.66	33	B
SODAxx_XI	SKS	EQ961882136	18.29	42.38	178	4.5	1.6	0.2	66.03	21.97	142.83	241	B
SODAxx_XI	SKS	EQ961971651	18.29	42.38	1	7.5	1.1	0.2	68.09	18.73	145.63	176	B
SODAxx_XI	SKS	EQ962550237	18.29	42.38	0	7	1.1	0.2	53.92	35.54	140.94	55	A
SODAxx_XI	SKS	EQ962981931	18.29	42.38	166	8	1.2	0.3	13.23	66.99	-173.23	19	A
SODAxx_XI	SKS	EQ970230215	18.29	42.38	175	2	1.6	0.2	253.34	-22	-65.72	276	B
SODAxx_XI	PKS	EQ963100941	18.29	42.38	9	9.5	0.9	0.2	116.78	-31.16	180	369	B
SODAxx_XI	PKS	EQ963160047	18.29	42.38	7	9	1.3	0.3	119.1	-32.54	-179.05	33	B
SODAxx_XI	PKS	EQ970112028	18.29	42.38	8	5	1.3	0.2	314.75	18.22	-102.76	33	B
SODAxx_XI	SKK	EQ960560308	18.29	42.38	165	14.5	1.1	0.3	308.74	15.98	-98.07	21	B
SODAxx_XI	SKK	EQ960561417	18.29	42.38	7	4	1.9	0.2	300.73	12.96	-91.06	8	B
SODAxx_XI	SKK	EQ963100941	18.29	42.38	165	6.5	1.2	0.2	116.78	-31.16	180	369	A
SODAxx_XI	SKK	EQ963112000	18.29	42.38	173	13.5	1.2	0.4	60.19	28	143.54	9	B
TAIFxx_XI	SKS	EQ961610112	21.28	40.35	4	9.5	1.8	0.5	68.25	17.44	145.46	149	B
TAIFxx_XI	SKS	EQ961731357	21.28	40.35	12	5.5	1.3	0.3	33.17	51.57	159.12	20	B
TAIFxx_XI	SKS	EQ961780322	21.28	40.35	3	5	1.5	0.2	61.04	27.73	139.75	468	B
TAIFxx_XI	SKS	EQ961821132	21.28	40.35	171	12	1	0.2	32.79	51.73	159.81	33	B
TAIFxx_XI	SKS	EQ961882136	21.28	40.35	18	6	0.9	0.2	65.17	21.97	142.83	241	B
TAIFxx_XI	SKS	EQ961971651	21.28	40.35	14	5.5	1.2	0.2	67.01	18.73	145.63	176	B
TAIFxx_XI	SKK	EQ961821132	21.28	40.35	174	6	1.1	0.2	32.79	51.73	159.81	33	B
BGCAxx_GT	SKS	EQ001680755	5.18	18.42	23	16.5	0.85	0.45	236.3	-33.88	-70.09	120	B
BGCAxx_GT	SKS	EQ003341025	5.18	18.42	40	17	1.1	0.6	245.31	-24.87	-70.89	58	B
BGCAxx_GT	SKS	EQ003551123	5.18	18.42	20	14.5	1	0.28	231.42	-39.01	-74.66	11	B
BGCAxx_GT	SKS	EQ010071018	5.18	18.42	7	6.5	0.95	0.13	236.88	-33.44	-72.23	10	B
BGCAxx_GT	SKS	EQ010470559	5.18	18.42	82	5	0.8	0.23	96.36	-7.16	117.49	521	B

BGCAxx_GT	SKS	EQ010471319	5.18	18.42	24	4.5	0.7	0.08	254.71	-15.35	-70.47	210	B
BGCAxx_GT	SKS	EQ010621158	5.18	18.42	17	7.5	1.15	0.23	231.66	-38.77	-74.56	33	B
BGCAxx_GT	SKS	EQ010741302	5.18	18.42	4	13	0.8	0.2	237.95	-32.32	-71.49	37	B
BGCAxx_GT	SKS	EQ010750436	5.18	18.42	21	11	0.75	0.15	249.54	-20.41	-68.74	115	B
BGCAxx_GT	SKS	EQ010990900	5.18	18.42	28	7	1	0.2	237.7	-32.67	-73.11	11	B
BGCAxx_GT	SKS	EQ011700932	5.18	18.42	27	11	0.65	0.17	247.15	-22.74	-67.88	146	B
BGCAxx_GT	SKS	EQ011770418	5.18	18.42	34	16	0.75	0.3	252.43	-17.75	-71.65	24	B
BGCAxx_GT	SKS	EQ011801835	5.18	18.42	17	7.5	0.65	0.1	250.17	-19.52	-66.25	273	A
BGCAxx_GT	SKS	EQ011861353	5.18	18.42	58	14.5	1.35	0.57	254.26	-16.09	-73.99	62	B
BGCAxx_GT	SKS	EQ012400656	5.18	18.42	16	14	0.75	0.23	248.37	-21.72	-70.11	65	B
BGCAxx_GT	SKS	EQ013431815	5.18	18.42	77	7.5	1.15	0.48	88.68	0	122.87	156	B
BGCAxx_GT	SKS	EQ013461402	5.18	18.42	27	9.5	0.5	0.15	132.88	-42.81	124.69	10	B
BGCAxx_GT	SKS	EQ020322155	5.18	18.42	16	13	0.85	0.38	40.04	45.46	136.72	355	B
BGCAxx_GT	SKS	EQ020911959	5.18	18.42	36	15	1	0.38	240.58	-29.67	-71.38	71	B
BGCAxx_GT	SKS	EQ021480404	5.18	18.42	15	13.5	0.75	0.25	240.91	-28.94	-66.8	22	B
BGCAxx_GT	SKS	EQ942930115	5.18	18.42	5	3.5	0.9	0.1	231.07	-39.19	-70.81	161	A
BGCAxx_GT	SKS	EQ943192018	5.18	18.42	22	15.5	0.65	0.27	95.38	-5.59	110.19	560	B
BGCAxx_GT	SKS	EQ943460741	5.18	18.42	18	7	0.6	0.1	252.52	-17.48	-69.6	148	B
BGCAxx_GT	SKS	EQ950031611	5.18	18.42	11	3.5	1.3	0.22	212.3	-57.7	-65.88	13	B
BGCAxx_GT	SKS	EQ950201549	5.18	18.42	75	2.5	2.3	0.5	87.15	1.18	126	56	B
BGCAxx_GT	SKS	EQ950412026	5.18	18.42	11	14	0.6	0.2	250.01	-19.94	-68.76	118	B
BGCAxx_GT	SKS	EQ950451553	5.18	18.42	11	7	0.7	0.12	246.51	-23.37	-67.69	147	B
BGCAxx_GT	SKS	EQ950500017	5.18	18.42	67	4	0.7	0.15	82.92	5.24	126.26	75	B
BGCAxx_GT	SKS	EQ951471303	5.18	18.42	17	8.5	1.7	0.75	31.5	52.63	142.83	11	B
BGCAxx_GT	SKS	EQ951481959	5.18	18.42	10	14.5	0.6	0.22	241.26	-28.98	-71.22	42	B
BGCAxx_GT	SKS	EQ952522058	5.18	18.42	22	14.5	0.5	0.15	249.87	-20.14	-69.32	75	B
BGCAxx_GT	SKS	EQ953021924	5.18	18.42	75	8	0.95	0.38	87.49	0.86	125.89	68	B
BGCAxx_GT	SKS	EQ953040155	5.18	18.42	12	14	0.7	0.18	241.31	-28.94	-71.39	33	B
BGCAxx_GT	SKS	EQ953050035	5.18	18.42	22	18.5	0.75	0.5	241.34	-28.91	-71.42	19	B
BGCAxx_GT	SKS	EQ960531340	5.18	18.42	15	8.5	0.8	0.12	236.62	-33.67	-71.67	43	B
BGCAxx_GT	SKS	EQ961100019	5.18	18.42	0	15.5	0.85	0.3	246.17	-23.94	-70.09	49	B
BGCAxx_GT	SKS	EQ962492342	5.18	18.42	52	3	1.6	0.28	66.77	21.9	121.5	20	B
BGCAxx_GT	SKS	EQ962530020	5.18	18.42	7	5.5	0.9	0.12	238.37	-31.9	-71.56	39	B
BGCAxx_GT	SKS	EQ970230215	5.18	18.42	34	8	0.75	0.18	247.66	-22	-65.72	276	B
BGCAxx_GT	SKS	EQ971101953	5.18	18.42	1	7.5	0.75	0.1	236.14	-34.04	-69.98	104	A
BGCAxx_GT	SKS	EQ971870954	5.18	18.42	35	12.5	1.3	0.42	240.23	-30.06	-71.87	19	B
BGCAxx_GT	SKS	EQ980842102	5.18	18.42	10	11	0.85	0.25	245.48	-24.34	-66.99	197	B
BGCAxx_GT	SKS	EQ980912242	5.18	18.42	26	7	1.25	0.28	230.11	-40.32	-74.87	9	B
BGCAxx_GT	SKS	EQ980932201	5.18	18.42	55	16	0.65	0.32	262.16	-8.15	-74.24	164	B
BGCAxx_GT	SKS	EQ982100714	5.18	18.42	9	19	0.75	0.35	237.95	-32.31	-71.29	51	B
BGCAxx_GT	SKS	EQ982810451	5.18	18.42	20	9	0.65	0.12	254.03	-16.12	-71.4	136	A
BGCAxx_GT	SKS	EQ983481625	5.18	18.42	8	5.5	0.85	0.1	232.06	-38.21	-71.03	138	A
BGCAxx_GT	SKS	EQ990611745	5.18	18.42	21	14	0.5	0.18	247.23	-22.72	-68.5	110	B
BGCAxx_GT	SKS	EQ991451642	5.18	18.42	20	17	0.7	0.33	241.92	-27.93	-66.93	169	B
BGCAxx_GT	SKS	EQ992612128	5.18	18.42	10	2.5	1.55	0.2	26.74	51.21	157.56	60	B
BGCAxx_GT	SKS	EQ993250351	5.18	18.42	8	9	0.85	0.18	248.22	-21.75	-68.78	101	A

BGCAxx_GT	SKS	EQ993340401	5.18	18.42	23	15.5	0.7	0.22	251.08	-18.9	-69.17	128	A
BGCAxx_GT	PKS	EQ003061035	5.18	18.42	45	10	1.05	0.35	150.34	-45.07	167.01	24	B
BGCAxx_GT	PKS	EQ981901445	5.18	18.42	43	8	1.85	0.53	148.95	-30.49	-178.99	129	B
BGCAxx_GT	SKK	EQ000881100	5.18	18.42	33	14.5	0.9	0.4	60.68	22.34	143.73	126	B
BGCAxx_GT	SKK	EQ002190727	5.18	18.42	31	5.5	1.05	0.22	55.35	28.86	139.56	394	B
BGCAxx_GT	SKK	EQ002280430	5.18	18.42	37	2.5	1.35	0.2	148.43	-31.51	179.73	357	B
BGCAxx_GT	SKK	EQ011492337	5.18	18.42	54	18	1.15	0.5	94.71	-7.02	155.04	14	B
BGCAxx_GT	SKK	EQ012851502	5.18	18.42	47	6	1.35	0.23	71.02	12.69	144.98	37	B
BGCAxx_GT	SKK	EQ943002220	5.18	18.42	28	4.5	0.7	0.13	140.25	-25.78	179.34	518	A
BGCAxx_GT	SKK	EQ950162046	5.18	18.42	22	17.5	0.85	0.43	51.08	34.58	135.02	21	B
BGCAxx_GT	SKK	EQ952791139	5.18	18.42	23	12.5	1.1	0.35	137.8	-20	-175.92	197	B
BGCAxx_GT	SKK	EQ953040155	5.18	18.42	1	16	0.7	0.23	241.31	-28.94	-71.39	33	B
BGCAxx_GT	SKK	EQ960481421	5.18	18.42	41	8	1	0.15	87.97	-0.57	135.84	19	B
BGCAxx_GT	SKK	EQ960590944	5.18	18.42	54	5.5	1.15	0.15	86.54	1.76	126.05	115	B
BGCAxx_GT	SKK	EQ960762204	5.18	18.42	29	4	1	0.15	55.44	28.98	138.94	477	B
BGCAxx_GT	SKK	EQ961691122	5.18	18.42	27	16.5	0.9	0.32	96	-7.14	122.59	587	B
BGCAxx_GT	SKK	EQ962530020	5.18	18.42	1	16	0.7	0.25	238.37	-31.9	-71.56	39	B
BGCAxx_GT	SKK	EQ962882326	5.18	18.42	70	9	1	0.28	94.87	-7.13	155.57	24	B
BGCAxx_GT	SKK	EQ982100714	5.18	18.42	4	12.5	0.75	0.23	237.95	-32.31	-71.29	51	B
BGCAxx_GT	SKK	EQ982320640	5.18	18.42	28	3	1.15	0.12	55.36	28.93	139.33	440	B
BGCAxx_GT	SKK	EQ983610038	5.18	18.42	39	5.5	1.9	0.58	140.11	-21.63	-176.38	144	B
BGCAxx_GT	SKK	EQ990960822	5.18	18.42	31	16	0.7	0.2	94.19	-6.53	147.01	33	B
CM01xx_XB	SKK	EQ060331248	2.39	9.83	10	16	0.6	0.22	152.67	-17.75	-178.39	597	B
CM01xx_XB	SKK	EQ060570308	2.39	9.83	19	12.5	1.35	0.4	156.54	-23.61	-179.99	535	B
CM02xx_XB	SKS	EQ060232050	2.7	13.29	58	7.5	1.05	0.17	276.86	6.86	-77.79	14	B
CM02xx_XB	SKS	EQ060271658	2.7	13.29	51	3	1.05	0.07	94.75	-5.47	128.13	397	B
CM02xx_XB	SKS	EQ061752115	2.7	13.29	42	4.5	1	0.12	89.44	-0.39	123.19	26	A
CM02xx_XB	SKS	EQ062520413	2.7	13.29	48	2.5	0.85	0.07	96.68	-7.22	120.11	572	B
CM02xx_XB	SKS	EQ062590945	2.7	13.29	52	17	1.1	0.45	92.09	-3.08	129.44	17	B
CM02xx_XB	PKS	EQ061480312	2.7	13.29	57	3	1.05	0.07	95.51	-5.72	151.13	34	B
CM02xx_XB	PKS	EQ062001148	2.7	13.29	47	10	1.15	0.25	95.11	-5.47	150.68	28	B
CM02xx_XB	PKS	EQ062441018	2.7	13.29	53	3	0.9	0.08	97.5	-6.76	155.51	38	B
CM02xx_XB	PKS	EQ062900125	2.7	13.29	61	2.5	1.05	0.07	95.73	-5.88	150.98	32	A
CM02xx_XB	PKS	EQ063102056	2.7	13.29	70	15	1	0.45	94.92	-5.45	146.64	133	B
CM02xx_XB	PKS	EQ063111738	2.7	13.29	55	9	0.75	0.12	96.64	-6.48	151.2	11	B
CM02xx_XB	PKS	EQ063161821	2.7	13.29	56	3	1	0.08	96.24	-6.22	151.05	12	B
CM02xx_XB	PKS	EQ063171612	2.7	13.29	58	5.5	0.9	0.12	96.49	-6.38	151.23	11	B
CM02xx_XB	PKS	EQ063281231	2.7	13.29	55	2.5	0.9	0.07	95.88	-6	150.48	24	B
CM02xx_XB	SKK	EQ060271658	2.7	13.29	42	4	0.95	0.08	94.75	-5.47	128.13	397	A
CM02xx_XB	SKK	EQ062192218	2.7	13.29	54	3.5	0.9	0.1	118.99	-15.8	167.79	150	A
CM02xx_XB	SKK	EQ062900125	2.7	13.29	43	16.5	1	0.43	95.73	-5.88	150.98	32	B
CM03xx_XB	SKS	EQ061752115	3.52	15.03	16	16	0.5	0.2	89.26	-0.39	123.19	26	A
CM03xx_XB	SKS	EQ062090740	3.52	15.03	48	14.5	0.5	0.18	64.08	24.18	122.53	33	B
CM03xx_XB	PKS	EQ062441018	3.52	15.03	31	15	0.5	0.2	96.32	-6.76	155.51	38	B
CM03xx_XB	SKK	EQ060712054	3.52	15.03	75	7	0.95	0.28	93.65	-5.07	153.66	47	B
CM03xx_XB	SKK	EQ062192218	3.52	15.03	39	3	0.7	0.12	116.31	-15.8	167.79	150	B

CM04xx_XB	SKS	EQ060271658	2.98	11.96	70	11.5	0.95	0.28	94.6	-5.47	128.13	397	B
CM04xx_XB	SKS	EQ061752115	2.98	11.96	63	6	1	0.2	89.27	-0.39	123.19	26	B
CM04xx_XB	SKS	EQ061981545	2.98	11.96	61	8	0.8	0.12	99.08	-9.42	108.32	21	B
CM04xx_XB	SKS	EQ062590945	2.98	11.96	68	18	0.95	0.53	91.91	-3.08	129.44	17	B
CM04xx_XB	SKS	EQ063350358	2.98	11.96	63	3.5	1.2	0.15	86.78	3.39	99.08	204	B
CM04xx_XB	SKS	EQ063351401	2.98	11.96	67	9	0.9	0.2	97.68	-8.26	118.75	19	B
CM04xx_XB	PKS	EQ062441018	2.98	11.96	66	8	0.9	0.2	97.29	-6.76	155.51	38	B
CM04xx_XB	PKS	EQ062900125	2.98	11.96	70	6	0.95	0.17	95.5	-5.88	150.98	32	B
CM04xx_XB	PKS	EQ063111738	2.98	11.96	85	5.5	1.75	0.95	96.43	-6.48	151.2	11	B
CM04xx_XB	PKS	EQ063151510	2.98	11.96	69	13	0.95	0.33	95.54	-5.99	148.59	47	B
CM04xx_XB	PKS	EQ063161821	2.98	11.96	67	8	1	0.2	96.02	-6.22	151.05	12	B
CM04xx_XB	PKS	EQ063171612	2.98	11.96	78	4	1.5	0.33	96.28	-6.38	151.23	11	B
CM04xx_XB	PKS	EQ063281231	2.98	11.96	68	13	1	0.33	95.65	-6	150.48	24	B
CM04xx_XB	SKK	EQ060271658	2.98	11.96	63	12	0.7	0.18	94.6	-5.47	128.13	397	A
CM04xx_XB	SKK	EQ062192218	2.98	11.96	60	13.5	0.65	0.17	119.7	-15.8	167.79	150	B
CM04xx_XB	SKK	EQ062590945	2.98	11.96	63	11.5	0.85	0.22	91.91	-3.08	129.44	17	B
CM04xx_XB	SKK	EQ062900125	2.98	11.96	51	14	0.75	0.23	95.5	-5.88	150.98	32	B
CM04xx_XB	SKK	EQ063161821	2.98	11.96	61	15.5	0.95	0.3	96.02	-6.22	151.05	12	B
CM05xx_XB	SKS	EQ061462253	2.94	9.91	52	5.5	0.55	0.08	97.5	-7.96	110.45	12	B
CM05xx_XB	SKS	EQ061981545	2.94	9.91	69	11.5	0.55	0.17	99.03	-9.42	108.32	21	B
CM05xx_XB	SKS	EQ063350358	2.94	9.91	20	18	0.6	0.28	86.68	3.39	99.08	204	B
CM05xx_XB	SKS	EQ063461548	2.94	9.91	59	18	0.75	0.38	84.59	3.73	124.68	213	B
CM05xx_XB	PKS	EQ062900125	2.94	9.91	64	9	0.65	0.13	95.68	-5.88	150.98	32	B
CM05xx_XB	PKS	EQ063151510	2.94	9.91	43	16	0.5	0.23	95.69	-5.99	148.59	47	B
CM05xx_XB	SKK	EQ060570308	2.94	9.91	31	10	1	0.23	155.85	-23.61	-179.99	535	B
CM05xx_XB	SKK	EQ062900125	2.94	9.91	72	15	0.9	0.42	95.68	-5.88	150.98	32	B
CM06xx_XB	SKS	EQ050361223	2.38	11.27	58	3	0.95	0.13	83.39	5.29	123.34	525	B
CM06xx_XB	SKS	EQ050461442	2.38	11.27	52	2	0.95	0.05	83.69	4.76	126.42	39	B
CM06xx_XB	SKS	EQ050611042	2.38	11.27	53	6	0.75	0.12	96.1	-6.53	129.93	201	B
CM06xx_XB	SKS	EQ053131133	2.38	11.27	17	5	1.1	0.25	268.91	-1.02	-76.94	248	B
CM06xx_XB	SKS	EQ053251536	2.38	11.27	42	1.5	1.1	0.12	54.89	31.02	130	145	B
CM06xx_XB	SKS	EQ053572147	2.38	11.27	16	7.5	1.15	0.35	268.57	-1.39	-77.52	192	B
CM06xx_XB	SKS	EQ060271658	2.38	11.27	58	6.5	0.85	0.12	94.89	-5.47	128.13	397	A
CM06xx_XB	SKS	EQ060730657	2.38	11.27	59	7.5	0.95	0.2	92.83	-3.6	127.21	30	B
CM06xx_XB	SKS	EQ060902114	2.38	11.27	53	5	0.9	0.13	84.74	3.8	126.34	37	B
CM06xx_XB	SKS	EQ060911002	2.38	11.27	49	6.5	1.1	0.3	65.27	22.87	121.28	9	B
CM06xx_XB	SKS	EQ061462253	2.38	11.27	59	3.5	0.8	0.08	97.63	-7.96	110.45	12	B
CM06xx_XB	SKS	EQ061752115	2.38	11.27	59	5	1.05	0.15	89.47	-0.39	123.19	26	A
CM06xx_XB	SKS	EQ061980819	2.38	11.27	60	16	0.9	0.35	99.02	-9.28	107.42	20	B
CM06xx_XB	SKS	EQ061981545	2.38	11.27	60	9.5	0.8	0.12	99.14	-9.42	108.32	21	B
CM06xx_XB	SKS	EQ062590945	2.38	11.27	55	15.5	0.75	0.22	92.2	-3.08	129.44	17	B
CM06xx_XB	SKS	EQ063350358	2.38	11.27	69	2.5	1	0.12	86.72	3.39	99.08	204	B
CM06xx_XB	SKS	EQ063461548	2.38	11.27	58	7	1.1	0.25	84.95	3.73	124.68	213	B
CM06xx_XB	PKS	EQ050360334	2.38	11.27	50	2.5	1.3	0.22	66.22	16.01	145.87	142	A
CM06xx_XB	PKS	EQ050541133	2.38	11.27	41	16.5	0.75	0.25	96.76	-6.24	150.66	10	B
CM06xx_XB	PKS	EQ051551450	2.38	11.27	67	17	0.65	0.27	96.56	-6.32	146.85	26	B

CM06xx_XB	PKS	EQ052721550	2.38	11.27	40	4.5	0.7	0.07	95.63	-5.44	151.84	25	B
CM06xx_XB	PKS	EQ052721823	2.38	11.27	48	8	0.9	0.15	95.82	-5.56	151.87	28	B
CM06xx_XB	PKS	EQ052981940	2.38	11.27	48	9	0.7	0.15	97.65	-7.15	145.98	175	B
CM06xx_XB	PKS	EQ053451420	2.38	11.27	41	11	0.8	0.2	97.46	-6.58	152.22	17	B
CM06xx_XB	PKS	EQ060031227	2.38	11.27	51	1.5	1.25	0.1	69.2	13.84	145.29	78	A
CM06xx_XB	PKS	EQ060831227	2.38	11.27	62	12	0.75	0.2	92.2	-3.24	143.14	12	A
CM06xx_XB	PKS	EQ061480312	2.38	11.27	49	4.5	0.8	0.1	96.01	-5.72	151.13	34	A
CM06xx_XB	PKS	EQ062352315	2.38	11.27	52	6.5	0.75	0.12	93.8	-4.24	152.82	40	B
CM06xx_XB	PKS	EQ062581013	2.38	11.27	57	14.5	0.75	0.25	96.41	-6.02	150.47	27	B
CM06xx_XB	PKS	EQ063111738	2.38	11.27	64	16.5	0.7	0.18	97.19	-6.48	151.2	11	B
CM06xx_XB	PKS	EQ063151510	2.38	11.27	43	13	0.7	0.23	96.21	-5.99	148.59	47	B
CM06xx_XB	PKS	EQ063161821	2.38	11.27	37	9.5	0.8	0.17	96.77	-6.22	151.05	12	B
CM06xx_XB	PKS	EQ063171612	2.38	11.27	46	5	0.65	0.07	97.04	-6.38	151.23	11	B
CM06xx_XB	PKS	EQ063281231	2.38	11.27	54	8	0.7	0.13	96.38	-6	150.48	24	B
CM06xx_XB	SKK	EQ050360334	2.38	11.27	56	3	2.05	0.42	66.22	16.01	145.87	142	B
CM06xx_XB	SKK	EQ050461442	2.38	11.27	70	9.5	1	0.35	83.69	4.76	126.42	39	B
CM06xx_XB	SKK	EQ050611042	2.38	11.27	61	14	0.7	0.23	96.1	-6.53	129.93	201	B
CM06xx_XB	SKK	EQ060271658	2.38	11.27	62	7.5	0.9	0.17	94.89	-5.47	128.13	397	B
CM06xx_XB	SKK	EQ060570308	2.38	11.27	51	1.5	1.6	0.17	153.6	-23.61	-179.99	535	B
CM06xx_XB	SKK	EQ061462253	2.38	11.27	54	9	0.65	0.13	97.63	-7.96	110.45	12	B
CM06xx_XB	SKK	EQ062192218	2.38	11.27	52	4	0.8	0.15	121.38	-15.8	167.79	150	A
CM06xx_XB	SKK	EQ063161821	2.38	11.27	58	8	0.8	0.12	96.77	-6.22	151.05	12	B
CM06xx_XB	SKK	EQ063351401	2.38	11.27	43	8	0.8	0.17	97.86	-8.26	118.75	19	B
CM07xx_XB	SKS	EQ060232050	3.87	11.46	138	10.5	0.65	0.1	276.75	6.86	-77.79	14	B
CM07xx_XB	SKS	EQ062950855	3.87	11.46	95	18	1.1	0.47	135.78	-45.73	95.99	10	B
CM07xx_XB	SKS	EQ063350358	3.87	11.46	166	11.5	1.1	0.45	86.8	3.39	99.08	204	B
CM07xx_XB	SKK	EQ063161821	3.87	11.46	142	18	0.55	0.43	95.02	-6.22	151.05	12	B
CM09xx_XB	SKS	EQ061462253	4.23	9.33	20	2.5	1.25	0.22	97.22	-7.96	110.45	12	B
CM09xx_XB	PKS	EQ060451527	4.23	9.33	25	6.5	1.2	0.23	57.83	20.82	146.18	40	B
CM10xx_XB	SKS	EQ061462253	4.22	10.62	49	4	0.9	0.1	97.29	-7.96	110.45	12	B
CM10xx_XB	SKS	EQ061981545	4.22	10.62	35	10	0.8	0.23	98.86	-9.42	108.32	21	B
CM10xx_XB	SKS	EQ063350358	4.22	10.62	30	13.5	0.6	0.17	86.75	3.39	99.08	204	B
CM10xx_XB	SKK	EQ060570308	4.22	10.62	51	3	1.5	0.38	152.99	-23.61	-179.99	535	B
CM10xx_XB	SKK	EQ060902114	4.22	10.62	40	7.5	0.7	0.12	83.82	3.8	126.34	37	B
CM10xx_XB	SKK	EQ062192218	4.22	10.62	47	4.5	0.95	0.23	118.76	-15.8	167.79	150	B
CM11xx_XB	SKS	EQ062731626	3.98	13.19	14	6.5	0.75	0.12	254.28	-15.59	-73.16	107	A
CM11xx_XB	SKK	EQ060331248	3.98	13.19	21	5.5	0.7	0.1	141.2	-17.75	-178.39	597	A
CM11xx_XB	SKK	EQ060551415	3.98	13.19	27	3.5	0.75	0.1	139.03	-18	-179.59	622	A
CM11xx_XB	SKK	EQ060570308	3.98	13.19	32	13.5	0.8	0.3	148.08	-23.61	-179.99	535	A
CM11xx_XB	SKK	EQ061600558	3.98	13.19	29	8	0.85	0.2	139.89	-17.53	-178.75	564	B
CM11xx_XB	SKK	EQ070082052	3.98	13.19	25	9.5	0.8	0.2	144.19	-18.58	-177.85	406	B
CM12xx_XB	SKS	EQ062731626	4.48	11.63	59	18.5	1	0.5	254.12	-15.59	-73.16	107	B
CM12xx_XB	SKS	EQ062731750	4.48	11.63	12	15.5	1.4	0.73	29.51	46.35	153.17	11	B
CM12xx_XB	SKS	EQ063601226	4.48	11.63	174	9.5	1.3	0.37	66	21.8	120.55	10	B
CM12xx_XB	SKK	EQ062192218	4.48	11.63	130	14.5	0.95	0.5	117.37	-15.8	167.79	150	B
CM12xx_XB	SKK	EQ062761803	4.48	11.63	138	6.5	1.6	0.45	124.68	-18.84	169	161	B

CM12xx_XB	SKK	EQ070300454	4.48	11.63	14	17.5	0.55	0.28	152.15	-54.74	146.3	11	B
CM13xx_XB	SKK	EQ060230602	4.59	9.46	175	9	0.9	0.18	122.52	-17.39	167.71	23	B
CM13xx_XB	SKK	EQ060331248	4.59	9.46	11	14.5	1.05	0.35	150.17	-17.75	-178.39	597	B
CM13xx_XB	SKK	EQ060551415	4.59	9.46	16	9.5	1.2	0.23	147.11	-18	-179.59	622	B
CM13xx_XB	SKK	EQ060570308	4.59	9.46	21	10	1.25	0.3	155.14	-23.61	-179.99	535	B
CM13xx_XB	SKK	EQ060902114	4.59	9.46	9	6	0.9	0.22	83.49	3.8	126.34	37	B
CM15xx_XB	SKS	EQ063350358	5.03	9.93	11	4	1.2	0.23	86.72	3.39	99.08	204	B
CM15xx_XB	SKS	EQ063601226	5.03	9.93	174	12.5	1.6	0.6	65.5	21.8	120.55	10	B
CM15xx_XB	SKK	EQ060570308	5.03	9.93	14	5.5	1.05	0.17	153.58	-23.61	-179.99	535	B
CM15xx_XB	SKK	EQ062192218	5.03	9.93	4	15	0.65	0.22	117.88	-15.8	167.79	150	A
CM15xx_XB	SKK	EQ062761803	5.03	9.93	3	7	1	0.18	125.66	-18.84	169	161	B
CM16xx_XB	SKK	EQ060331248	5.48	10.57	8	16	0.8	0.33	145.05	-17.75	-178.39	597	B
CM16xx_XB	SKK	EQ060570308	5.48	10.57	34	18	0.9	0.4	151.6	-23.61	-179.99	535	B
CM17xx_XB	SKS	EQ060271658	5.55	12.31	24	4.5	1.55	0.27	93.36	-5.47	128.13	397	B
CM17xx_XB	SKS	EQ060911002	5.55	12.31	25	4.5	1.5	0.17	64.64	22.87	121.28	9	B
CM17xx_XB	SKS	EQ061752115	5.55	12.31	25	16	1.3	0.45	88.31	-0.39	123.19	26	B
CM17xx_XB	SKS	EQ061981545	5.55	12.31	31	9	0.95	0.25	98.8	-9.42	108.32	21	B
CM17xx_XB	SKS	EQ062731626	5.55	12.31	35	4.5	1.55	0.18	254.13	-15.59	-73.16	107	B
CM17xx_XB	SKS	EQ062821001	5.55	12.31	37	4	2.15	0.28	67.13	20.65	120.02	14	B
CM17xx_XB	SKS	EQ063350358	5.55	12.31	23	5.5	1.25	0.23	86.95	3.39	99.08	204	B
CM17xx_XB	PKS	EQ062900125	5.55	12.31	20	2	1.55	0.15	92.57	-5.88	150.98	32	B
CM17xx_XB	PKS	EQ063161821	5.55	12.31	30	11.5	1.05	0.3	93.08	-6.22	151.05	12	B
CM17xx_XB	PKS	EQ063171612	5.55	12.31	18	2.5	1.7	0.25	93.32	-6.38	151.23	11	B
CM17xx_XB	SKK	EQ060271658	5.55	12.31	17	5	1.55	0.42	93.36	-5.47	128.13	397	B
CM17xx_XB	SKK	EQ060331248	5.55	12.31	22	3.5	1.4	0.18	140.1	-17.75	-178.39	597	B
CM17xx_XB	SKK	EQ060551415	5.55	12.31	24	7.5	1.15	0.3	137.78	-18	-179.59	622	B
CM17xx_XB	SKK	EQ060570308	5.55	12.31	31	5.5	1.5	0.25	147.8	-23.61	-179.99	535	B
CM17xx_XB	SKK	EQ061600558	5.55	12.31	26	3.5	1.65	0.2	138.66	-17.53	-178.75	564	B
CM17xx_XB	SKK	EQ070211127	5.55	12.31	16	7	1.55	0.4	86.4	1.07	126.28	22	B
CM18xx_XB	SKS	EQ050281546	5.72	9.35	99	4.5	1.7	0.42	268.97	-1.09	-81.16	10	B
CM18xx_XB	SKS	EQ050300706	5.72	9.35	103	14.5	1.15	0.53	269.26	-0.79	-81.07	28	B
CM18xx_XB	SKS	EQ051680621	5.72	9.35	102	17.5	1.75	0.6	323.01	40.77	-126.57	12	B
CM18xx_XB	SKS	EQ053572147	5.72	9.35	112	16.5	0.55	0.28	268.31	-1.39	-77.52	192	B
CM18xx_XB	SKK	EQ050461442	5.72	9.35	103	4	1.45	0.22	81.86	4.76	126.42	39	B
CM19xx_XB	SKS	EQ062950855	5.97	11.23	9	16	1	0.28	135.77	-45.73	95.99	10	B
CM19xx_XB	SKS	EQ063350358	5.97	11.23	12	4	1.5	0.3	86.87	3.39	99.08	204	B
CM19xx_XB	SKK	EQ060551415	5.97	11.23	13	18	0.6	0.2	139.47	-18	-179.59	622	B
CM19xx_XB	SKK	EQ060570308	5.97	11.23	29	16	0.75	0.23	149.51	-23.61	-179.99	535	B
CM20xx_XB	SKS	EQ062970303	6.22	10.05	62	13.5	0.9	0.3	81.79	4.9	125.29	10	B
CM20xx_XB	SKK	EQ062731750	6.22	10.05	15	3	1.4	0.22	28.16	46.35	153.17	11	B
CM21xx_XB	SKS	EQ060271658	6.47	12.62	48	9.5	0.85	0.2	92.94	-5.47	128.13	397	B
CM21xx_XB	SKS	EQ060730657	6.47	12.62	46	18.5	1	0.55	90.98	-3.6	127.21	30	B
CM21xx_XB	SKS	EQ061202140	6.47	12.62	36	7	1.35	0.28	242.39	-27.21	-71.06	12	B
CM21xx_XB	SKS	EQ061752115	6.47	12.62	49	5	1.3	0.15	88.01	-0.39	123.19	26	B
CM21xx_XB	SKS	EQ061971142	6.47	12.62	38	16.5	1.1	0.4	241.09	-28.72	-72.54	10	B
CM21xx_XB	SKS	EQ062590945	6.47	12.62	61	7	1.65	0.33	90.17	-3.08	129.44	17	B

CM21xx_XB	SKS	EQ062731626	6.47	12.62	43	12	0.9	0.3	254.12	-15.59	-73.16	107	B
CM21xx_XB	SKS	EQ062731750	6.47	12.62	47	8.5	1.65	0.55	29.54	46.35	153.17	11	B
CM21xx_XB	SKS	EQ063350358	6.47	12.62	64	3.5	1.45	0.22	87.04	3.39	99.08	204	B
CM21xx_XB	PKS	EQ062900125	6.47	12.62	60	16	0.7	0.35	91.55	-5.88	150.98	32	B
CM21xx_XB	PKS	EQ063161821	6.47	12.62	66	15	0.8	0.25	92.06	-6.22	151.05	12	B
CM21xx_XB	PKS	EQ063281231	6.47	12.62	76	7	1	0.28	91.77	-6	150.48	24	B
CM21xx_XB	SKK	EQ060570308	6.47	12.62	29	16.5	0.5	0.23	145.88	-23.61	-179.99	535	B
CM22xx_XB	SKS	EQ060271658	6.48	13.27	71	16.5	1.1	0.52	92.99	-5.47	128.13	397	B
CM22xx_XB	SKS	EQ060871332	6.48	13.27	70	11	1.15	0.38	50.76	31.71	137.75	401	B
CM22xx_XB	SKS	EQ061752115	6.48	13.27	66	12.5	1.25	0.43	88.08	-0.39	123.19	26	B
CM22xx_XB	SKS	EQ062362150	6.48	13.27	71	8.5	0.85	0.12	23.93	51.15	157.52	43	B
CM22xx_XB	PKS	EQ060831227	6.48	13.27	68	5	1.1	0.2	88.81	-3.24	143.14	12	B
CM22xx_XB	PKS	EQ062900125	6.48	13.27	69	9	1.3	0.38	91.59	-5.88	150.98	32	B
CM22xx_XB	PKS	EQ063161821	6.48	13.27	72	7.5	1.15	0.27	92.09	-6.22	151.05	12	B
CM22xx_XB	PKS	EQ063281231	6.48	13.27	61	7	1.2	0.23	91.81	-6	150.48	24	B
CM22xx_XB	SKK	EQ060331248	6.48	13.27	75	4	1.45	0.17	135.57	-17.75	-178.39	597	A
CM22xx_XB	SKK	EQ060551415	6.48	13.27	80	5.5	1.5	0.25	133.53	-18	-179.59	622	B
CM22xx_XB	SKK	EQ060570308	6.48	13.27	81	4.5	1.55	0.23	144.56	-23.61	-179.99	535	B
CM22xx_XB	SKK	EQ062900125	6.48	13.27	72	12.5	0.8	0.3	91.59	-5.88	150.98	32	B
CM22xx_XB	SKK	EQ063171612	6.48	13.27	82	4	1.75	0.45	92.32	-6.38	151.23	11	B
CM23xx_XB	PKS	EQ063161821	6.37	10.79	79	10	1.45	0.52	92.05	-6.22	151.05	12	B
CM23xx_XB	SKK	EQ060570308	6.37	10.79	31	14.5	0.5	0.2	149.95	-23.61	-179.99	535	B
CM24xx_XB	SKS	EQ050611042	6.52	14.29	82	2	1.25	0.2	94.07	-6.53	129.93	201	B
CM24xx_XB	SKS	EQ051651710	6.52	14.29	66	15.5	0.65	0.2	10.93	51.24	179.31	17	B
CM24xx_XB	SKS	EQ060271658	6.52	14.29	82	11	1.1	0.52	93.06	-5.47	128.13	397	B
CM24xx_XB	SKS	EQ060730657	6.52	14.29	72	11	0.95	0.25	91.13	-3.6	127.21	30	B
CM24xx_XB	PKS	EQ050330628	6.52	14.29	79	3	1.7	0.3	94.22	-7.48	145.04	26	B
CM24xx_XB	PKS	EQ052721550	6.52	14.29	77	2.5	1.45	0.25	90.91	-5.44	151.84	25	B
CM24xx_XB	PKS	EQ063111738	6.52	14.29	81	3.5	2.1	0.62	92.49	-6.48	151.2	11	B
CM24xx_XB	PKS	EQ063161821	6.52	14.29	83	3.5	1.25	0.4	92.12	-6.22	151.05	12	B
CM24xx_XB	PKS	EQ063171612	6.52	14.29	80	6	1.5	0.5	92.34	-6.38	151.23	11	B
CM24xx_XB	PKS	EQ063281231	6.52	14.29	79	3	1.3	0.25	91.85	-6	150.48	24	B
CM24xx_XB	SKK	EQ051680621	6.52	14.29	86	3.5	1.45	0.15	326.08	40.77	-126.57	12	B
CM24xx_XB	SKK	EQ060331248	6.52	14.29	65	8.5	0.9	0.25	133.17	-17.75	-178.39	597	B
CM24xx_XB	SKK	EQ060570308	6.52	14.29	84	11.5	0.95	0.28	142.55	-23.61	-179.99	535	A
CM25xx_XB	PKS	EQ063281231	6.76	11.81	42	17.5	0.6	0.28	91.38	-6	150.48	24	B
CM25xx_XB	SKK	EQ063372052	6.76	11.81	82	6	1.75	0.38	285.61	13.99	-91.21	61	B
CM26xx_XB	SKS	EQ050611042	7.26	13.55	52	16.5	0.6	0.3	93.64	-6.53	129.93	201	B
CM26xx_XB	SKS	EQ060271658	7.26	13.55	26	8	0.9	0.25	92.65	-5.47	128.13	397	B
CM26xx_XB	SKS	EQ063192122	7.26	13.55	45	12	1.15	0.43	28.6	47.28	154.15	12	B
CM26xx_XB	PKS	EQ051551450	7.26	13.55	55	16.5	0.55	0.2	91.81	-6.32	146.85	26	B
CM26xx_XB	PKS	EQ052721550	7.26	13.55	71	15	0.75	0.33	90.01	-5.44	151.84	25	B
CM26xx_XB	PKS	EQ052981940	7.26	13.55	53	13.5	0.75	0.2	93.02	-7.15	145.98	175	B
CM26xx_XB	PKS	EQ053091048	7.26	13.55	26	17.5	0.65	0.27	87.27	-3.15	148.14	25	B
CM26xx_XB	PKS	EQ062900125	7.26	13.55	79	7	0.95	0.45	90.77	-5.88	150.98	32	B
CM26xx_XB	PKS	EQ063111738	7.26	13.55	69	17	0.65	0.32	91.63	-6.48	151.2	11	B

CM26xx_XB	PKS	EQ063161821	7.26	13.55	49	17	0.55	0.25	91.26	-6.22	151.05	12	B
CM26xx_XB	PKS	EQ063171612	7.26	13.55	39	14	0.6	0.2	91.48	-6.38	151.23	11	B
CM26xx_XB	PKS	EQ063281231	7.26	13.55	50	17.5	0.55	0.25	91	-6	150.48	24	B
CM26xx_XB	SKK	EQ060331248	7.26	13.55	65	15	1.15	0.43	132.95	-17.75	-178.39	597	B
CM26xx_XB	SKK	EQ062192218	7.26	13.55	70	12	0.65	0.2	110.88	-15.8	167.79	150	B
CM26xx_XB	SKK	EQ062881707	7.26	13.55	43	11.5	1.3	0.37	339.17	19.88	-155.93	38	B
CM27xx_XB	PKS	EQ063111738	7.36	12.67	55	10	0.65	0.1	91.43	-6.48	151.2	11	B
CM27xx_XB	PKS	EQ063171612	7.36	12.67	60	18	0.65	0.25	91.28	-6.38	151.23	11	B
CM28xx_XB	SKS	EQ060630811	8.47	13.24	71	17.5	1.3	0.47	284.45	12.6	-89.36	27	B
CM28xx_XB	SKS	EQ061752115	8.47	13.24	24	6.5	1.1	0.22	87.37	-0.39	123.19	26	B
CM28xx_XB	SKK	EQ060271658	8.47	13.24	73	9.5	0.9	0.32	92.05	-5.47	128.13	397	B
CM29xx_XB	SKS	EQ050361223	9.35	13.39	49	17.5	0.5	0.25	81.18	5.29	123.34	525	B
CM29xx_XB	SKS	EQ050461442	9.35	13.39	53	14	0.75	0.28	81.06	4.76	126.42	39	B
CM29xx_XB	SKS	EQ051651710	9.35	13.39	66	10	1.05	0.27	10.02	51.24	179.31	17	B
CM29xx_XB	SKS	EQ052260239	9.35	13.39	50	17.5	1.1	0.55	249.33	-19.78	-68.98	113	B
CM29xx_XB	SKS	EQ053131133	9.35	13.39	36	9.5	1.05	0.27	269.05	-1.02	-76.94	248	B
CM29xx_XB	SKS	EQ053341653	9.35	13.39	65	7.5	1.25	0.35	80.02	6.27	124.03	13	B
CM29xx_XB	SKS	EQ061980819	9.35	13.39	73	13	1.15	0.48	98.49	-9.28	107.42	20	B
CM29xx_XB	SKS	EQ061981545	9.35	13.39	65	3.5	1.05	0.1	98.49	-9.42	108.32	21	B
CM29xx_XB	SKS	EQ062641854	9.35	13.39	51	19	0.85	0.38	97.83	-9.05	110.36	25	B
CM29xx_XB	SKS	EQ063350358	9.35	13.39	48	9	1.05	0.2	87.36	3.39	99.08	204	B
CM29xx_XB	SKS	EQ063461548	9.35	13.39	55	8	1.2	0.32	82.51	3.73	124.68	213	B
CM29xx_XB	PKS	EQ062441018	9.35	13.39	65	6.5	1.1	0.23	88.96	-6.76	155.51	38	B
CM29xx_XB	PKS	EQ062900125	9.35	13.39	59	11	0.9	0.23	88.45	-5.88	150.98	32	B
CM29xx_XB	PKS	EQ063111738	9.35	13.39	45	14	1.2	0.38	89.3	-6.48	151.2	11	B
CM29xx_XB	PKS	EQ063161821	9.35	13.39	51	11	0.95	0.23	88.94	-6.22	151.05	12	B
CM29xx_XB	PKS	EQ063171612	9.35	13.39	49	13	0.9	0.18	89.14	-6.38	151.23	11	B
CM29xx_XB	SKK	EQ050461442	9.35	13.39	43	4.5	1.4	0.15	81.06	4.76	126.42	39	B
CM29xx_XB	SKK	EQ062192218	9.35	13.39	51	5.5	1.05	0.15	106.97	-15.8	167.79	150	B
CM29xx_XB	SKK	EQ063411910	9.35	13.39	45	9.5	1.3	0.57	28.78	46.15	154.39	16	B
CM30xx_XB	SKS	EQ061462253	9.76	13.95	39	15.5	1.3	0.42	96.76	-7.96	110.45	12	B
CM30xx_XB	SKS	EQ061752115	9.76	13.95	57	4.5	0.85	0.1	87.04	-0.39	123.19	26	A
CM30xx_XB	SKS	EQ061892040	9.76	13.95	61	12	1.1	0.3	9.42	51.21	-179.31	22	B
CM30xx_XB	SKS	EQ061981545	9.76	13.95	51	3.5	1.1	0.1	98.53	-9.42	108.32	21	B
CM30xx_XB	SKS	EQ063372052	9.76	13.95	31	8	2	0.62	286.61	13.99	-91.21	61	B
CM30xx_XB	PKS	EQ061480312	9.76	13.95	51	13.5	0.95	0.38	87.85	-5.72	151.13	34	B
CM30xx_XB	PKS	EQ062900125	9.76	13.95	44	7.5	0.85	0.12	88.12	-5.88	150.98	32	B
CM30xx_XB	PKS	EQ063111738	9.76	13.95	34	12.5	1	0.2	88.95	-6.48	151.2	11	B
CM30xx_XB	PKS	EQ063161821	9.76	13.95	38	8	1	0.18	88.6	-6.22	151.05	12	B
CM30xx_XB	PKS	EQ063171612	9.76	13.95	44	8	0.9	0.15	88.8	-6.38	151.23	11	B
CM30xx_XB	PKS	EQ063612015	9.76	13.95	48	13	0.75	0.25	87.14	-5.72	154.42	355	B
CM30xx_XB	SKK	EQ060551415	9.76	13.95	56	4	1.4	0.18	123.4	-18	-179.59	622	B
CM30xx_XB	SKK	EQ061200817	9.76	13.95	42	10.5	1.25	0.3	104.26	-15.1	167.44	127	B
CM30xx_XB	SKK	EQ061600558	9.76	13.95	66	4	1.4	0.17	123.4	-17.53	-178.75	564	B
CM30xx_XB	SKK	EQ062192218	9.76	13.95	45	4	1.45	0.2	105.94	-15.8	167.79	150	A
CM30xx_XB	SKK	EQ070082052	9.76	13.95	56	4	1.85	0.4	128.77	-18.58	-177.85	406	B

CM31xx_XB	SKS	EQ060271658	10.33	15.26	65	7	1.1	0.2	91.51	-5.47	128.13	397	B
CM31xx_XB	SKS	EQ061102325	10.33	15.26	55	8	0.85	0.1	13.84	60.95	167.09	22	B
CM31xx_XB	SKS	EQ061110432	10.33	15.26	59	15	0.55	0.17	14.62	60.53	165.82	9	B
CM31xx_XB	SKS	EQ061111114	10.33	15.26	78	12	1.3	0.52	13.45	61.35	167.52	12	B
CM31xx_XB	SKS	EQ061421112	10.33	15.26	50	17.5	0.9	0.45	14.53	60.77	165.74	19	B
CM31xx_XB	SKS	EQ061462253	10.33	15.26	61	14	1	0.35	96.9	-7.96	110.45	12	B
CM31xx_XB	SKS	EQ061752115	10.33	15.26	58	13	1.15	0.33	87.1	-0.39	123.19	26	B
CM31xx_XB	SKS	EQ061892040	10.33	15.26	57	5.5	1	0.13	10.27	51.21	-179.31	22	B
CM31xx_XB	SKS	EQ061981545	10.33	15.26	47	11.5	1	0.28	98.69	-9.42	108.32	21	B
CM31xx_XB	SKS	EQ062362150	10.33	15.26	78	10.5	0.95	0.2	24.32	51.15	157.52	43	B
CM31xx_XB	SKS	EQ062590945	10.33	15.26	49	12.5	1.15	0.4	88.72	-3.08	129.44	17	B
CM31xx_XB	SKS	EQ062900125	10.33	15.26	64	10.5	1.15	0.35	87.79	-5.88	150.98	32	B
CM31xx_XB	PKS	EQ061480312	10.33	15.26	63	17	1	0.35	87.54	-5.72	151.13	34	B
CM31xx_XB	PKS	EQ062900125	10.33	15.26	66	13.5	0.95	0.35	87.79	-5.88	150.98	32	B
CM31xx_XB	PKS	EQ063161821	10.33	15.26	61	14	0.9	0.28	88.26	-6.22	151.05	12	B
CM31xx_XB	SKK	EQ060271658	10.33	15.26	58	10	1.05	0.23	91.51	-5.47	128.13	397	B
CM31xx_XB	SKK	EQ061731053	10.33	15.26	65	9	0.95	0.23	32.77	45.42	149.34	95	B
CM31xx_XB	SKK	EQ062192218	10.33	15.26	60	2	1.2	0.08	104.41	-15.8	167.79	150	A
CM31xx_XB	SKK	EQ062362150	10.33	15.26	67	15.5	0.5	0.2	24.32	51.15	157.52	43	B
CM32xx_XB	SKS	EQ050611042	10.62	14.37	56	8	0.75	0.1	92.08	-6.53	129.93	201	B
CM32xx_XB	SKS	EQ053251536	10.62	14.37	18	13	0.65	0.2	53.53	31.02	130	145	B
CM32xx_XB	SKS	EQ061110432	10.62	14.37	36	18.5	1	0.4	14.2	60.53	165.82	9	B
CM32xx_XB	SKS	EQ061752115	10.62	14.37	64	8.5	1.05	0.23	86.83	-0.39	123.19	26	B
CM32xx_XB	SKS	EQ061981545	10.62	14.37	39	15.5	0.85	0.32	98.52	-9.42	108.32	21	B
CM32xx_XB	SKS	EQ062362150	10.62	14.37	84	8	0.85	0.2	23.81	51.15	157.52	43	B
CM32xx_XB	SKS	EQ062641854	10.62	14.37	52	11	1	0.22	97.81	-9.05	110.36	25	B
CM32xx_XB	SKS	EQ062731626	10.62	14.37	62	5	1.35	0.38	254.33	-15.59	-73.16	107	B
CM32xx_XB	SKS	EQ063351401	10.62	14.37	39	12	0.9	0.18	95.68	-8.26	118.75	19	B
CM32xx_XB	PKS	EQ051551450	10.62	14.37	47	18.5	0.5	0.33	88.8	-6.32	146.85	26	B
CM32xx_XB	PKS	EQ052981940	10.62	14.37	36	15	0.75	0.23	90.07	-7.15	145.98	175	A
CM32xx_XB	PKS	EQ053561220	10.62	14.37	43	7.5	1.2	0.32	202.12	-54.72	-135.87	10	B
CM32xx_XB	PKS	EQ063161821	10.62	14.37	77	2	2.05	0.3	87.76	-6.22	151.05	12	B
CM32xx_XB	SKK	EQ050611042	10.62	14.37	52	3	1.25	0.08	92.08	-6.53	129.93	201	A
CM32xx_XB	SKK	EQ060271658	10.62	14.37	42	7	1.5	0.22	91.24	-5.47	128.13	397	B
CM32xx_XB	SKK	EQ060551415	10.62	14.37	55	3.5	1.75	0.23	120.06	-18	-179.59	622	B
CM32xx_XB	SKK	EQ061600558	10.62	14.37	58	13.5	1.25	0.4	119.83	-17.53	-178.75	564	B
CM32xx_XB	SKK	EQ062192218	10.62	14.37	52	3.5	0.8	0.08	104.12	-15.8	167.79	150	A
CM32xx_XB	SKK	EQ062761803	10.62	14.37	67	8.5	1.3	0.2	111.38	-18.84	169	161	B
EKNAxx_AF	SKKS	EQ082051526	4.23	9.33	19	5	1.5	0.28	40.3	39.802	141.464	108	B
IFExxx_AF	SKS	EQ092461951	7.55	4.46	131	9	1	0.33	65.97	24.33	94.67	95	B
IFExxx_AF	SKS	EQ092501612	7.55	4.46	126	7	1.45	0.32	98.34	-10.2	110.63	23	B
IFExxx_AF	SKS	EQ092771058	7.55	4.46	143	9.5	0.8	0.2	78.41	6.74	123.38	620	A
IFExxx_AF	SKS	EQ092862021	7.55	4.46	138	7	2	0.4	354.1	52.6	-167.12	14	B
IFExxx_AF	SKS	EQ093030703	7.55	4.46	115	19.5	0.9	0.45	52.49	29.22	129.78	34	B
IFExxx_AF	SKS	EQ093121941	7.55	4.46	137	13	1.4	0.42	95.55	-8.21	118.63	18	B
IFExxx_AF	SKK	EQ092771058	7.55	4.46	134	9	1.1	0.23	78.41	6.74	123.38	620	B

IFExxx_AF	SKK	EQ092860537	7.55	4.46	139	4.5	1.35	0.15	354.05	52.75	-167	24	B
IFExxx_AF	SKK	EQ092862021	7.55	4.46	150	6	1.45	0.28	354.1	52.6	-167.12	14	B
MSKUxx_IU	SKS	EQ000480454	-1.66	13.61	68	14.5	1.4	0.42	115.59	-10.9	166.69	33	B
MSKUxx_IU	SKS	EQ000571824	-1.66	13.61	31	5	1.25	0.28	279.29	9.41	-78.53	65	A
MSKUxx_IU	SKS	EQ000722221	-1.66	13.61	47	12.5	1.25	0.33	285.01	14.98	-92.44	62	B
MSKUxx_IU	SKS	EQ000881100	-1.66	13.61	51	9	1.15	0.43	63.01	22.34	143.73	126	B
MSKUxx_IU	SKS	EQ000941520	-1.66	13.61	64	2	1	0.1	86.29	4.08	125.61	150	B
MSKUxx_IU	SKS	EQ001042054	-1.66	13.61	35	17	0.65	0.4	79.59	10.3	126.52	33	B
MSKUxx_IU	SKS	EQ001580958	-1.66	13.61	28	13.5	0.95	0.35	95.03	-5.09	102.7	33	B
MSKUxx_IU	SKS	EQ001592345	-1.66	13.61	24	18.5	1	0.48	94.53	-4.61	101.9	33	B
MSKUxx_IU	SKS	EQ001621823	-1.66	13.61	39	7.5	0.7	0.15	65.72	23.84	121.22	33	B
MSKUxx_IU	SKS	EQ001661700	-1.66	13.61	22	16	0.75	0.28	85.8	4.54	127.72	89	B
MSKUxx_IU	SKS	EQ002030153	-1.66	13.61	61	16	0.9	0.3	279.21	9.42	-85.33	33	B
MSKUxx_IU	SKS	EQ002102028	-1.66	13.61	25	15	0.6	0.22	66.24	23.36	120.92	33	B
MSKUxx_IU	SKS	EQ002201433	-1.66	13.61	71	10.5	1.05	0.32	97.98	-7.02	123.36	648	B
MSKUxx_IU	SKS	EQ021671831	-1.66	13.61	57	5.5	0.85	0.12	92.29	-2.34	102.56	231	B
MSKUxx_IU	SKS	EQ031710619	-1.66	13.61	45	3.5	1.15	0.13	262.55	-7.61	-71.72	558	B
MSKUxx_IU	SKS	EQ031820552	-1.66	13.61	65	3.5	0.95	0.12	85.81	4.53	122.51	635	B
MSKUxx_IU	SKS	EQ991161817	-1.66	13.61	48	4.5	1.25	0.15	268.32	-1.65	-77.78	172	B
MSKUxx_IU	PKS	EQ000371133	-1.66	13.61	37	9.5	0.7	0.15	100.25	-5.84	150.88	33	B
MSKUxx_IU	PKS	EQ000431629	-1.66	13.61	66	10	0.7	0.15	102.37	-6.57	155.01	33	B
MSKUxx_IU	PKS	EQ000460205	-1.66	13.61	50	3.5	1.05	0.18	68.27	17.67	145.4	521	B
MSKUxx_IU	PKS	EQ001120435	-1.66	13.61	56	8	1.1	0.2	9.5	51.42	-178.14	33	B
MSKUxx_IU	PKS	EQ001610127	-1.66	13.61	48	16	0.7	0.38	99.48	-5.07	152.49	33	B
MSKUxx_IU	PKS	EQ002272211	-1.66	13.61	29	7	1.2	0.38	106.23	-9.38	153.85	10	B
MSKUxx_IU	PKS	EQ032021353	-1.66	13.61	55	14	0.5	0.15	99.33	-5.48	148.85	189	B
MSKUxx_IU	PKS	EQ032060937	-1.66	13.61	63	5.5	0.7	0.1	93.9	-1.53	149.69	24	A
MSKUxx_IU	PKS	EQ990951108	-1.66	13.61	53	6	0.65	0.07	99.62	-5.59	149.57	150	A
MSKUxx_IU	PKS	EQ990960822	-1.66	13.61	75	7	0.7	0.15	100.41	-6.53	147.01	33	B
MSKUxx_IU	PKS	EQ991011650	-1.66	13.61	57	8.5	0.7	0.12	99.98	-6	148.49	58	B
MSKUxx_IU	PKS	EQ991051354	-1.66	13.61	66	7	0.7	0.12	100.16	-6.35	146.98	31	B
MSKUxx_IU	PKS	EQ991131856	-1.66	13.61	41	18	0.8	0.35	74.16	13.12	145.14	52	B
MSKUxx_IU	PKS	EQ991302033	-1.66	13.61	51	11.5	0.6	0.13	99.27	-5.16	150.88	138	A
MSKUxx_IU	PKS	EQ991360051	-1.66	13.61	67	8	0.65	0.1	99	-4.75	152.49	73	B
MSKUxx_IU	SKK	EQ000371133	-1.66	13.61	51	16.5	0.6	0.25	100.25	-5.84	150.88	33	B
MSKUxx_IU	SKK	EQ000431629	-1.66	13.61	46	3	0.95	0.1	102.37	-6.57	155.01	33	A
MSKUxx_IU	SKK	EQ000632209	-1.66	13.61	57	15.5	0.6	0.2	98.75	-7.32	128.49	141	B
MSKUxx_IU	SKK	EQ000881100	-1.66	13.61	48	10.5	1.1	0.35	63.01	22.34	143.73	126	B
MSKUxx_IU	SKK	EQ000941520	-1.66	13.61	49	8	0.8	0.15	86.29	4.08	125.61	150	B
MSKUxx_IU	SKK	EQ001610127	-1.66	13.61	41	18	0.65	0.32	99.48	-5.07	152.49	33	B
MSKUxx_IU	SKK	EQ001660215	-1.66	13.61	34	5	1.55	0.27	151.87	-25.52	178.05	604	B
MSKUxx_IU	SKK	EQ002172113	-1.66	13.61	24	4	2	0.52	34.99	48.79	142.25	10	B
MSKUxx_IU	SKK	EQ002201433	-1.66	13.61	53	7	0.7	0.1	97.98	-7.02	123.36	648	A
MSKUxx_IU	SKK	EQ002280430	-1.66	13.61	32	15	0.8	0.23	159.35	-31.51	179.73	357	B
MSKUxx_IU	SKK	EQ002411505	-1.66	13.61	65	16	1	0.3	95.18	-4.11	127.39	16	B
MSKUxx_IU	SKK	EQ032021353	-1.66	13.61	57	16	0.65	0.27	99.33	-5.48	148.85	189	B

MSKUxx_IU	SKK	EQ032051023	-1.66	13.61	43	10	0.7	0.15	90.48	0.14	124.58	73	B
MSKUxx_IU	SKK	EQ032080204	-1.66	13.61	47	13.5	1.05	0.4	156.69	-21.08	-176.59	212	B
MSKUxx_IU	SKK	EQ990600851	-1.66	13.61	50	17	0.5	0.25	93.9	-2.97	126.53	33	B
MSKUxx_IU	SKK	EQ990951108	-1.66	13.61	54	6.5	0.75	0.07	99.62	-5.59	149.57	150	A
MSKUxx_IU	SKK	EQ990960822	-1.66	13.61	64	16.5	0.55	0.22	100.41	-6.53	147.01	33	B
MSKUxx_IU	SKK	EQ991031038	-1.66	13.61	48	9	0.9	0.25	157.29	-21.42	-176.46	164	B
MSKUxx_IU	SKK	EQ991131856	-1.66	13.61	38	9	0.85	0.2	74.16	13.12	145.14	52	B
MSKUxx_IU	SKK	EQ991371007	-1.66	13.61	60	14.5	0.6	0.25	99.69	-5.16	152.88	27	B
TOROxx_NJ	SKS	EQ121640559	10.99	8.12	-50	6	1.8	0.3	94.19	-5.677	105.494	163.9	B
TOROxx_NJ	SKS	EQ121682218	10.99	8.12	-50	15	0.85	0.32	69.86	15.593	119.563	28	B
TOROxx_NJ	SKS	EQ121750434	10.99	8.12	-65	14.5	1.3	0.6	87.11	3.009	97.896	95	B

BIBLIOGRAPHY

Abdelsalam, M. G., J.-P. Liégeois, and R. J. Stern (2002), The Saharan Metacraton, Journal of African Earth Sciences, 34(3–4), 119-136.

Abdelsalam, M. G., S. S. Gao, and J.-P. Liégeois (2011), Upper mantle structure of the Saharan Metacraton, Journal of African Earth Sciences, 60(5), 328-336.

Aka, F. T., K. Nagao, M. Kusakabe, H. Sumino, G. Tanyileke, B. Ateba, and J. Hell (2004), Symmetrical Helium isotope distribution on the Cameroon Volcanic Line, West Africa, Chemical Geology, 203(3–4), 205-223.

Anderson, D. L. (1994), The sublithospheric mantle as the source of continental flood basalts; the case against the continental lithosphere and plume head reservoirs, Earth and Planetary Science Letters, 123(1–3), 269-280.

Anderson, D. L. (2000), The thermal state of the upper mantle; No role for mantle plumes, Geophysical Research Letters, 27(22), 3623-3626.

Artemieva, I. M., and W. D. Mooney (2002), On the relations between cratonic lithosphere thickness, plate motions, and basal drag, Tectonophysics, 358(1–4), 211-231.

Avigad, D., and Z. Gvirtzman (2009), Late Neoproterozoic rise and fall of the northern Arabian–Nubian shield: The role of lithospheric mantle delamination and subsequent thermal subsidence, Tectonophysics, 477(3–4), 217-228.

Babuška, V., and J. Plomerová (1989), Seismic anisotropy of the subcrustal lithosphere in Europe: Another clue to recognition of accreted terranes, 209-217 pp., AGU, Washington, D. C.

Bagley, B., and A. A. Nyblade (2013), Seismic anisotropy in eastern Africa, mantle flow, and the African superplume, Geophysical Research Letters, 40(8), 1500-1505.

Barruol, G., and R. Hoffmann (1999), Upper mantle anisotropy beneath the Geoscope stations, Journal of Geophysical Research: Solid Earth, 104(B5), 10757-10773.

Barruol, G., and W. B. Ismail (2001), Upper mantle anisotropy beneath the African IRIS and Geoscope stations, Geophysical Journal International, 146(2), 549-561.

Barruol, G., and F. R. Fontaine (2013), Mantle flow beneath La Réunion hotspot track from SKS splitting, Earth and Planetary Science Letters, 362(0), 108-121.

Bastow, I. D., and D. Keir (2011), The protracted development of the continent-ocean transition in Afar, Nature Geosci, 4(4), 248-250.

Begg, G. C., et al. (2009), The lithospheric architecture of Africa: Seismic tomography, mantle petrology, and tectonic evolution, Geosphere, 5(1), 23-50.

Behn, M. D., C. P. Conrad, and P. G. Silver (2004), Detection of upper mantle flow associated with the African Superplume, Earth and Planetary Science Letters, 224(3–4), 259-274.

Ben-Ismail, W., G. Barruol, and D. Mainprice (2001), The Kaapvaal craton seismic anisotropy: Petrophysical analyses of upper mantle kimberlite nodules, Geophys. Res. Lett., 28, 2497-2500.

Berhe, S. M. (1990), Ophiolites in Northeast and East Africa: implications for Proterozoic crustal growth, J. Geol. Soc. London, 147, 41-57.

Birch, F. (1960), The velocity of compressional waves in rocks to 10 kilobars: 1, Journal of Geophysical Research, 65(4), 1083-1102.

Bosworth, W., P. Huchon, and K. McClay (2005), The Red Sea and Gulf of Aden Basins, Journal of African Earth Sciences, 43(1–3), 334-378.

Burke, K. (2001), Origin of the Cameroon Line of Volcano-Capped Swells, The Journal of Geology, 109(3), 349-362.

Burke, K., and J. F. Dewey (1973), Plume-generated triple junctions: key Indicators in applying plate tectonics to old rocks, The Journal of Geology, 81(4), 406-433.

Burke, K., and J. T. Wilson (1976), Hot spots on the earth's surface, Scientific American, 235(2), 46-60.

Camp, V. E., and M. J. Roobol (1992), Upwelling asthenospher beneath western Arabia and Its regional implications, J. Geophys. Res., 97(B11), 15,255-215,271.

Castaing, C., J. L. Feybesse, D. Thiéblemont, C. Triboulet, and P. Chèvremont (1994), Palaeogeographical reconstructions of the Pan-African/Brasiliano orogen: closure of an oceanic domain or intracontinental convergence between major blocks?, Precambrian Research, 69(1–4), 327-344.

Chang, S.-J., and S. Van der Lee (2011), Mantle plumes and associated flow beneath Arabia and East Africa, Earth and Planetary Science Letters, 302, 448-454.

Chastel, Y. B., P. R. Dawson, H.-R. Wenk, and K. Bennett (1993), Anisotropic convection with implications for the upper mantle, Journal of Geophysical Research: Solid Earth, 98(B10), 17757-17771.

Chevrot, S. (2000), Multichannel analysis of shear wave splitting, Journal of Geophysical Research: Solid Earth, 105(B9), 21579-21590.

Conrad, C. P., and B. H. Hager (2001), Mantle convection with strong subduction zones, Geophysical Journal International, 144(2), 271-288.

Conrad, C. P., and M. D. Behn (2010), Constraints on lithosphere net rotation and asthenospheric viscosity from global mantle flow models and seismic anisotropy, Geochemistry, Geophysics, Geosystems, 11(5), Q05W05.

Conrad, C. P., M. D. Behn, and P. G. Silver (2007), Global mantle flow and the development of seismic anisotropy: Differences between the oceanic and continental upper mantle, Journal of Geophysical Research: Solid Earth, 112(B7), B07317.

Conrad, C. P., T. A. Bianco, E. I. Smith, and P. Wessel (2011), Patterns of intraplate volcanism controlled by asthenospheric shear, Nature Geosci, 4(5), 317-321.

Courtillot, V., A. Davaille, J. Besse, and J. Stock (2003), Three distinct types of hotspots in the Earth's mantle, Earth and Planetary Science Letters, 205(3–4), 295-308.

Davies, G. F. (1994), Thermomechanical erosion of the lithosphere by mantle plumes, Journal of Geophysical Research: Solid Earth, 99(B8), 15709-15722.

DeMets, C., R. G. Gordon, D. F. Argus, and S. Stein (1994), Effect of recent revisions to the geomagnetic reversal time scale on estimates of current plate motions, Geophysical Research Letters, 21(20), 2191-2194.

Dercourt, J., et al. (1986), Geological evolution of the tethys belt from the atlantic to the pamirs since the LIAS, Tectonophysics, 123(1–4), 241-315.

Déruelle, B., I. Ngounouno, and D. Demaiffe (2007), The 'Cameroon Hot Line' (CHL): A unique example of active alkaline intraplate structure in both oceanic and continental lithospheres, Comptes Rendus Geoscience, 339(9), 589-600.

Déruelle, B., C. Moreau, C. Nkoumbou, R. Kambou, J. Lissom, E. Njonfang, R. T. Ghogomu, and A. Nono (1991), The Cameroon Line: A Review, in Magmatism in Extensional Structural Settings, edited by A. B. Kampunzu and R. T. Lubala, pp. 274-327, Springer Berlin Heidelberg.

Djomani, Y. H. P., J. M. Nnange, M. Diament, C. J. Ebinger, and J. D. Fairhead (1995), Effective elastic thickness and crustal thickness variations in west central Africa inferred from gravity data, Journal of Geophysical Research: Solid Earth, 100(B11), 22047-22070.

Doglioni, C., E. Carminati, M. Cuffaro, and D. Scrocca (2007), Subduction kinematics and dynamic constraints, Earth-Science Reviews, 83(3–4), 125-175.

Dorbath, C., L. Dorbath, J. D. Fairhead, and G. W. Stuart (1986), A teleseismic delay time study scross the central African shear zone In the Adamawa region of Cameroon, west Africa, Geophysical Journal of the Royal Astronomical Society, 86(3), 751-766.

Doubrovine, P. V., B. Steinberger, and T. H. Torsvik (2012), Absolute plate motions in a reference frame defined by moving hot spots in the Pacific, Atlantic, and Indian oceans, Journal of Geophysical Research: Solid Earth, 117(B9), B09101.

Druken, K. A., C. Kincaid, and R. W. Griffiths (2013), Directions of seismic anisotropy in laboratory models of mantle plumes, Geophysical Research Letters, 40(14), 3544-3549.

Ebinger, C. J., and N. H. Sleep (1998), Cenozoic magmatism throughout east Africa resulting from impact of a single plume, Nature, 395(6704), 788-791.

Faccenna, C., T. W. Becker, L. Jolivet, and M. Keskin (2013), Mantle convection in the Middle East: Reconciling Afar upwelling, Arabia indentation and Aegean trench rollback, Earth and Planetary Science Letters, 375(0), 254-269.

Fairhead, J. D. (1988), Mesozoic plate tectonic reconstructions of the central South Atlantic Ocean: The role of the West and Central African rift system, Tectonophysics, 155(1–4), 181-191.

Fairhead, J. D., and C. S. Okereke (1987), A regional gravity study of the West African rift system in Nigeria and Cameroon and its tectonic interpretation, Tectonophysics, 143(1–3), 141-159.

Fitton, J. G. (1987), The Cameroon line, West Africa: a comparison between oceanic and continental alkaline volcanism, Geological Society, London, Special Publications, 30(1), 273-291.

Fitton, J. G., and D. J. Hughes (1981), Strontian melilite in nephelinite lava from Etinde, in Mineralogical Magazine, edited, pp. 261– 264.

Fitton, J. G., and H. M. Dunlop (1985), The Cameroon line, West Africa, and its bearing on the origin of oceanic and continental alkali basalt, Earth and Planetary Science Letters, 72(1), 23-38.

Forte, A. M., S. Quéré, R. Moucha, N. A. Simmons, S. P. Grand, J. X. Mitrovica, and D. B. Rowley (2010), Joint seismic–geodynamic-mineral physical modelling of African geodynamics: A reconciliation of deep-mantle convection with surface geophysical constraints, Earth and Planetary Science Letters, 295(3–4), 329-341.

Fouch, M. J., and S. Rondenay (2006), Seismic anisotropy beneath stable continental interiors, Physics of the Earth and Planetary Interiors, 158(2–4), 292-320.

Fouch, M. J., P. G. Silver, D. R. Bell, and J. N. Lee (2004), Small-scale variations in seismic anisotropy near Kimberley, South Africa, Geophysical Journal International, 157(2), 764-774.

Fouch, M. J., K. M. Fischer, E. M. Parmentier, M. E. Wysession, and T. J. Clarke (2000), Shear wave splitting, continental keels, and patterns of mantle flow, Journal of Geophysical Research: Solid Earth, 105(B3), 6255-6275.

Funiciello, F., M. Moroni, C. Piromallo, C. Faccenna, A. Cenedese, and H. A. Bui (2006), Mapping mantle flow during retreating subduction: Laboratory models analyzed by feature tracking, Journal of Geophysical Research: Solid Earth, 111(B3), B03402.

Gallacher, R. J., and I. D. Bastow (2012), The development of magmatism along the Cameroon Volcanic Line: Evidence from teleseismic receiver functions, Tectonics, 31(3), TC3018.

Gao, S. S., and K. H. Liu (2009), Significant seismic anisotropy beneath the southern Lhasa Terrane, Tibetan Plateau, Geochemistry, Geophysics, Geosystems, 10(2), Q02008.

Gao, S. S., K. H. Liu, and M. G. Abdelsalam (2010), Seismic anisotropy beneath the Afar Depression and adjacent areas: Implications for mantle flow, Journal of Geophysical Research: Solid Earth, 115(B12), B12330.

Gao, S. S., K. H. Liu, R. J. Stern, G. R. Keller, J. P. Hogan, J. Pulliam, and E. Y. Anthony (2008), Characteristics of mantle fabrics beneath the south-central United States: Constraints from shear-wave splitting measurements, Geosphere, 4(2), 411-417.

Gao, S., P. M. Davis, H. Liu, P. D. Slack, Y. A. Zorin, V. V. Mordvinova, V. M. Kozhevnikov, and R. P. Meyer (1994), Seismic anisotropy and mantle flow beneath the Baikal rift zone, Nature, 371(6493), 149-151.

Gao, S., P. M. Davis, H. Liu, P. D. Slack, A. W. Rigor, Y. A. Zorin, V. V. Mordvinova, V. M. Kozhevnikov, and N. A. Logatchev (1997), SKS splitting beneath continental rift zones, Journal of Geophysical Research: Solid Earth, 102(B10), 22781-22797.

Gashawbeza, E. M., S. L. Klemperer, A. A. Nyblade, K. T. Walker, and K. M. Keranen (2004), Shear-wave splitting in Ethiopia: Precambrian mantle anisotropy locally modified by Neogene rifting, Geophysical Research Letters, 31(18), L18602.

Gripp, A. E., and R. G. Gordon (2002), Young tracks of hotspots and current plate velocities, Geophysical Journal International, 150(2), 321-361.

Hansen, S. E., A. A. Nyblade, and J. Julià (2009), Estimates of crustal and lithospheric thickness in Sub-Saharan Africa from S-wave receiver functions, South African Journal of Geology, 112(3-4), 229-240.

Hansen, S., S. Schwartz, A. Al-Amri, and A. Rodgers (2006), Combined plate motion and density-driven flow in the asthenosphere beneath Saudi Arabia: Evidence from shear-wave splitting and seismic anisotropy, Geology, 34, 869–872.

Hansen, S., A. Rodgers, S. Schwartz, and A. Al-Amri (2007), Imaging ruptured lithosphere beneath the Red Sea and Arabian Peninsula, Earth Planet. Sci. Lett., 259, 256-265.

James, D. E., and M. Assumpção (1996), Tectonic implications of S-wave anisotropy beneath SE Brazil, Geophysical Journal International, 126(1), 1-10.

Jolivet, L., and C. Faccenna (2000), Mediterranean extension and the Africa-Eurasia collision, Tectonics, 19(6), 1095-1106.

Karato, S. C., H. Jung, I. Katayama, and P. Skemer (2008), Geodynamic Significance of Seismic Anisotropy of the Upper Mantle: New Insights from Laboratory Studies, Annual Review of Earth and Planetary Sciences, 36(1), 59-95.

Kaviani, A., R. Hofstetter, G. Rümpker, and M. Weber (2013), Investigation of seismic anisotropy beneath the Dead Sea fault using dense networks of broadband stations, Journal of Geophysical Research: Solid Earth, 118(7), 3476-3491.

Kaviani, A., G. Rumpker, M. Weber, and G. Asch (2011), Short-scale variations of shear wave splitting across the Dead Sea basin: Evidence for the effects of sedimentary fill, Geophys. Res. Lett., 38, L04308, doi:10.1029/2010GL046464.

Kendall, J. M., G. W. Stuart, C. J. Ebinger, I. D. Bastow, and D. Keir (2005), Magma-assisted rifting in Ethiopia, Nature, 433(7022), 146-148.

Kendall, J. M., S. Pilidou, D. Keir, I. D. Bastow, G. W. Stuart, and A. Ayele (2006), Mantle upwellings, melt migration and the rifting of Africa: insights from seismic anisotropy, Geological Society, London, Special Publications, 259(1), 55-72.

King, S. D., and D. L. Anderson (1995), An alternative mechanism of flood basalt formation, Earth and Planetary Science Letters, 136(3–4), 269-279.

King, S. D., and D. L. Anderson (1998), Edge-driven convection, Earth and Planetary Science Letters, 160(3–4), 289-296.

King, S. D., and J. Ritsema (2000), African hot spot volcanism: Small-scale convection in the upper mantle beneath cratons, Science, 290(5494), 1137-1140.

Koch, F. W., D. A. Wiens, A. A. Nyblade, P. J. Shore, R. Tibi, B. Ateba, C. T. Tabod, and J. M. Nnange (2012), Upper-mantle anisotropy beneath the Cameroon Volcanic Line and Congo Craton from shear wave splitting measurements, Geophysical Journal International, 190(1), 75-86.

Kreemer, C. (2009), Absolute plate motions constrained by shear wave splitting orientations with implications for hot spot motions and mantle flow, Journal of Geophysical Research: Solid Earth, 114(B10), B10405.

Lazar, M., Z. Ben-Avraham, and Z. Garfunkel (2012), The Red Sea – New insights from recent geophysical studies and the connection to the Dead Sea fault, Journal of African Earth Sciences, 68(0), 96-110.

Lee, D.-C., A. N. Halliday, J. G. Fitton, and G. Poli (1994), Isotopic variations with distance and time in the volcanic islands of the Cameroon line: evidence for a mantle plume origin, Earth and Planetary Science Letters, 123(1–3), 119-138.

Levin, V., and J. Park (2000), Shear zones in the Proterozoic lithosphere of the Arabian Shield and the nature of the Hales discontinuity, Tectonophysics, 323(3–4), 131-148.

Levin, V., A. Henza, J. Park, and A. Rodgers (2006), Texture of mantle lithosphere along the Dead Sea Rift: Recently imposed or inherited?, Physics of the Earth and Planetary Interiors, 158(2–4), 174-189.

Li, A., and C. Chen (2006), Shear wave splitting beneath the central Tien Shan and tectonic implications, Geophysical Research Letters, 33(22), L22303.

Lithgow-Bertelloni, C., and M. A. Richards (1998), The dynamics of Cenozoic and Mesozoic plate motions, Reviews of Geophysics, 36(1), 27-78.

Liu, K. H. (2009), NA-SWS-1.1: A uniform database of teleseismic shear wave splitting measurements for North America, Geochemistry, Geophysics, Geosystems, 10(5), Q05011.

Liu, K. H., and S. S. Gao (2013), Making Reliable Shear-Wave Splitting Measurements, Bulletin of the Seismological Society of America, 103(5), 2680-2693.

Liu, K. H., and S. S. Gao (2013), Making Reliable Shear-Wave Splitting Measurements, Bulletin of the Seismological Society of America, 103(5), 2680-2693.

Liu, H., P. M. Davis, and S. Gao (1995), SKS splitting beneath southern California, Geophysical Research Letters, 22(7), 767-770.

Liu, K. H., S. S. Gao, Y. Gao, and J. Wu (2008), Shear wave splitting and mantle flow associated with the deflected Pacific slab beneath northeast Asia, Journal of Geophysical Research: Solid Earth, 113(B1), B01305.

Mainprice, D., and P. G. Silver (1993), Interpretation of SKS-waves using samples from the subcontinental lithosphere, Phys. Earth Planet. Inter., 78, 257-280.

Marone, F., and B. Romanowicz (2007), The depth distribution of azimuthal anisotropy in the continental upper mantle, Nature, 447(7141), 198-201.

McKenzie, D. (1979), Finite deformation during fluid flow, Geophysical Journal of the Royal Astronomical Society, 58(3), 689-715.

McNamara, D. E., T. J. Owens, P. G. Silver, and F. T. Wu (1994), Shear wave anisotropy beneath the Tibetan Plateau, Journal of Geophysical Research: Solid Earth, 99(B7), 13655-13665.

McQuarrie, N., J. M. Stock, C. Verdel, and B. P. Wernicke (2003), Cenozoic evolution of Neotethys and implications for the causes of plate motions, Geophysical Research Letters, 30(20), 2036.

Meyers, J. B., B. R. Rosendahl, C. G. A. Harrison, and Z.-D. Ding (1998), Deep-imaging seismic and gravity results from the offshore Cameroon Volcanic Line, and speculation of African hotlines, Tectonophysics, 284(1–2), 31-63.

Milelli, L., L. Fourel, and C. Jaupart (2012), A lithospheric instability origin for the Cameroon Volcanic Line, Earth and Planetary Science Letters, 335–336(0), 80-87.

Morgan, W. J. (1972), Deep Mantle Convection Plumes and Plate Motions, AAPG Bulletin, 56(2), 203-213.

Morgan, W. J. (1983), Hotspot tracks and the early rifting of the Atlantic, Tectonophysics, 94(1–4), 123-139.

Nicolas, A., and N. I. Christensen (1987), Formation of Anisotropy in Upper Mantle Peridotites - A Review, in Composition, Structure and Dynamics of the Lithosphere-Asthenosphere System, edited, pp. 111-123, American Geophysical Union.

Nnange, J. M., V. Ngako, J. D. Fairhead, and C. J. Ebinger (2000), Depths to density discontinuities beneath the Adamawa Plateau region, Central Africa, from spectral analyses of new and existing gravity data, Journal of African Earth Sciences, 30(4), 887-901.

Nowacki, A., J. Wookey, and J. M. Kendall (2010), Deformation of the lowermost mantle from seismic anisotropy, Nature, 467(7319), 1091-1094.

Obrebski, M., S. Kiselev, L. Vinnik, and J. P. Montagner (2010), Anisotropic stratification beneath Africa from joint inversion of SKS and P receiver functions, Journal of Geophysical Research: Solid Earth, 115(B9), B09313.

Plomerová, J., V. Babuška, C. Dorbath, L. Dorbath, and R. J. Lillie (1993), Deep lithospheric structure across the Central African Shear Zone in Cameroon, Geophysical Journal International, 115(2), 381-390.

Priestley, K., D. McKenzie, E. Debayle, and S. Pilidou (2008), The African upper mantle and its relationship to tectonics and surface geology, Geophysical Journal International, 175(3), 1108-1126.

Refayee, H. A., B. B. Yang, K. H. Liu, and S. S. Gao Mantle flow and lithosphere–asthenosphere coupling beneath the southwestern edge of the North American craton: Constraints from shear-wave splitting measurements, Earth and Planetary Science Letters(0).

Reilinger, R., and S. McClusky (2011), Nubia–Arabia–Eurasia plate motions and the dynamics of Mediterranean and Middle East tectonics, Geophysical Journal International, 186(3), 971-979.

Reilinger, R., S. McClusky, M. B. Oral, R. W. King, M. N. Toksoz, A. A. Barka, I. Kinik, O. Lenk, and I. Sanli (1997), Global Positioning System measurements of present-day crustal movements in the Arabia-Africa-Eurasia plate collision zone, J. Geophys. Res., 102, 9983-9999.

Reusch, A. M., A. A. Nyblade, D. A. Wiens, P. J. Shore, B. Ateba, C. T. Tabod, and J. M. Nnange (2010), Upper mantle structure beneath Cameroon from body wave tomography and the origin of the Cameroon Volcanic Line, Geochemistry, Geophysics, Geosystems, 11(10), Q10W07.

Reusch, A. M., A. A. Nyblade, R. Tibi, D. A. Wiens, P. J. Shore, A. Bekoa, C. T. Tabod, and J. M. Nnange (2011), Mantle transition zone thickness beneath Cameroon: evidence for an upper mantle origin for the Cameroon Volcanic Line, Geophysical Journal International, 187(3), 1146-1150.

Ribe, N. M. (1989), Seismic anisotropy and mantle flow, Journal of Geophysical Research: Solid Earth, 94(B4), 4213-4223.

Ribe, N. M., and Y. Yu (1991), A theory for plastic deformation and textural evolution of olivine polycrystals, Journal of Geophysical Research: Solid Earth, 96(B5), 8325-8335.

Ribe, N. M., and U. R. Christensen (1994), Three-dimensional modeling of plume-lithosphere interaction, Journal of Geophysical Research: Solid Earth, 99(B1), 669-682.

Ritsema, J., and H. van Heijst (2000), New seismic model of the upper mantle beneath Africa, Geology, 28(1), 63-66.

Sandvol, E., D. Seber, A. Calvert, and M. Barazangi (1998), Grid search modeling of receiver functions: Implications for crustal structure in the Middle East and North Africa, Journal of Geophysical Research: Solid Earth, 103(B11), 26899-26917.

Savage, M. K. (1999), Seismic anisotropy and mantle deformation: What have we learned from shear wave splitting?, Reviews of Geophysics, 37(1), 65-106.

Schlüter, T. (2006), Geological Atlas of Africa: With Notes on Stratigraphy, Tectonics, Economic Geology, Geohazards and Geosites of Each Country, 1 st ed., Springer, New York.

Schmid, C., S. Van Der Lee, and D. Giardini (2004), Delay times and shear wave splitting in the Mediterranean region, Geophysical Journal International, 159(1), 275-290.

Silver, P. G. (1996), Seismic anisotropy beneath the continents: probing the depths of geology, Annual Review of Earth and Planetary Sciences, 24(1), 385-432.

Silver, P. G., and W. W. Chan (1991), Shear wave splitting and subcontinental mantle deformation, Journal of Geophysical Research: Solid Earth, 96(B10), 16429-16454.

Silver, P. G., and M. K. Savage (1994), The Interpretation of Shear-Wave Splitting Parameters In the Presence of Two Anisotropic Layers, Geophysical Journal International, 119(3), 949-963.

Silver, P. G., S. S. Gao, and K. H. Liu (2001), Mantle deformation beneath southern Africa, Geophysical Research Letters, 28(13), 2493-2496.

Sleep, N. H. (1994), Lithospheric thinning by midplate mantle plumes and the thermal history of hot plume material ponded at sublithospheric depths, Journal of Geophysical Research: Solid Earth, 99(B5), 9327-9343.

Stern, R. J., and P. Johnson (2010), Continental lithosphere of the Arabian Plate: A geologic, petrologic, and geophysical synthesis, Earth-Science Reviews, 101(1-2), 29-67.

Stoeser, D. B., and V. E. Camo (1985), Pan-African microplate accretion of the Arabian Shield, Geological Society of America Bulletin, 96(7), 817-826.

Stuart, G. W., J. D. Fairhead, L. Dorbath, and C. Dorbath (1985), A seismic refraction study of the crustal structure associated with the Adamawa Plateau and Garoua Rift, Cameroon, West Africa, Geophysical Journal International, 81(1), 1-12.

Tabod, C. T., J. D. Fairhead, G. W. Stuart, B. Ateba, and N. Ntepe (1992), Seismicity of the Cameroon Volcanic Line, 1982–1990, Tectonophysics, 212(3–4), 303-320.

Tadjou, J. M., R. Nouayou, J. Kamguia, and H. L. Kande (2009), Gravity analysis of the boundary between the Congo craton and the Pan-African belt of Cameroon, Austrian Journal of Earth Sciences, 102, 71-79.

Tokam, A.-P. K., C. T. Tabod, A. A. Nyblade, J. Julià, D. A. Wiens, and M. E. Pasyanos (2010), Structure of the crust beneath Cameroon, West Africa, from the joint inversion of Rayleigh wave group velocities and receiver functions, Geophysical Journal International, 183(2), 1061-1076.

Tommasi, A. (1998), Forward modeling of the development of seismic anisotropy in the upper mantle, Earth and Planetary Science Letters, 160(1–2), 1-13.

Tommasi, A., A. Vauchez, and R. Russo (1996), Seismic anisotropy in ocean basins: Resistive drag of the sublithospheric mantle?, Geophysical Research Letters, 23(21), 2991-2994.

Toteu, S. F., J. Penaye, and Y. P. Djomani (2004), U-Pb and Sm-Nd evidence for Eburnean and Pan-African high-grade metamorphism in cratonic rocks of southern Cameroon, Canadian Journal of Earth Sciences, 41, 73–85.

Turcotte, D. L., and E. R. Oxburgh (1978), Intra-Plate Volcanism [and Discussion], Philosophical Transactions of the Royal Society of London. Series A, Mathematical and Physical Sciences, 288(1355), 561-579.

Van Houten, F. B. (1983), Sirte Basin, north-central Libya: Cretaceous rifting above a fixed mantle hotspot?, Geology, 11(2), 115-118.

Vauchez, A., A. Tommasi, G. Barruol, and J. Maumus (2000), Upper mantle deformation and seismic anisotropy in continental rifts, Physics and Chemistry of the Earth, Part A: Solid Earth and Geodesy, 25(2), 111-117.

Vinnik, L. P., V. Farra, and B. Romanowicz (1989), Azimuthal anisotropy in the earth from observations of SKS at GEOSCOPE and NARS broadband stations, Bulletin of the Seismological Society of America, 79(5), 1542-1558.

Walker, K. T., G. H. R. Bokelmann, and S. L. Klemperer (2001), Shear-wave splitting to test mantle deformation models around Hawaii, Geophysical Research Letters, 28(22), 4319-4322.

Walker, K. T., G. H. R. Bokelmann, S. L. Klemperer, and G. Bock (2005), Shear-wave splitting around the Eifel hotspot: evidence for a mantle upwelling, Geophysical Journal International, 163(3), 962-980.

Walker, K. T., A. A. Nyblade, S. L. Klemperer, G. H. R. Bokelmann, and T. J. Owens (2004), On the relationship between extension and anisotropy: Constraints from shear wave splitting across the East African Plateau, Journal of Geophysical Research: Solid Earth, 109(B8), B08302.

Wilson, M., and R. Guiraud (1992), Magmatism and rifting in Western and Central Africa, from Late Jurassic to Recent times, Tectonophysics, 213(1–2), 203-225.

Wolfe, C. J., and S. C. Solomon (1998), Shear-Wave Splitting and Implications for Mantle Flow Beneath the MELT Region of the East Pacific Rise, Science, 280(5367), 1230-1232.

Wolfe, C. J., F. L. Vernon, and A. Al-Amri (1999), Shear-wave splitting across western Saudi Arabia: The pattern of upper mantle anisotropy at a Proterozoic shield, Geophys. Res. Lett., 26, 779-782.

Zhang, S., and S. I. Karato (1995), Lattice preferred orientation of olivine aggregates deformed in simple shear, Nature, 375(6534), 774-777.

Zhu, L., and H. Kanamori (2000), Moho depth variation in southern California from teleseismic receiver functions, Journal of Geophysical Research: Solid Earth, 105(B2),2969-2980.

VITA

Ahmed Elsheikh was born and raised in Khartoum, Sudan. He received his Bachelor's degree in Geology and Physics from University of Khartoum Sudan in 2004. In 2009, he earned a Master degree in Geology and Geophysics from Missouri University of Science and Technology, Rolla. In 2010, he joined the PhD program in Geology and Geophysics at Missouri University of Science and Technology Rolla.